A FINE STRUCTURAL AND CYTOCHEMICAL INVESTIGATION INTO PATHOGENICITY OF ENTAMOEBA HISTOLYTICA STRAINS USING CELL LINE MONOLAYERS

A thesis submitted for the degree of
Ph.D (Faculty of Medicine)
of
the University of London
by
THOMAS FORREST McCAIL

from

the Electron Microscopy Unit,
The London School of Hygiene and Tropical Medicine

VOLUME II

SEPTEMBER, 1976

CONTENTS

VOLUME II		page
A.	Key to lettering used in figures	1
B.	Figures (photographs)	3

KEY TO LETTERING USED IN PLATES

A	Amoeba
B	Bacterium
BD	BD-VI liver cell-line
BR	Rhesus Monkey Brain cell
C	Catalase reaction product
Cb	Chromatoid body
Ce	Euchromatin
Ch	Heterochromatin
Cj	Cell Junction
Cm	Cytoplasmic membrane (of bacteria)
Cr	Chromatin
Cv	CV-1 kidney cells
Cy	Cytoplasm
Cz	Contact zone
D	Cellular debris
Db	Dense body
E	Envelope
Ec	Ectoplasm
ER	Endoplasmic reticulum
F	Filaments
Fp	Filopodium
G	Golgi-like complex
Gl	Glomerulus
H	Ribonucleoprotein helix
Ic	Infected cell
If	Interdigitating folds
Ih	Inner helix
K	Karyosome
L	Lysosome
Le	Lesion
Mb	Bundle of microfilaments
Mc	Mitochondrial cristae
M, Mi.	Mitochondria
Mf	Myelin-like figures
Mt	Microtubule
Mv	Microvilli
N	Nucleus
Ne	Nuclear envelope
Ni	Nuclear inclusion
Nic	Non-infected cell
Np	Nuclear pore
Nu	Nucleolus

Oh	Outer helix
Om	Outer membrane (of bacteria)
P	Plasmalemma
Pb	Phagocytotic bulb
Pc	Phagocytotic channel
Pg	Perichromatin granule
Pi	Pinocytotic channel
Ps	Micropseudopodia
Pr	Polyribosomes
Ps	Pseudopodium
R	Rosette
Rf	Ruffle
Rh	Rhabdovirus
RH	Ribosomal helix
Ri	Ribosomes
RV	RV13 cell
Sp	Subpellicular body
T	Tubule
Tj	Tight junction
Tm	Mucoid threads
U	Uroid
V	Vacuole
Ve	Vesicle

Fig. 1 Trophozoite of E. histolytica from monoxenic strain (Evans) showing an oval-shaped nucleus (N) and a number of vacuoles (V). Pseudopodia are engulfing cellular debris from lysed RK13 cultured cells. x 4400

Fig. 2a Evans strain (monoxenic). The nuclear membrane shows a double membrane with nuclear pores (Np). The microtubules (arrowheads) are radiating from a centrally situated karyosome (K). x 44000

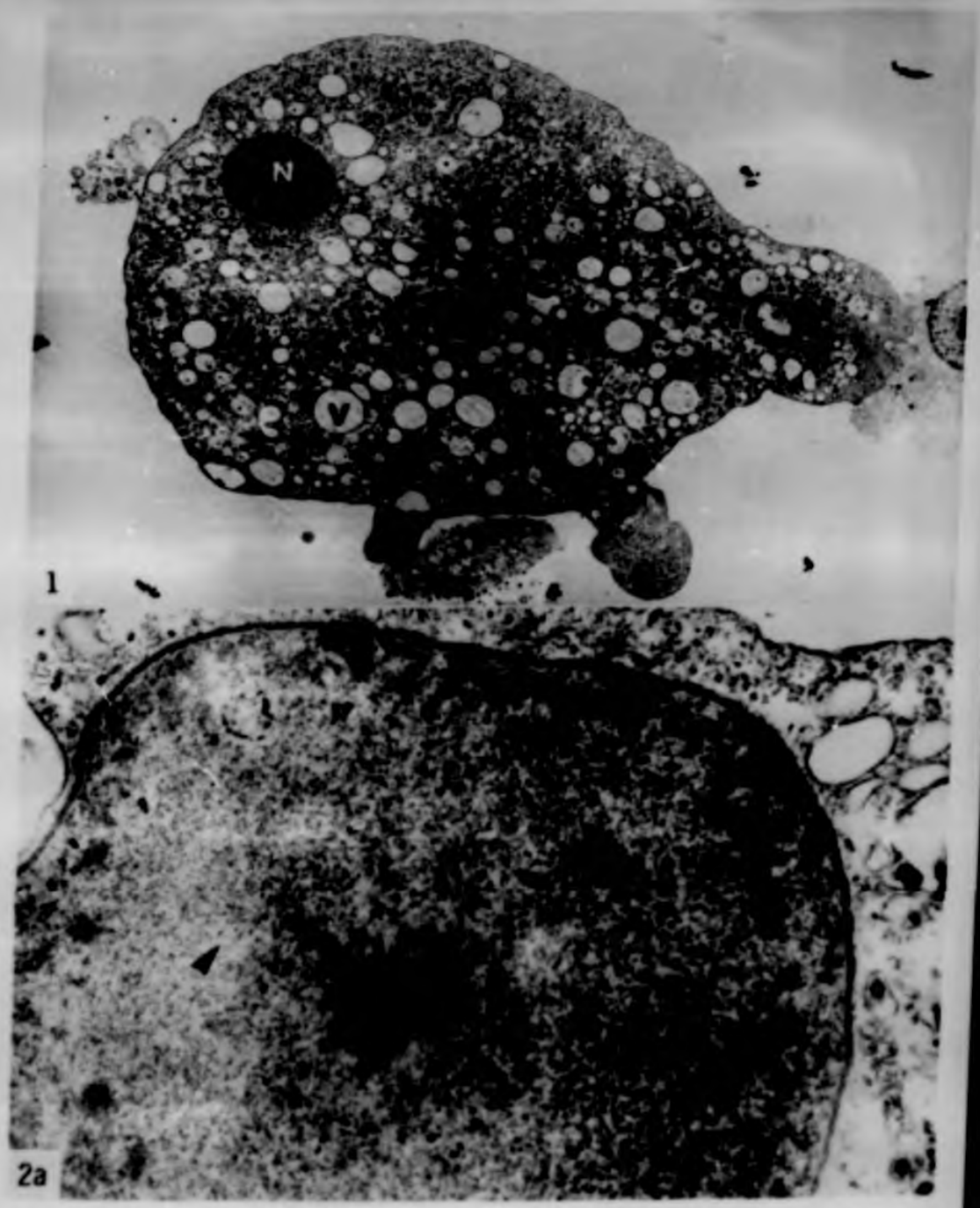
N
V
1
2a

Fig. 2b Ax. 200 strain (axenic). Part of an amoeba showing nucleus and its nuclear inclusions (Ni). x 7350

Fig. 3 Twms strain (monozenic). Nuclear pore illustrating a diaphragm (arrow). x 87500

Figs. 4 & 5 Trophozoite of E. histolytica from monozenic strain (Liggins) :

Fig. 4 Part of an amoeba showing 3 nuclei with numerous nuclear inclusions x 7350

Fig. 5 Higher magnification of Fig. 4 showing numerous membrane-bound intra-nuclear bodies (Ni), some of which contain membranous material (white arrow) in the heterochromatin border (Ch). Note in the euchromatin (Ce) a non-membrane bound inclusion with granular material (arrowhead). x 36,750

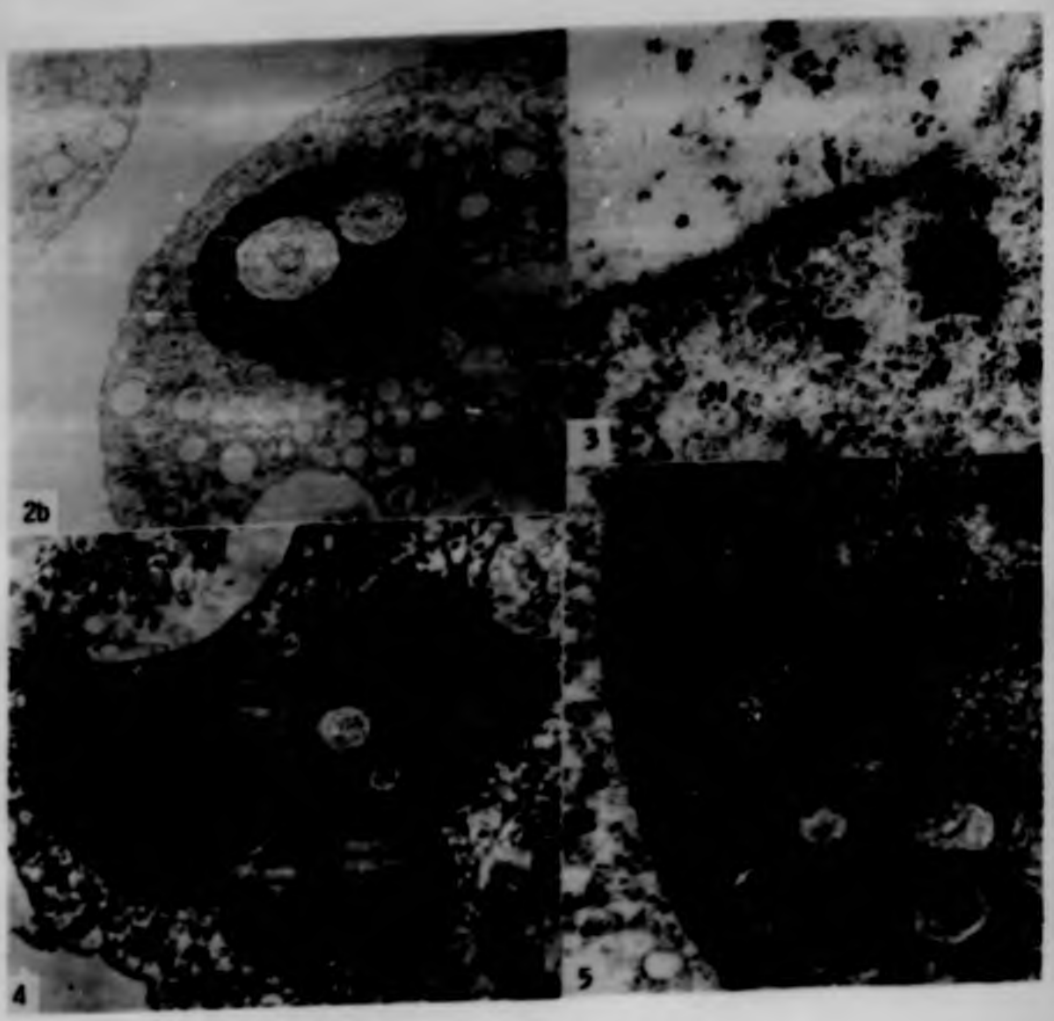
2b
3
4
5

Fig. 6 Swanwick strain (monoxenic). Part of the nucleus showing numerous membrane-bound intranuclear inclusions in the heterochromatin. Ribosomal material (arrow) is seen in one of the inclusions. x 43,480

Fig. 7a Swanwick strain (monoxenic). Part of the nucleus showing an inclusion body about to pass through the nuclear membrane. x 43,480

Fig. 7b Evans strain (monoxenic). The vesicle has passed through the nuclear membrane releasing its contents into the cytoplasm. x 69,570

Fig. 8 Part of the nucleus of a monoxenically cultivated amoeba (Evans strain) containing nuclear inclusions and clusters of filamentous strands (arrowheads) of unknown origin. x 36,720

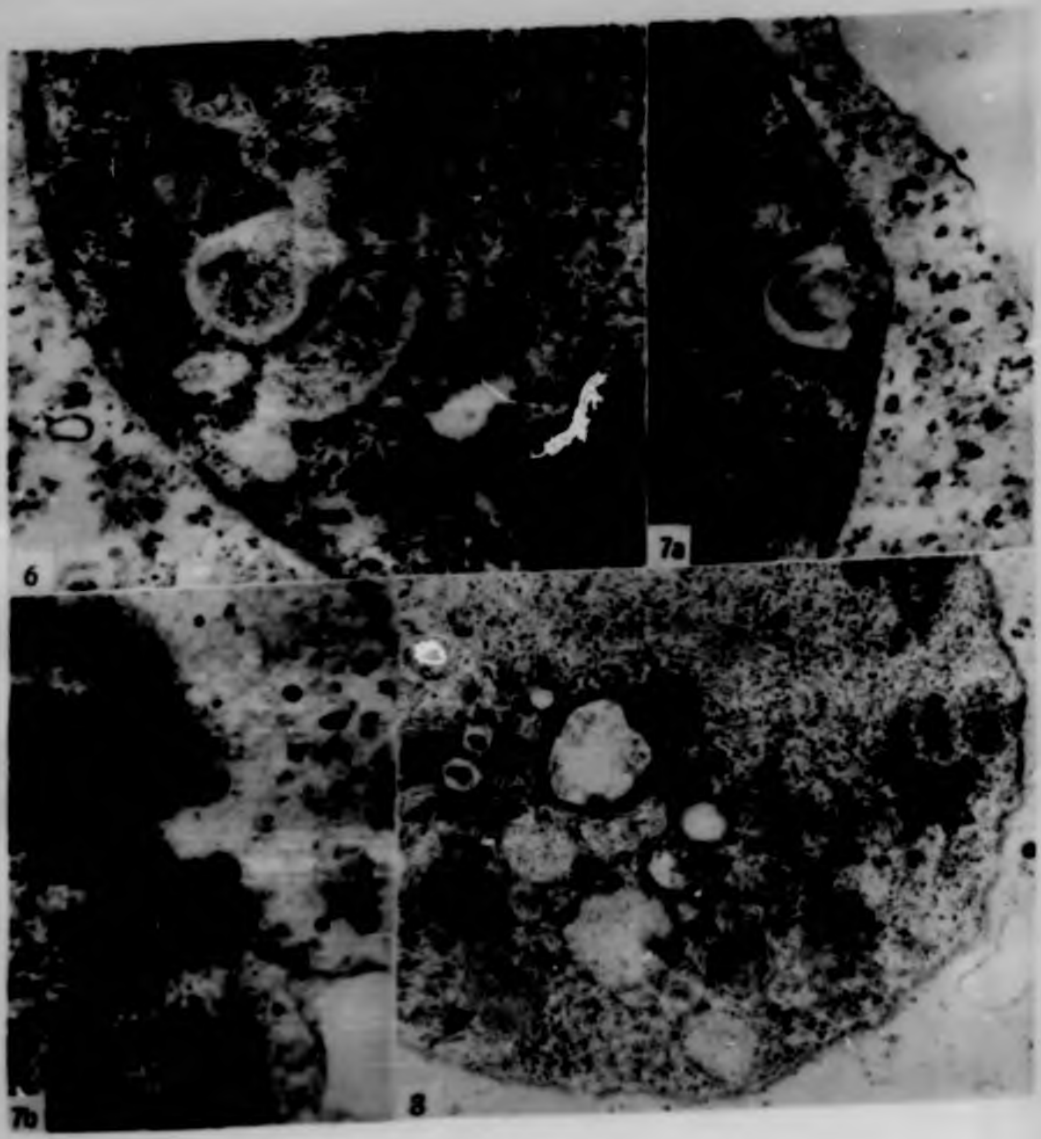
6
7a
7b
8

Fig. 9 Evans strain (monoxenic). Shows a typical tri-laminar plasma membrane (P). x 132,300

Fig. 1 Evans strain (monoxenic). A section of an amoeba illustrating the subpellicular body (Sp). x 132,300

Fig. 11 Ax. 200 strain (axenic). Part of a trophozoite showing the development of the sub pellicular bodies (arrowheads). A fully formed sub-pellicular body is also seen. x 84,000

Fig. 12 An intranuclear inclusion (Ni) is observed in this section in the cytoplasm of an axenically cultivated amoeba (Ax. 200 strain). A sub-pellicular body (arrow) is also seen and it resembles the non-vesicular type nuclear inclusion. x 36,230

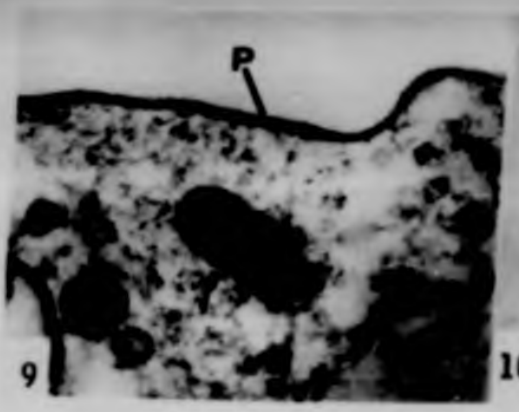

9

10

11

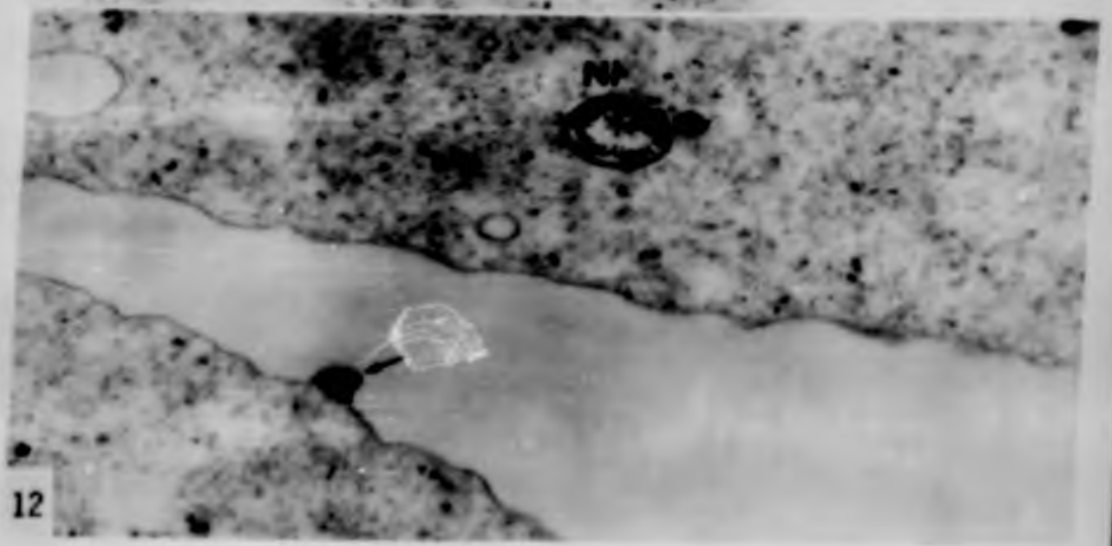

12

Fig. 13 DKB strain (monoxenic). A section through the amoebic cytoplasm showing 2 collapsed vacuoles (arrows) which give an appearance suggestive of a 'surface lysosome'. x 16,800

Fig. 14 A bacterium present in the amoebic culture shows a rigid polysaccharide cell wall which is comprised of an outer membrane (Om) and a cytoplasmic membrane (Cm). x 126,000

Fig. 15 Swanwick strain (monoxenic). A vacuole containing ingested bacteria (B). The outer membranes (Om) of the bacteria have broken down, releasing the cytoplasm (arrowhead) into the amoebic vacuole. Further decomposition leads to the formation of myelin-like figures (Mf). x 50,000

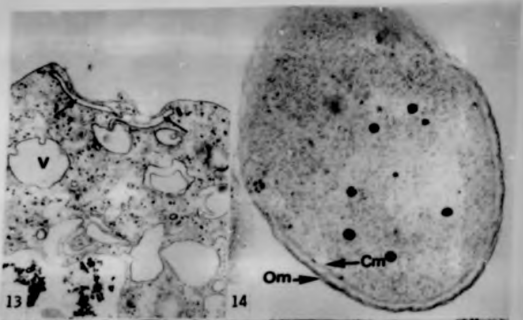

13 14

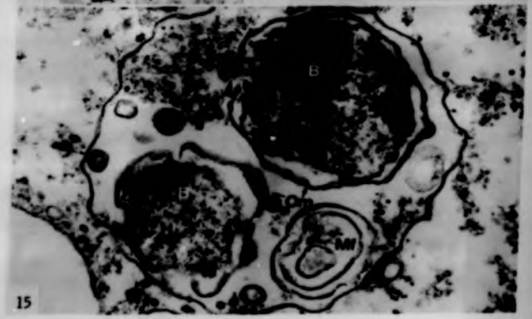

15

Figs. 16 & 17 Light microscope localisation of acid phosphatase activity in E. histolytica (Evans strain).

Fig. 16 Incubation in a medium containing naphthol AS-B1 phosphate as a substrate. A diffused reaction product is seen. Note : the amoebae were fixed in situ revealing the uroids (U). x 1800

Fig. 17 Incubation in a medium containing sodium β-glycerophosphate as a substrate. x 1420

Figs. 18, 19 & 20 Electron microscope localisation of acid phosphatase activity in amoebic vacuoles (Evans strain).

Fig. 18 Incubation in Barka and Anderson's medium containing sodium β-glycerophosphate as a substrate. The reaction deposits are confined to the walls of the vacuoles (V). x 22,540

Figs. 19 & 20 Incubation in Novikoff's medium containing cytidine 5'-monophosphate as a substrate. Fig. 19 The lead reaction product is restricted either to the walls of the vacuoles and their contents (V) or to whole lysosomes (L). Droplets observed in one of the vacuoles are perhaps fat bodies released from decomposed erithidia. x 8230

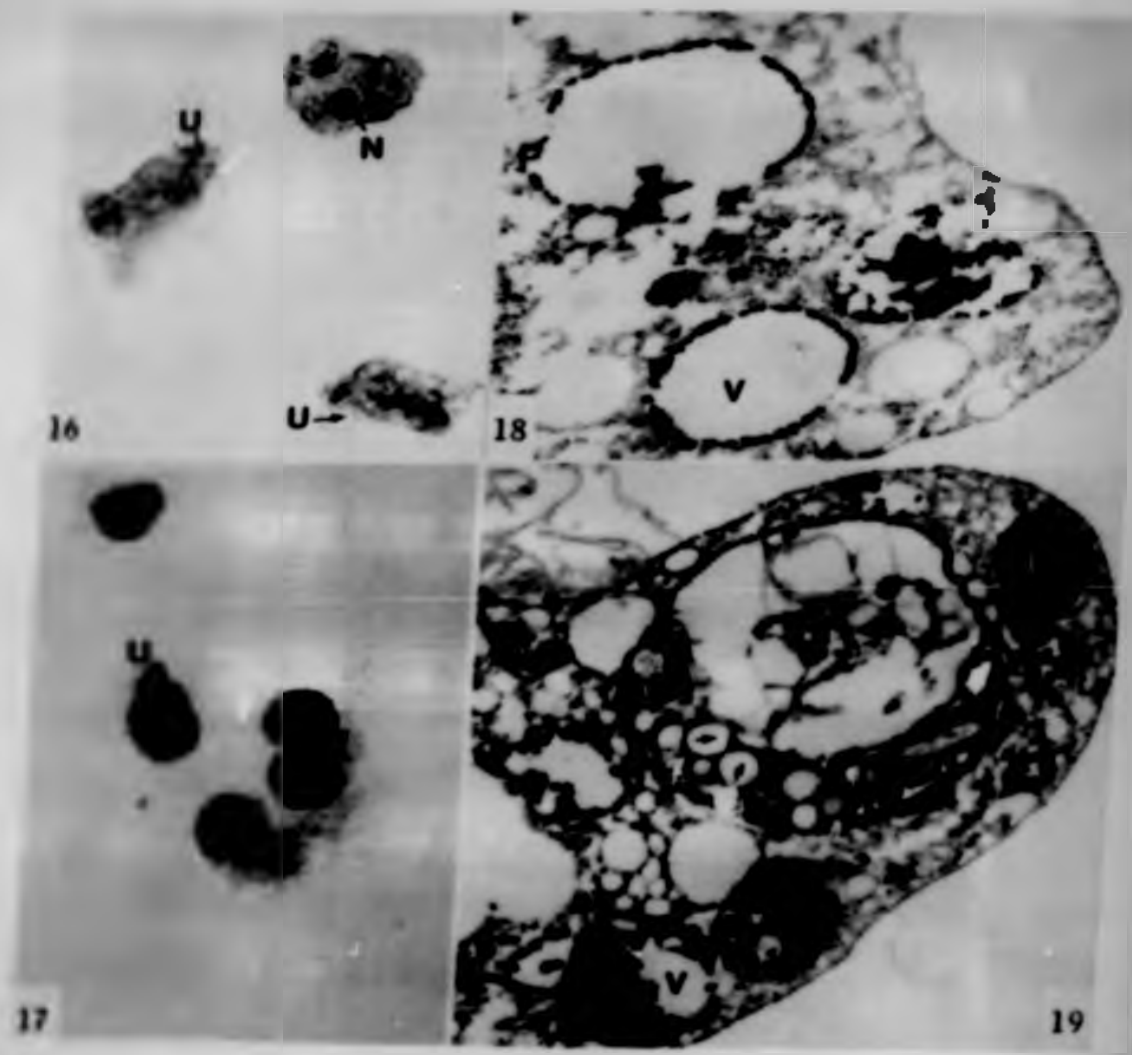
U
N
U
16
V
18
U
17
V
19

Fig. 20 The reaction product for acid phosphatase is not present in the intranuclear bodies (arrows). x 8000

Fig. 21 Light microscope localization of catalase (C) activity in the vacuoles of E. histolytica. x 3570

Fig. 22 Electron microscope localization of catalase (C) activity in the amoebic vacuoles. The reaction deposits are confined to the contents of the vacuoles. x 6860

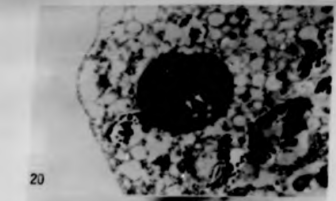

20

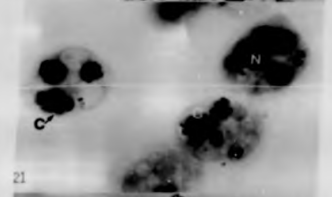

21

22

Fig. 23 Electron microscope localisation of catalase activity in E. histolytica. The trophozoites were fixed in situ revealing extracellular components, the uroid (U) and filopodia (Fp) which are not evident in sections of trophozoites fixed after centrifugation. Cellular debris containing the reaction deposits for catalase are taken into the amoebic cytoplasm through the uroid by phagocytosis (arrowhead). Eventually the debris are trapped in a vacuole (arrow). x 8250

Fig. 25 Light microscope localisation of thiamine pyrophosphatase (TPPase) activity in a trophozoite (A) of E. histolytica. Reaction product in amoebic vacuoles (arrow). Fixed in 4% formaldehyde. x 3995

23

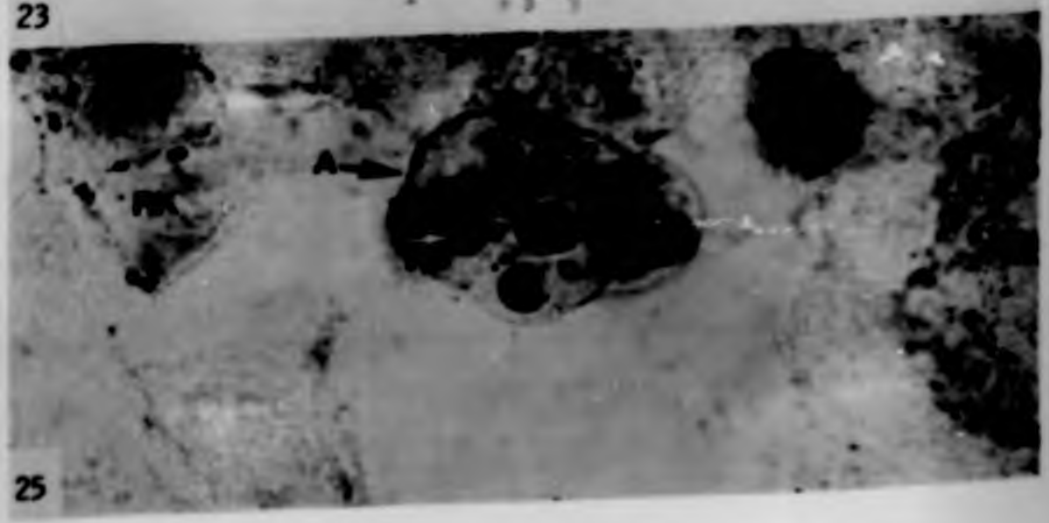

25

Fig. 24 Trophozoites of E. histolytica from monoxenic strain (Evans) showing an absence of staining for catalase activity when incubated in a substrate depleted medium. x 1500

Fig. 26 Reaction product (arrowheads) in the amoebic nucleus, after incubation in presence of TPP. Fixed for 3 mins. in 3% glutaraldehyde. x 3750

Fig. 27 Part of an amoeba showing reaction product for TPPase at electron microscopic level in the amoebic nucleus (N). An electron microscope localisation. Fixed for 15 mins. in 3% glutaraldehyde. x 23,000

Fig. 28 Electron microscope localisation of TPPase activity in E. histolytica (Evans strain). 30 mins. fixation in 4% formaldehyde. Reaction product observed in the vacuoles. None is seen in both the nucleus (N) and the nuclear inclusions (Ni). x 8,400


24
27
28

Fig. 29 At a higher magnification, the reaction product for TPPase is confined either to the vacuolar contents or to the wall of the vacuoles (arrow). x 20,700

Figs. 30a, b Part of an amoeba showing small invaginations of the vacuolar membrane (black arrows) resembling pinocytotic vesicles. A pinocytotic vesicle can also be seen on the surface of the plasmalemma (white arrow).

Fig. 30a Arnell strain (monoxenic) x 20,700
30b Swanwich strain (monoxenic) x 20,700

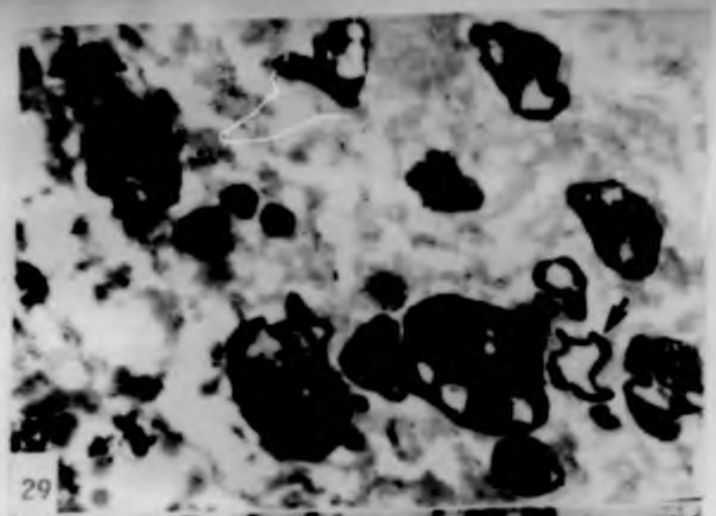

29

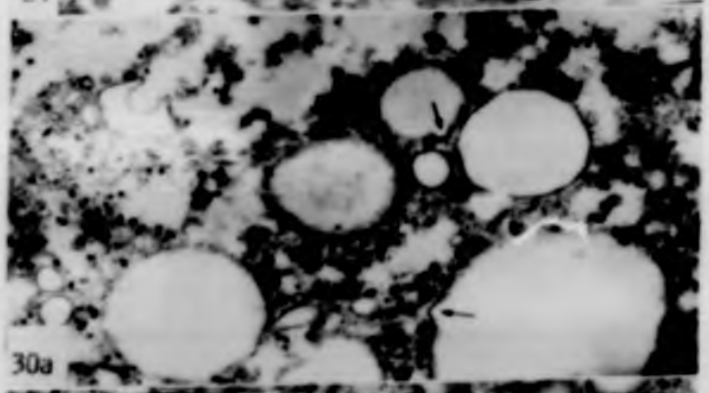

30a

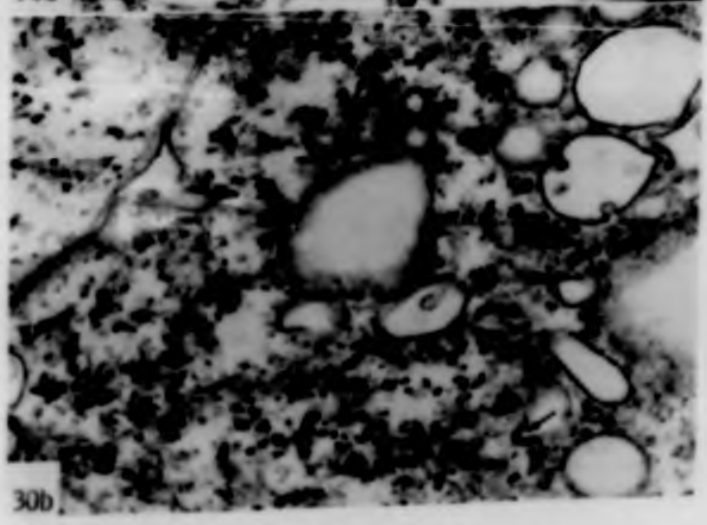

30b

Fig. 31 Ax. 200 strain (axenic). Part of amoebic cytoplasm showing a crystalloid structure resembling the chromatoid body (Ch). x 19,200

Fig. 32 Asante strain (monoxenic). Section through the cytoplasm and nucleus of a trophozoite illustrating rosettes of rhabdovirus particles (arrowheads). x 4510

Fig. 33 Swanwick strain (monoxenic). Particles showing characteristics of a rhabdovirus; a bullet shaped virion with an outer envelope (E) and two distinguishable helices (Ih and Oh). x 66,770

Fig. 34 Ax. 200 strain (axenic). Part of amoebic cytoplasm showing a granular mass resembling paranuclear bodies. x 19,200

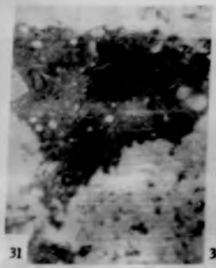

31

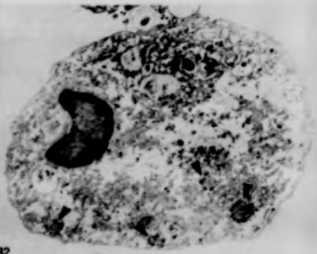

32

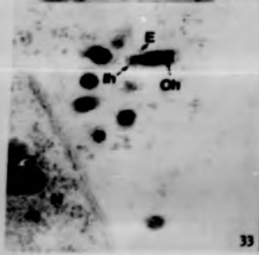

33

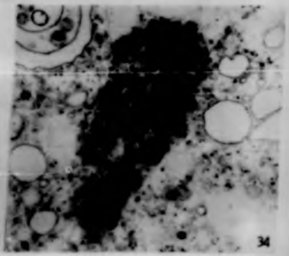

34

Fig. 35 Ax. 200 strain (axenic). A fibre-like structure resembling microfilaments is shown (Mb).
x 53,850

Fig. 36 Evans strain (monoxenic) Filaments (F) are occasionally seen in the cytoplasm of trophozoites cultivated monoxenically. x 86,150

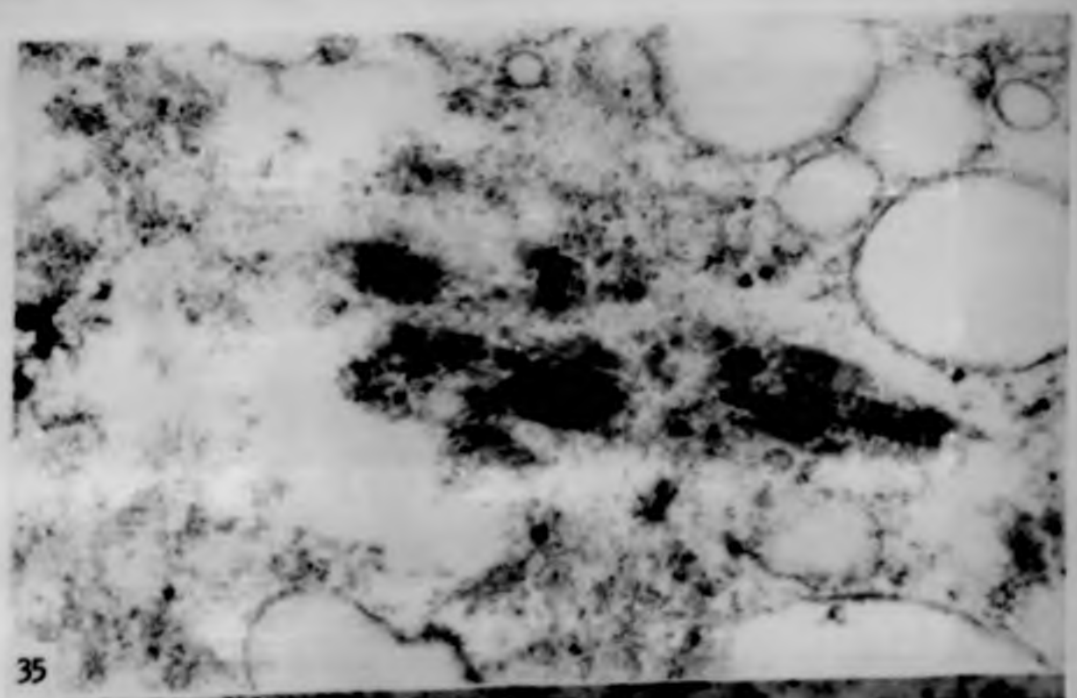

35

36

Figs. 37 to 40 Scanning electron microscopy of E. histolytica trophozoites of monoxenic strain (Cysms). The amoebae were fixed in situ for 30 mins. with 3% glutaraldehyde.

Fig. 37 General appearance of an amoeba showing a single pseudopodium (Ps) x 3025

Fig. 38 A group of amoebae illustrating the tail end or uroid (U) and pseudopodia x 1352

Figs. 39 & 40 The amoebic surface is smooth with areas of minimal infolding. Large depressions or surface lysosomes have not been identified in the specimens used in this study.

Fig. 39 x 10,920

Fig. 40 x 14,040


37
38
39
40

Fig. 41 Amoebic pseudopodium (Ps) illustrating horizontal striations (arrowheads) on the surface. x 1404

Fig. 42 Another scanning electron micrograph of a E. histolytica trophozoite showing the uroid (U). x 3950

Fig. 43a A group of trophozoites. Filopodia can be seen to spread out from the uroid (U) of one amoeba. x 1850

Fig. 43b High magnification of an area marked U in Fig. 43a x 10,560

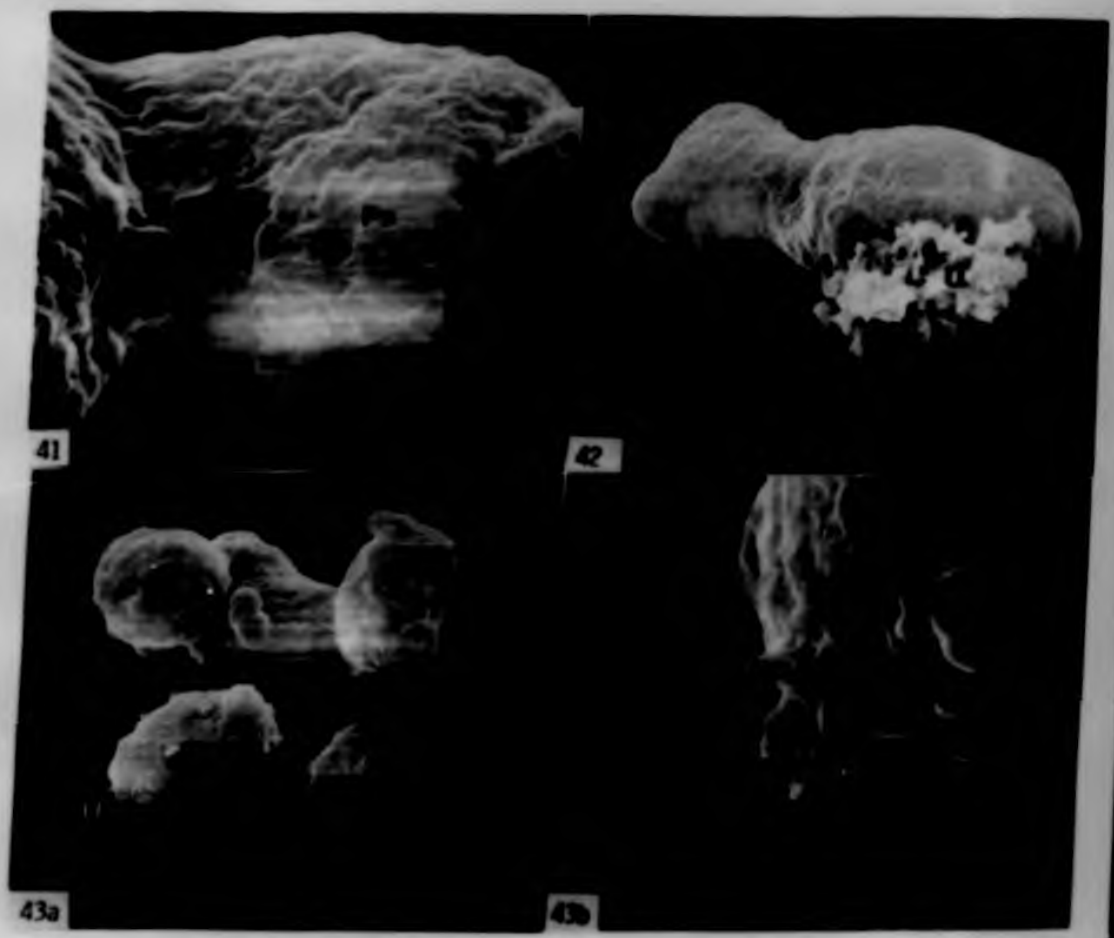
41
42
43a
43b

Fig. 44a Small filopodia, marked by arrows are seen to extend along the lateral edges of the amoeba. x 2160

Figs. 44b and 44c High magnification of the areas marked by arrows in Fig. 44a. Pleba (arrow in Fig. 44c) are occasionally seen at the end of such filopodia. x 10,560

44a

44b

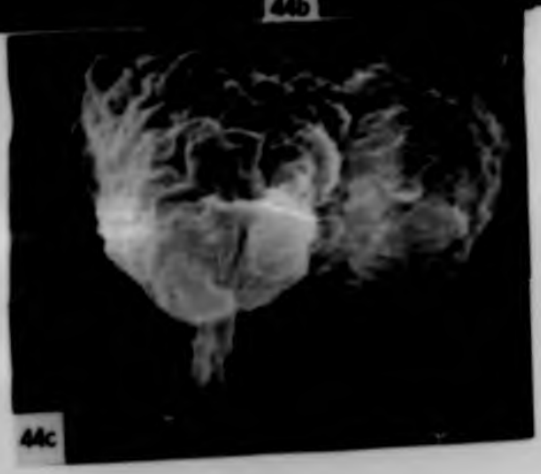

44c

Fig. 45 Section through a healthy Rhesus Monkey Brain cell from a control monolayer culture. x 5120

Fig. 46 Highly magnified view of a normal Monkey Brain cell from a control monolayer showing unaffected mitochondria (M) and endoplasmic reticulum (ER). Intramitochondrial granules (arrows) are clearly seen x 42,970

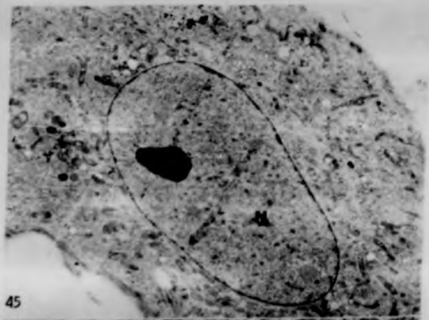

45

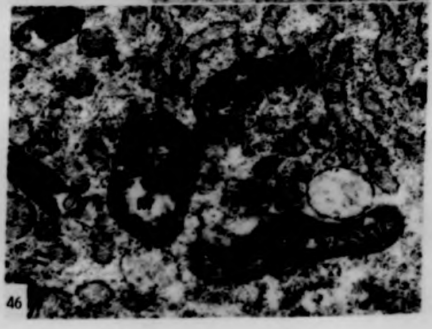

46

Fig. 47a Section through contact zone between E. histolytica (A) and Rhesus Brain cell (BR). x 2000

Fig. 47b High magnification of the area of contact between E. histolytica and Rhesus Monkey Brain cell as depicted in Fig. 47a. x 8400

Fig. 48 Section through healthy CV-1 cells from a control monolayer culture. The morphology of the nucleus (N) is clear; the dense area (arrow) represents the heterochromatin, the paler areas between the areas of heterochromatin being euchromatin (Ce). x 5000

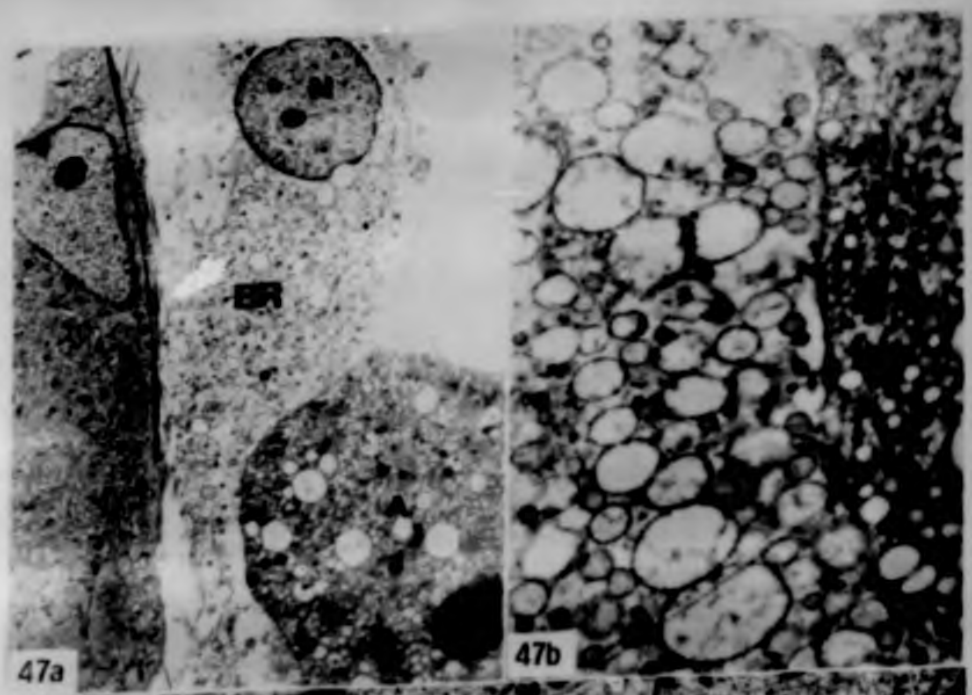

47a

47b

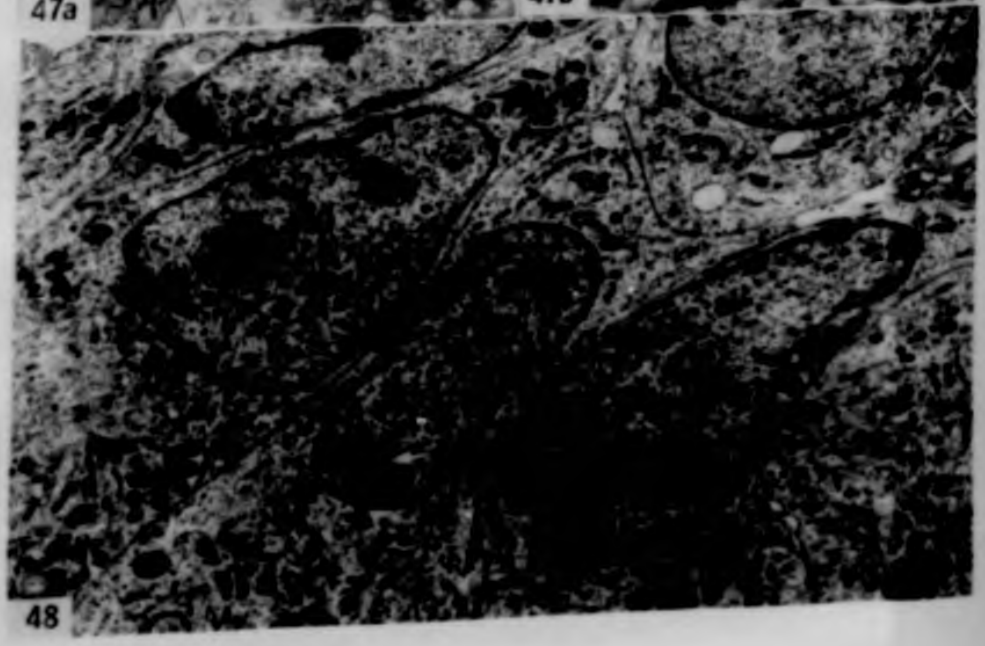

48

Fig. 49 Part of a healthy CV-1 cell from a control monolayer culture showing the various cell organelles; endoplasmic reticulum (ER), Golgi body (G), mitochondrion (M), microtubules (arrowhead). On the surface of the tangentially cut cisternae of endoplasmic reticulum can be seen numerous polyribosomes (arrows). x 48,750

Fig. 50 Contact zone between E. histolytica (A) and CV-1 cell (Cv) during the initial stage of interaction; the microvilli (Mv) of the cultured cells have increased in length. x 9750

49

50

Fig. 51a Portion of cytoplasm of an affected CV-1 cell in contact with *B. hyalolytica*. The mitochondria (M) and endoplasmic reticulum (ER) are swollen. Hyperactivity of the Golgi elements (G) is evidenced by an increase in the number of vesicles. The membranes of lysosomes (L) are intact. x 21,805

Fig. 51b High magnification of Fig. 51a. Moderately swollen mitochondria (M) showing peripherally placed and disintegrating cristae (Mc). The mitochondrial matrix has a patchy appearance due to development of multiple electron-lucent foci (arrowheads). The cisternae of endoplasmic reticulum are swollen with polyribosomes still intact (arrow). x 54,520

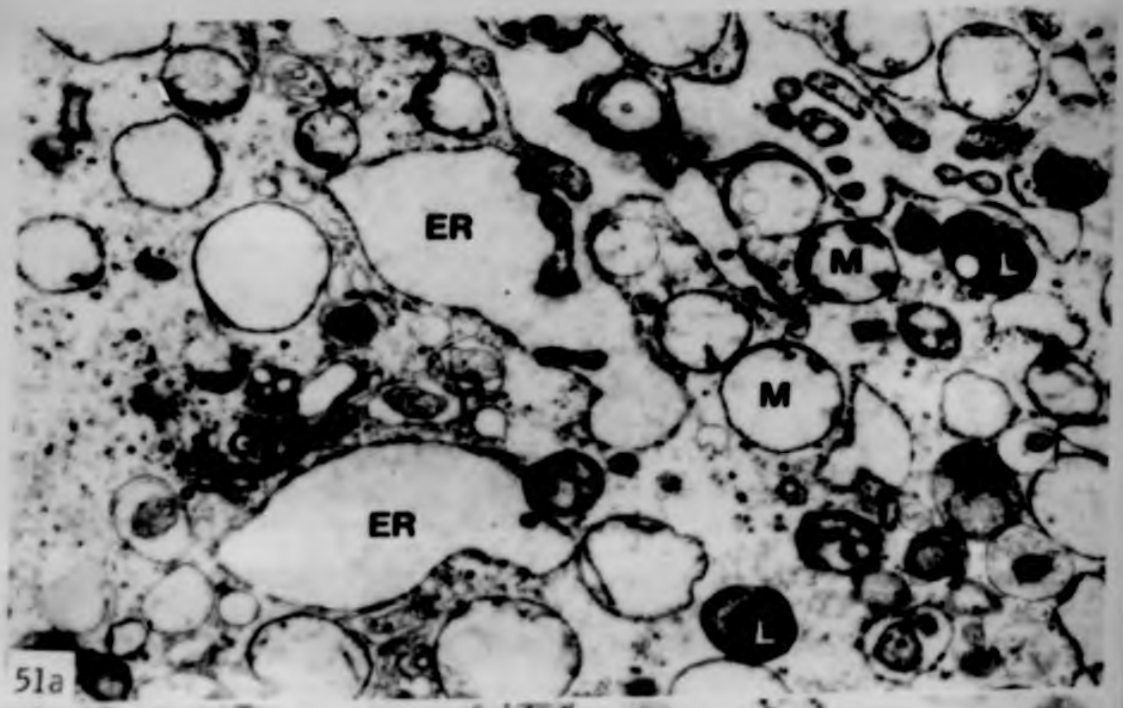

51a

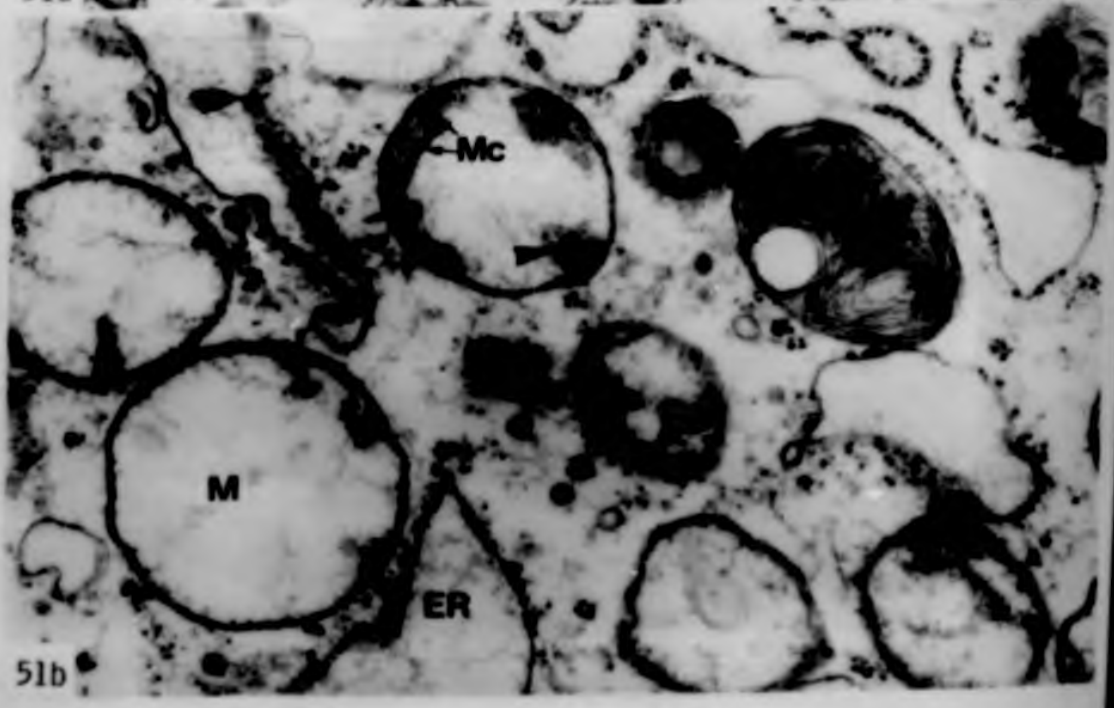

51b

Figs. 52 & 53 A later stage of interaction. Mitochondria (M) are markedly swollen with loss of matrix substance. Breaks in the mitochondrial limiting membranes are seen. Both vesiculation and dilatation of the cisternae of rough endoplasmic reticulum (ER) are also seen. Cytoplasmic filaments (black arrows) are present and may have arisen from dissolution of microtubules. Although some of the ribosomes have degranulated from the endoplasmic reticulum, most of the polyribosomes are still attached to the tangentially cut membranes of the cisternae of endoplasmic reticulum (white arrows). x 29,200

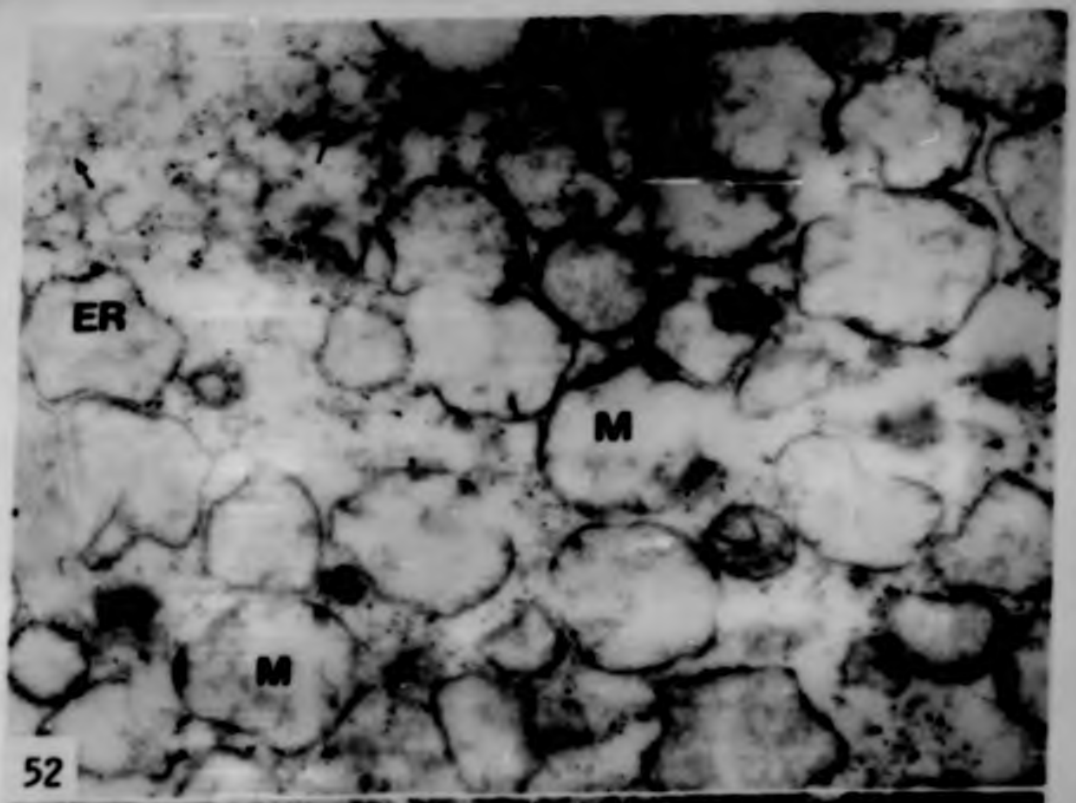

52

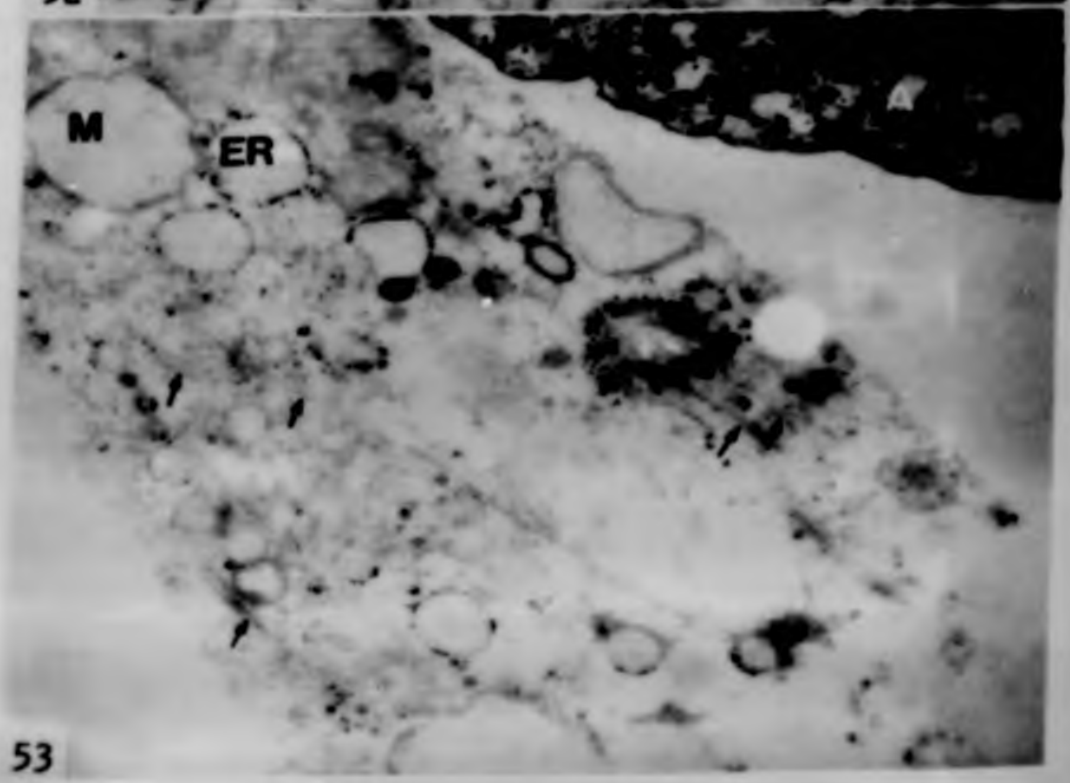

53

Fig. 54 Initial stage of contact between an amoeba and CV-1 cell. Condensation of the chromatin (Cr) is seen to occur along the inner membrane of the nuclear envelope. Endoplasmic reticulum and mitochondria are swollen. Note the amoebic uroid (U). x 5330

Fig. 55 Later stage of cell injury. The cell membrane of the affected cell next to a binucleate amoeba (A) has broken down. The damaged organelles are retained by the unbroken parts of the plasma membrane. The cell nucleus is also affected. Here, the nuclear envelope remains reasonably intact but the contents apart from the nucleolus (Nu) are almost completely lost. x 4000

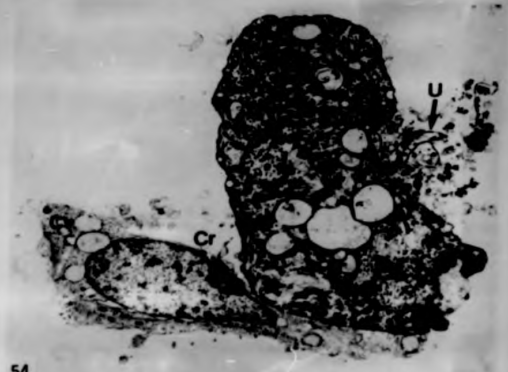

54

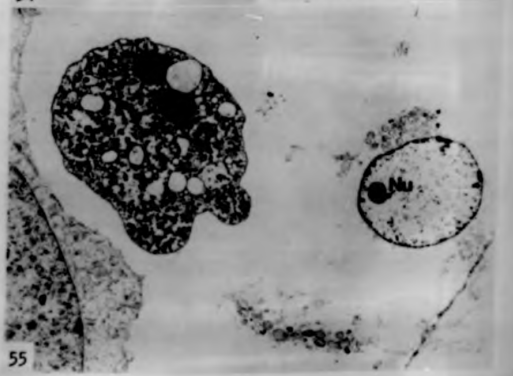

55

Figs. 56 to 62 **Stages of amoebic phagocytosis :**

Fig. 56 Amoebic micropseudopodia (Ps) are seen to indent the cell without breaking the cellular membrane (arrowhead) of the CV-1 cell. x 27,760

Fig. 57 A later stage of protrusion of micropseudopodia (Ps) into the cell. The cellular membrane (arrowheads) of the affected CV-1 cell is still unbroken. x 27,760

Fig. 58 Contact zone between the amoeba (A) and CV-1 cell showing the formation of a phagocytotic channel. x 26,020

Fig. 59 The phagocytotic channel (Ps) extends, and the end of the channel is seen to invaginate forming vesicles (arrow) which may bud off from the channel.

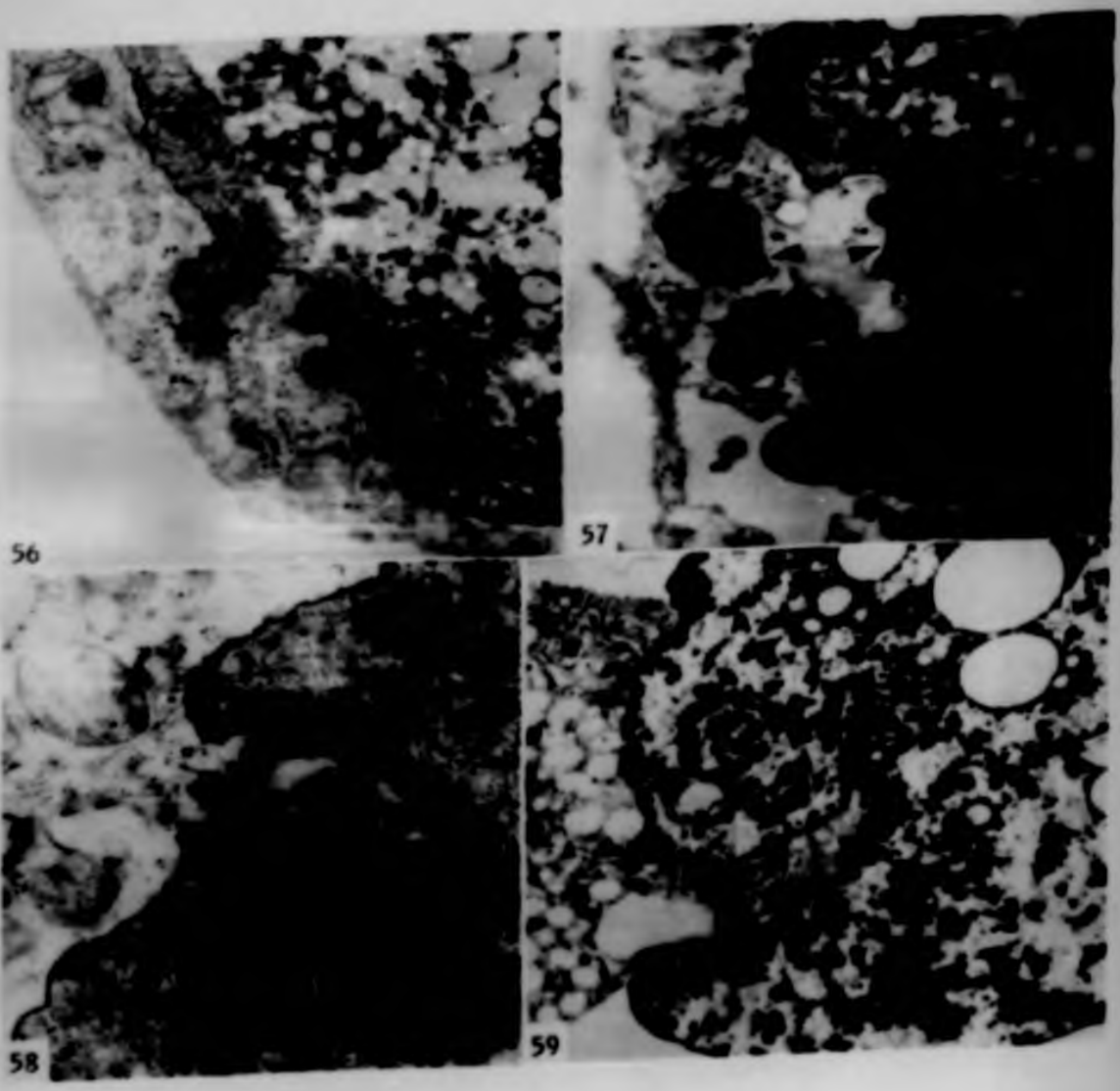

Fig. 60a Further extension of the phagocytotic channel (Pc). The amoebic microspseudopodia (Ps) expand encircling the trapped cellular debris. x 10,520

Fig. 60b Higher magnification of Fig. 60a. Detached pieces of cell plasma membrane (arrowheads) are observed along the lining of the phagocytotic channel; an indication that the cell has been phagocytosed with its membrane intact.
x 28,800

60a

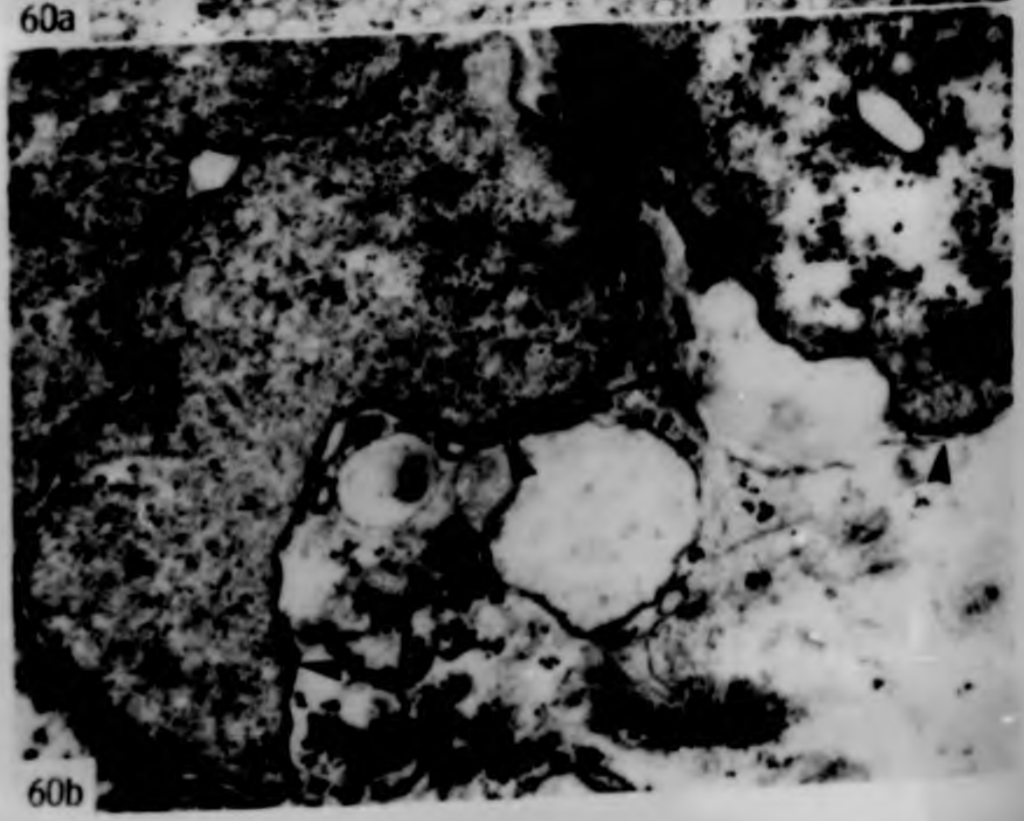

60b

Fig. 61a As for Fig. 60a; the micropseudopodia expand encircling the trapped cellular debris. x 13,950

Fig. 61b Higher magnification of Fig. 61a showing filaments (F), ruptured lysosomes (L) and degranulated ribosomes (Ri) in an amoebic phagocytotic channel. Detached pieces of cell plasma membrane (white arrows) within the phagocytotic channel are also observed. Note the filament-like structure (arrowheads) in the ectoplasm. x 56,760

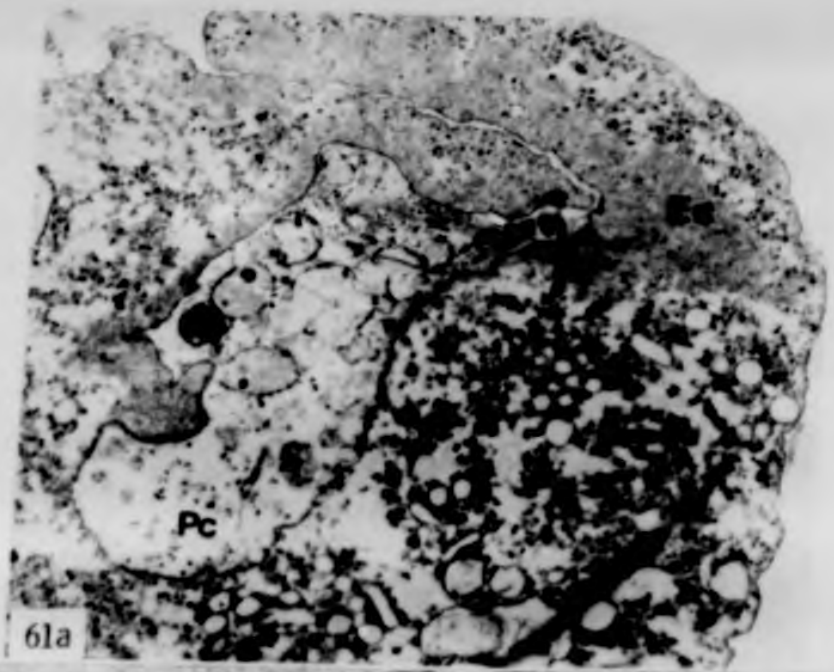

61a

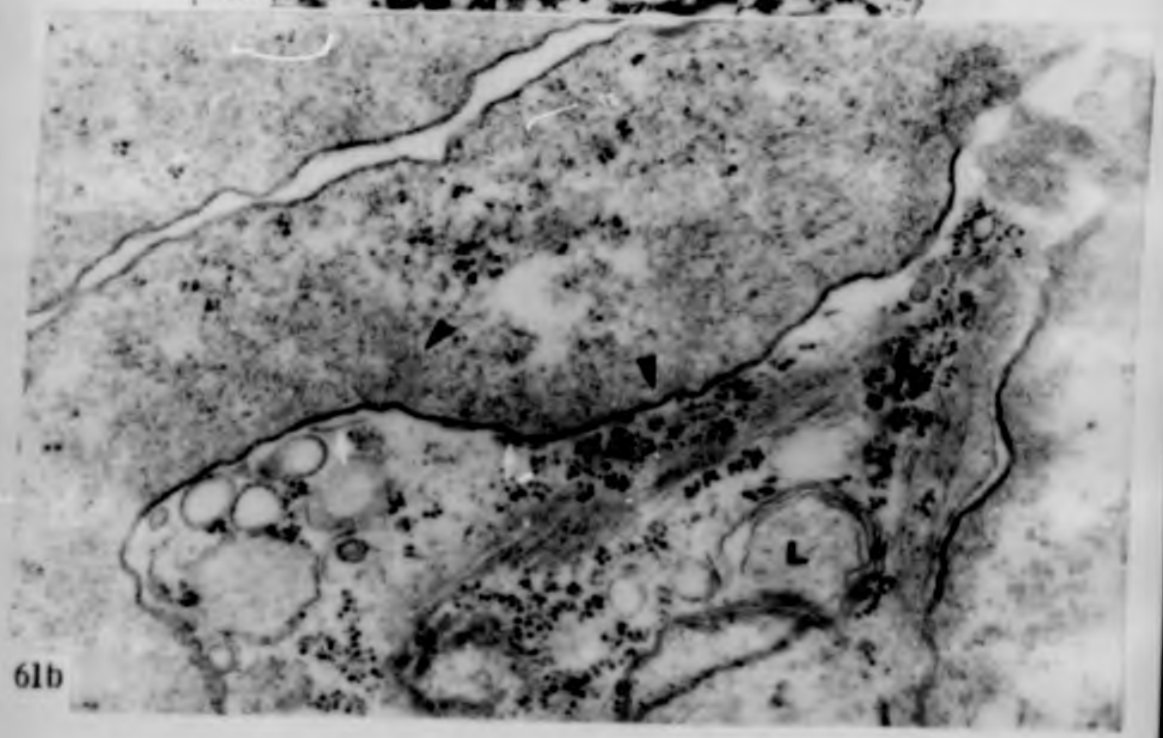

61b

Fig. 62 Higher magnification of the phagocytotic channel shown in Fig. 61a illustrating the dissolution of the cell mitochondria and its cristae (Mc). x 83,080

Fig. 63 Uroid of a trophozoite of E. histolytica. The particulate material (arrowhead) is seen to be taken into the amoeba by small cytoplasmic protrusions at the uroid end (U). Note the formation of a small vesicle (white arrow) adjacent to the inner coat of the vacuole. x 13,085

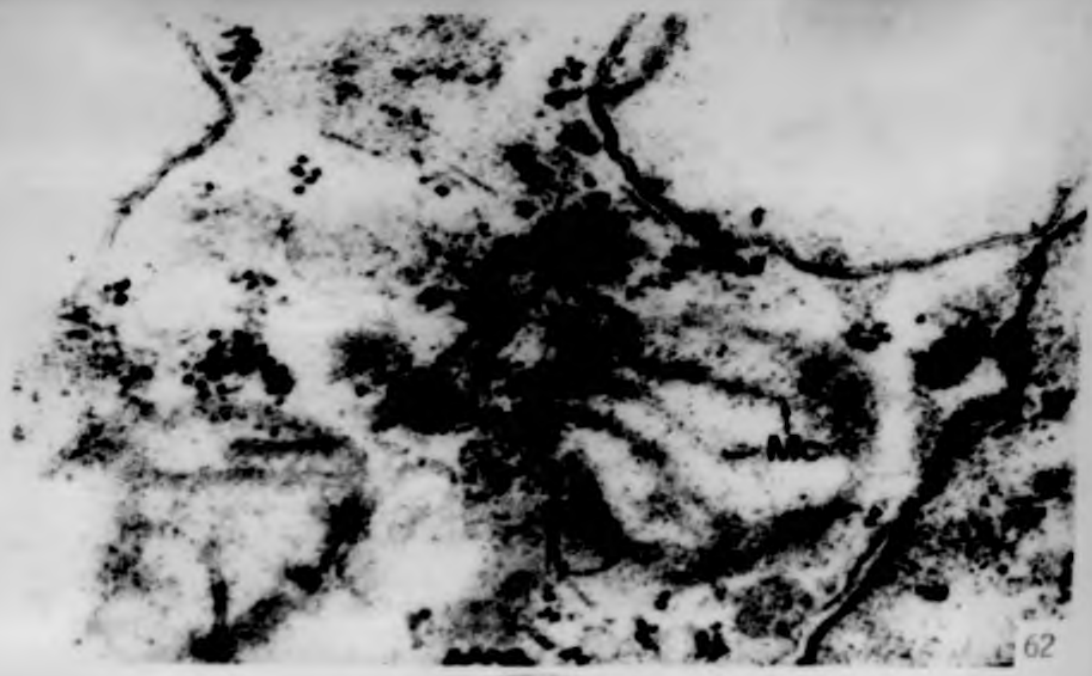

62

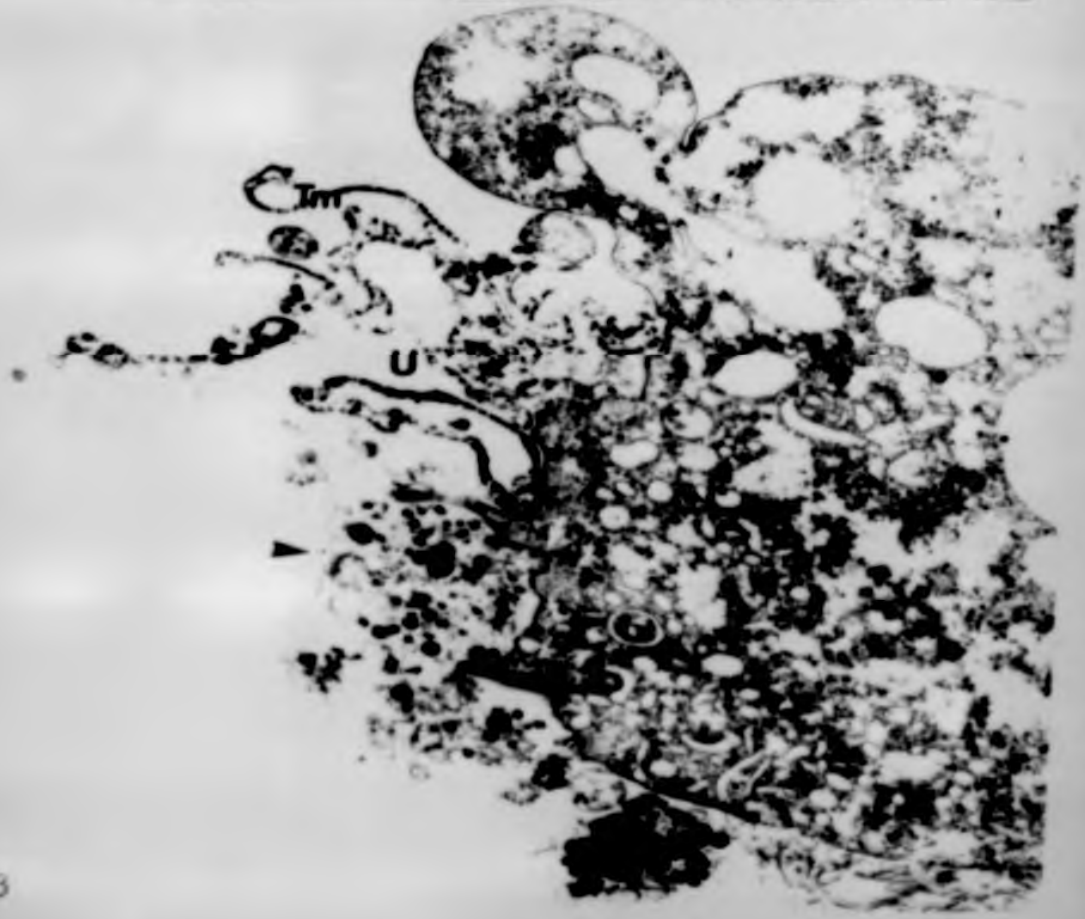

63

Fig. 64a *E. histolytica* trophozoite (A) in cell-denuded areas of a CV-1 cell monolayer (CV). The pseudopodium is seen to ingest a membrane-bound structure, probably a secondary lysosome (L). x 5485

Fig. 64b Higher magnification of the uroid shown in Fig. 64a. The uroid (U) is enclosed in a large clump of cellular debris (D) and microvilli (Mv). Pieces of ectoplasm (arrowheads) have almost detached themselves from the uroid. x 46,070

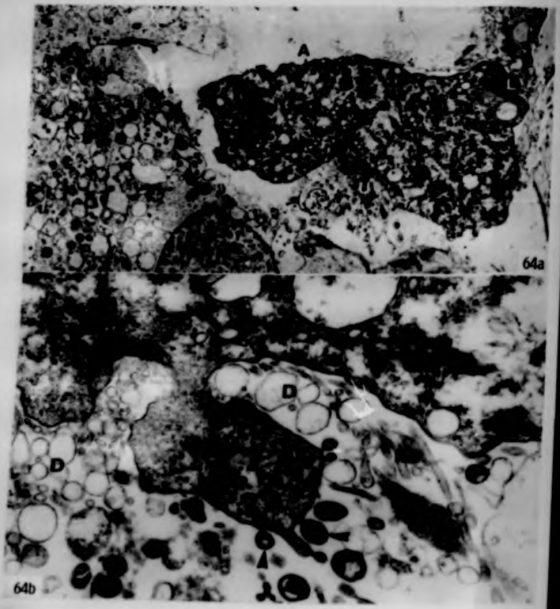
A
64a
D
D
64b

Fig. 65 *E. histolytica* trophozoite (A) in contact with a CV-1 cell, showing the uroid (U). Note the attraction of the microvilli (Mv) of the surrounding cultured cells for the uroid. x 7345

Fig. 66 Section through healthy BD-VI cells from a control monolayer culture. x 3510

65

66

Fig. 67 Part of cytoplasm of a healthy ED-VI cell from a control monolayer culture showing dense bodies (Db) resembling microbodies, mitochondria (M) and endoplasmic reticulum (ER). Note the fenestrated cristae (white arrows) in one of the mitochondria. x 51,790

Fig. 68 Section through part of cytoplasm of a healthy ED-VI cell illustrating endoplasmic reticulum (ER) and dense bodies (Db).

67

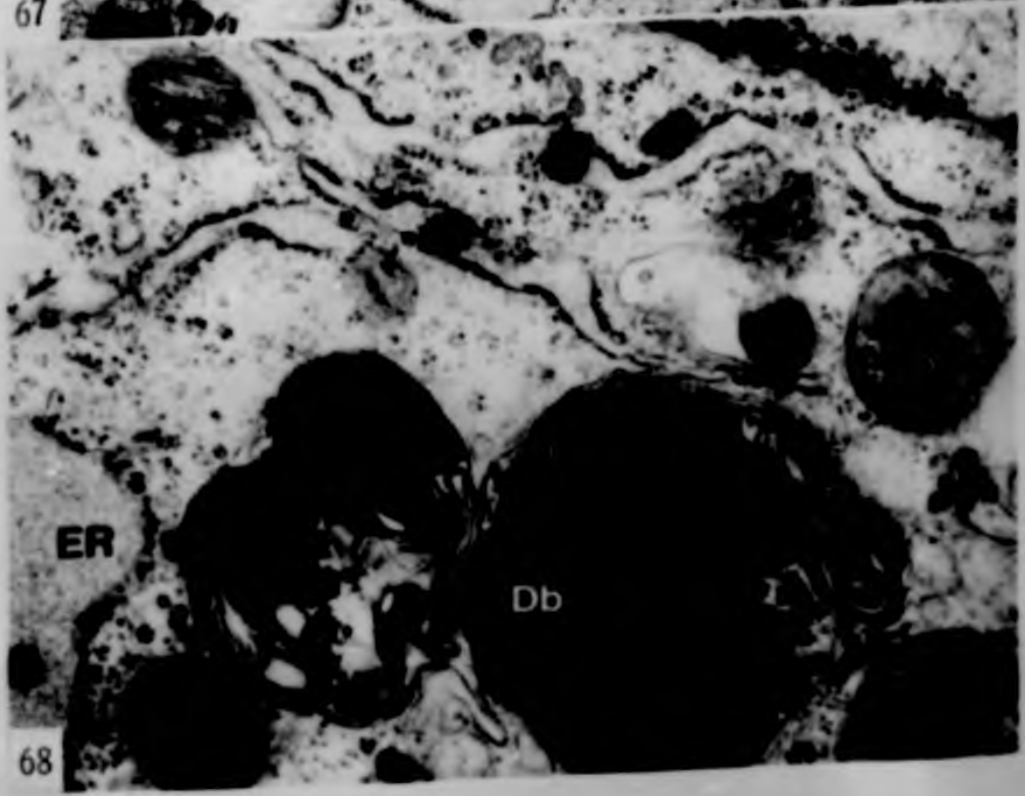

68

Fig. 69 Portion of cytoplasm of an affected BD-VI cell in contact with E. histolytica during the initial stage of interaction. Moderately swollen mitochondria showing peripherally placed and disintegrating cristae (arrowheads). The endoplasmic reticulum is not yet affected as its matrix is of normal density. x 34,460

Fig. 70 Initial stage of cell injury showing swollen mitochondria (M) with their membranes almost breaking up. The endoplasmic reticulum (ER) is not yet vesiculated. Hyperactivity of the Golgi elements (G) is evidenced by an increase in the number of vesicles. Condensation of chromatin (arrowheads) is seen to occur along the inner membrane of the nuclear envelope. x 21,540

69

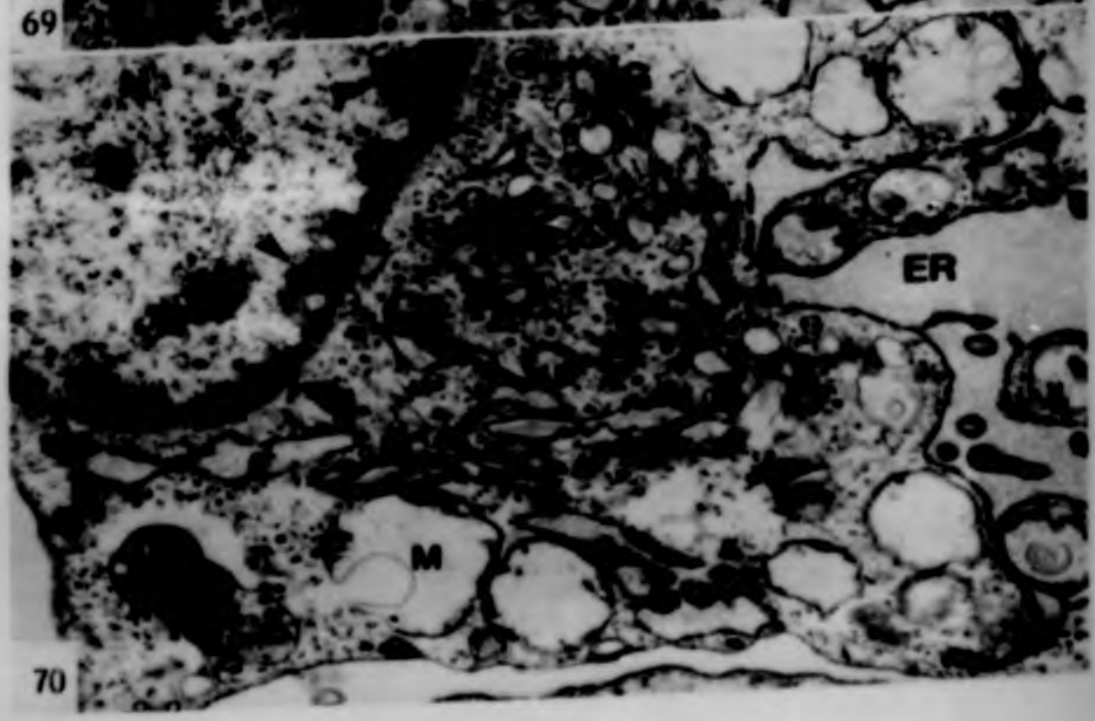

70

Fig. 71 Later stage of cell injury in BD-VI cell in contact with E. histolytica. Condensation of mitochondria (M) is evidenced by an increase in the density of the matrix and a reduction of mitochondrial size. Vesiculation of the cisternae of rough endoplasmic reticulum (ER) is observed. Most of the ribosomes (Ri) are still attached to the endoplasmic reticulum although some are seen in the cytoplasm. Cytoplasmic filaments (arrow) are present and may have arisen from dissolution of microtubules. Note the ballooning of the nuclear envelope (Ne). x 40,315

Fig. 72 Contact zone between an amoeba (A) and BD-VI cell showing a reduction in the density of the cytoplasmic matrix in the BD-VI cell. x 10,590

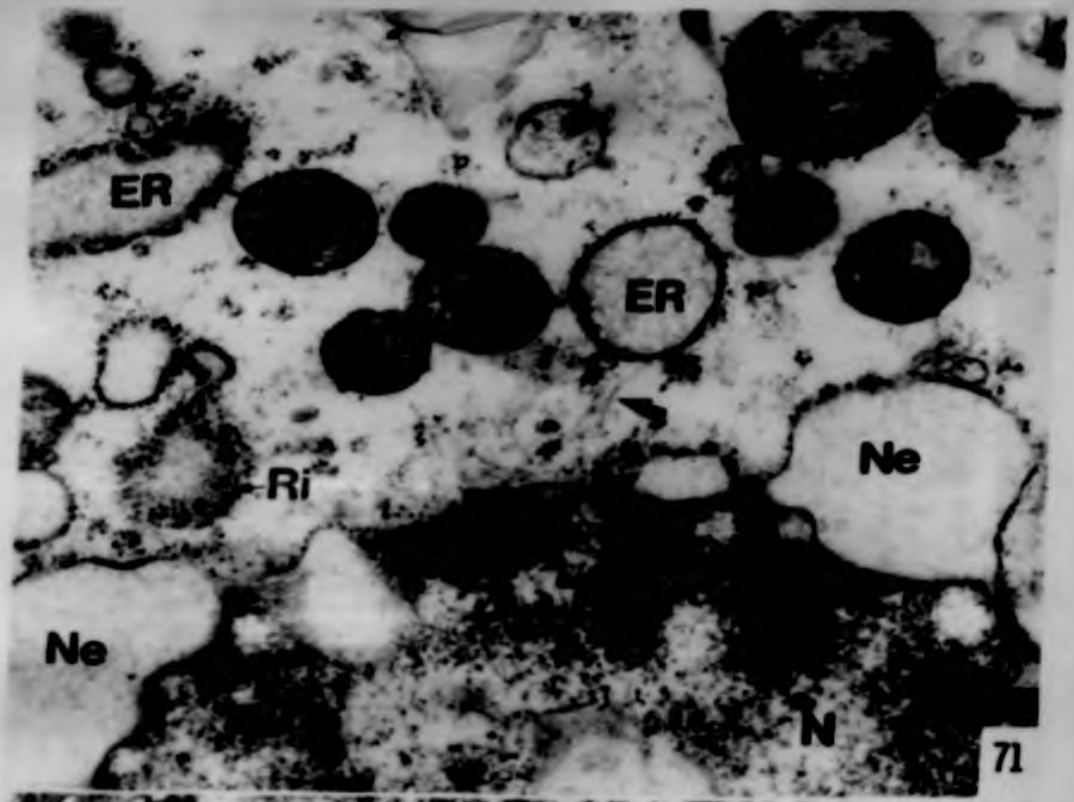

71

72

Fig. 73 Prior to lysis of cell in contact with E. histolytica (A) showing almost complete loss of cytoplasmic matrix. The vesiculated cisternae of the endoplasmic reticulum (ER) and the condensed mitochondria (arrow) still retain their shape. x 8360

Fig. 74 An affected BD-VI cell showing a breakdown in the cytoplasmic membrane (arrowheads). Note the almost complete loss of nuclear contents apart from the nucleolus (Nu). x 8775

Fig. 75 Section showing 2 lysed cells near the amoeba (A). The two nuclei (N) are seen to be distorted due to ballooning of the nuclear envelope. x 3343

73

74

75

Fig. 76a An amoeba (A) in contact with two BD-VI cells. x 5190

Fig. 76b Higher magnification of an area on the right hand side of Fig. 76a, showing organelle destruction within the BD-VI cell. x 13,085

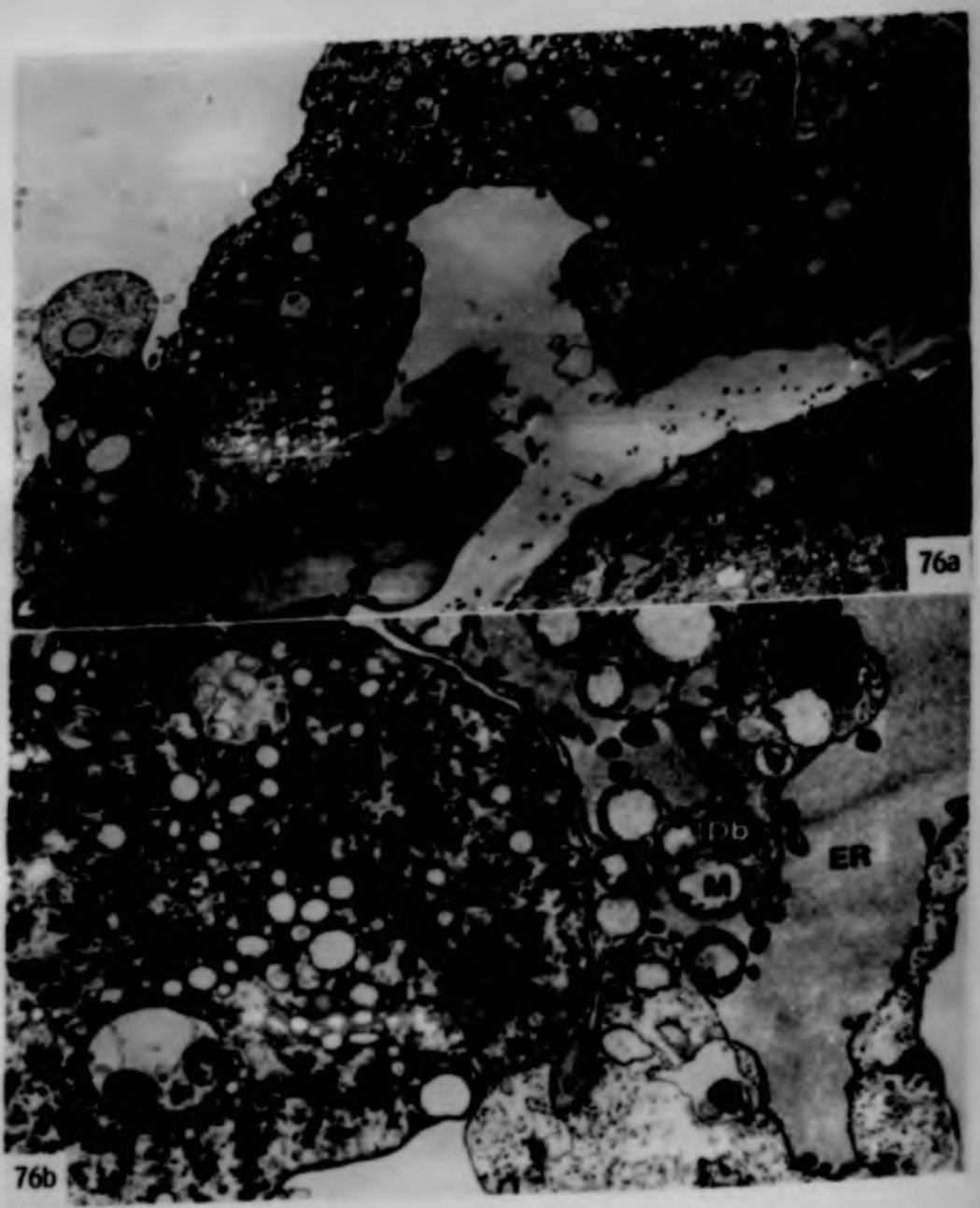
76a
IDb
M
ER
76b

Figs. 76a to 78a **Stages of amoebic phagocytosis :**

Fig. 76a Due to the active turnover of the amoebic plasmalemma, the cell plasma membrane shows marked infolding (arrows). x 13,400

Fig. 77a Contact zone between an amoeba and BD-VI cell; the membranes show fussiness and discontinuity (arrowhead). x 13,400

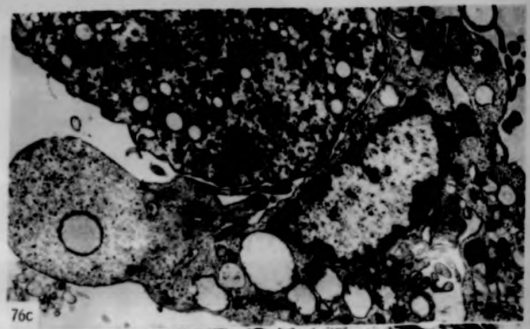

76c

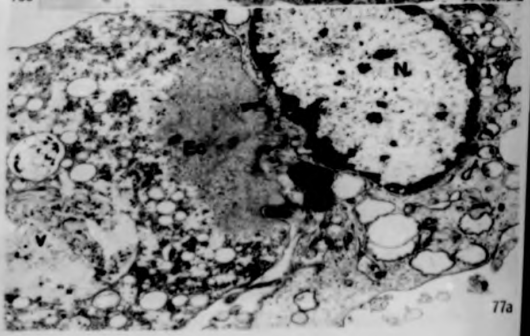

77a

Fig. 77b Higher magnification of the contact zone depicted in Fig. 77a; pieces of host cytoplasm (arrows) are drawn into the interior of the amoeba (A). Note the perichromatin granules (Pg) in the nucleus of BD-VI cell. x 34,200

Fig. 78a Phagocytotic channel (Pc) and bulb (Pb) of an amoeba. x 8460

77b

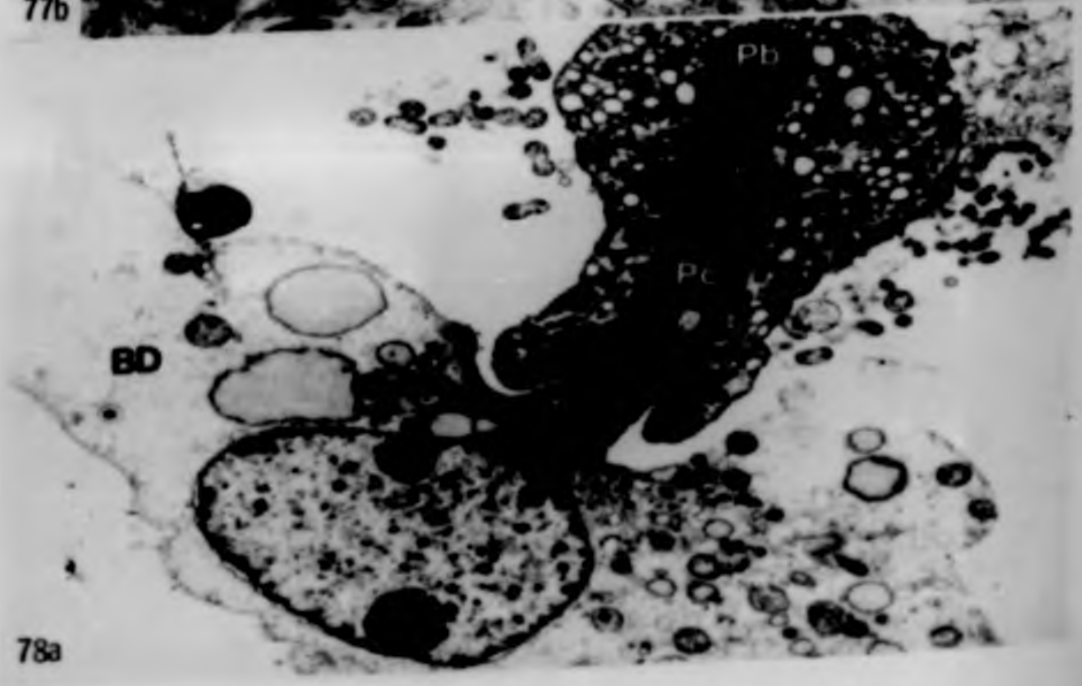

78a

Fig. 78b Higher magnification of the affected cell shown in Fig. 78a, showing the condensed mitochondria (M) and the vesiculated endoplasmic reticulum. x 52,750

Fig. 78a Higher magnification of the entrance of the phagocytotic channel shown in Fig. 78a, showing the tearing effect on the nucleus of the affected BM-VI cell. The nuclear pores (Np) can be observed. Note : cytoplasmic filaments (arrows) can be seen. x 40,190

78b

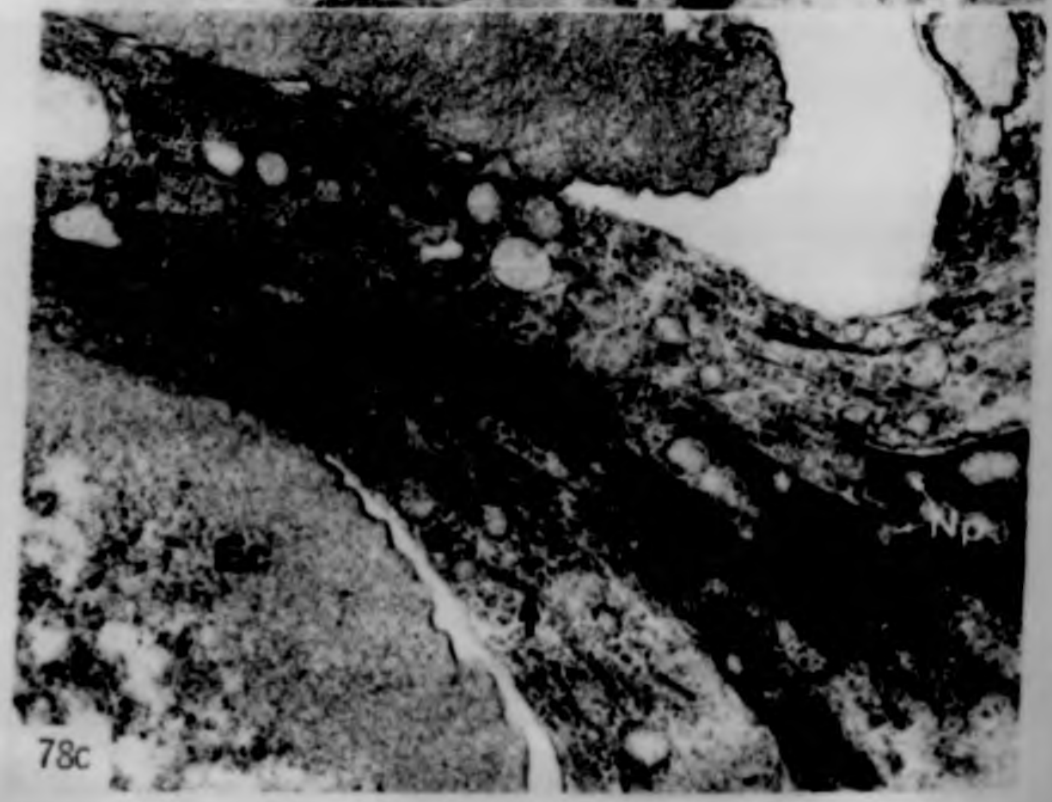

78c

Fig. 78d Higher magnification of the phagocytotic bulb shown in Fig. 78a illustrating small vesicles on the surface of the bulb. x 46,200

Fig. 79 A section of affected (Ie) and non-affected (Nie) cells in a lesion. Note the condensation of the chromatin (arrowheads) in the affected cell (Ie) in comparison with the nuclei of the non-affected cells (Nie). x 2200

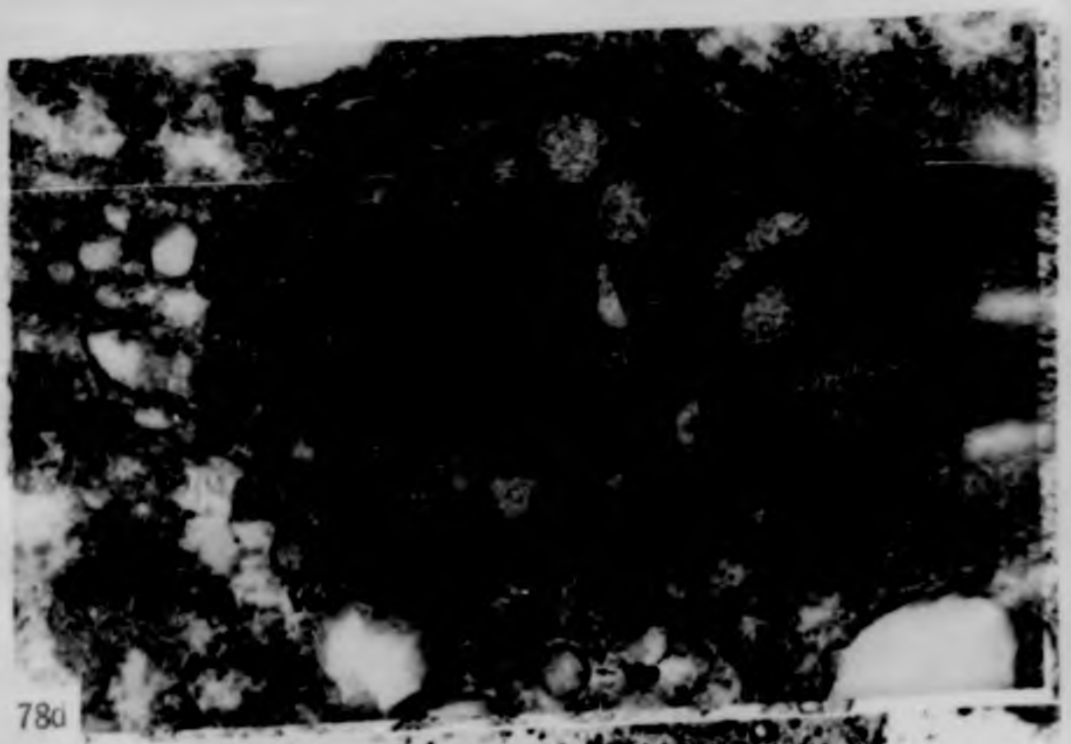

78a

79

Fig. 80 Scanning electron microscopy of BY13 cells from a control monolayer culture. Beneath area marked with arrow lies the nucleus. Fractures along the cell-junctions are artefacts induced by freeze-drying. x 620

Fig. 81 Scanning electron micrograph depicting details of the surface morphology of a rounded cell which is in the process of dividing. The surface is covered with small microvilli. x 5270

Fig. 82 A lateral view of amoeba in contact with the BY-13 cells. A fracture (arrow) along the cell-junctions induced by freeze-drying is easily seen. x 2540

Fig. 83 Higher magnification of the contact area between the amoeba (A) and the BY-13 cells shown in Fig. 82. The microvilli (Mv) surrounding the amoeba are seen to extend towards the parasite. x 6350

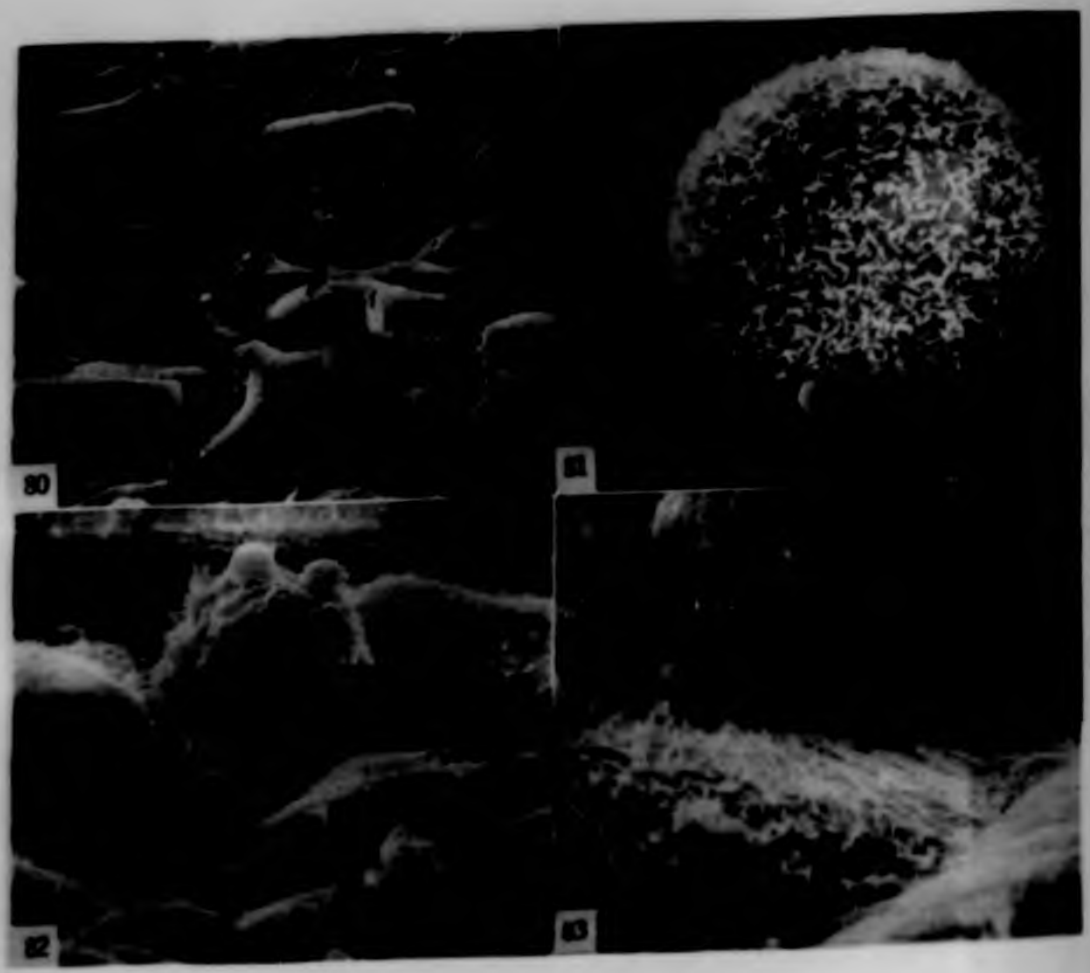
80
81
82
83

Fig. 84a A lateral view of amoeba (A) in contact with the HTLV cells. Early stage of infection. x 4420

Fig. 84b Higher magnification of Fig. 84a. The microvilli (Mv) near the amoeba are relatively longer than the ones further away from the trophozoite. Note that the elongated microvilli are not in contact with the amoebic surface membrane. x 17,000

Fig. 85 Here the cells surrounding the amoeba (A) in a later stage of cellular injury are rapidly destroyed. Fractures (arrows) along the cell-junctions are artefacts. x 1660

Fig. 86a The surface morphology of the affected cells (Ia) is rapidly altered. Here the microvilli are totally lost, and the surface is beginning to erode as evidenced by the appearance of microdots. The affected cells have also rounded up due to breakdown in cytoskeletal control. x 2040

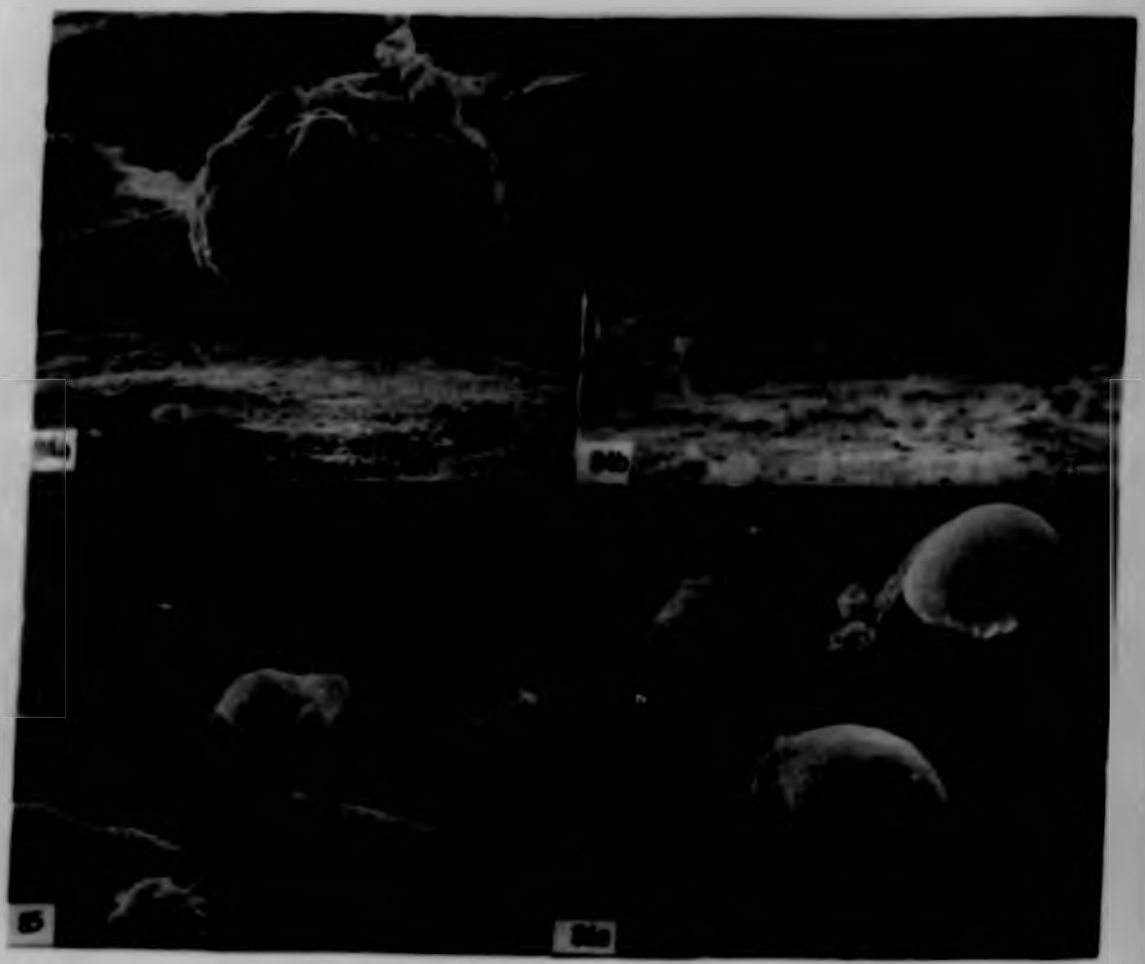

Fig. 86b Higher magnification of Fig. 86a showing a collection of cellular debris at the tail end of the uroid (U) of the amoeba (A). Erosion of the surface membrane (arrows) of the affected cell (Ia) is clearly seen. A filopodium (Fp) is shown emerging from the underside of the amoeba. x 5270

Fig. 87a E. histolytica trophozoite (A) burrowing between an affected cell and the supporting glass substrate. x 1530

Fig. 87b Higher magnification of the amoeba shown in Fig. 87a. The cellular debris (*) become agglutinated onto the surface of the affected cell and the uroid of the amoeba. x 8075

Fig. [illegible] E. histolytica trophozoite on an MF13 cell showing amoebic mucoid threads (Tm). x 11,475

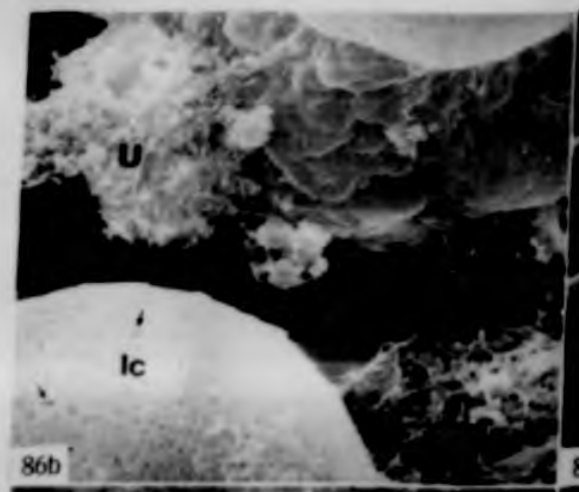

86b

87a

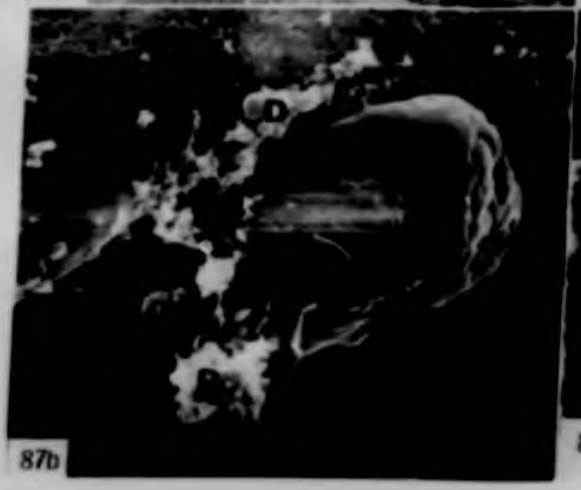

87b

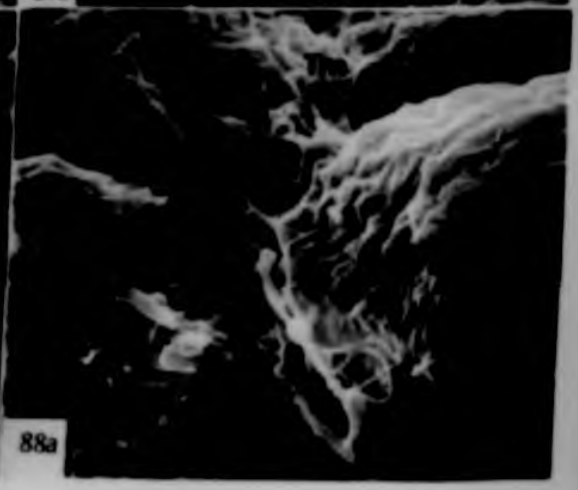

88a

Fig. 88b Scanning electron micrograph of RT1J cells grown on a nucleopore filter. The fractures (arrows) along cell-junctions are more extensive than those seen on glass-cultivated cells. x 1345

Fig. 88c E. histolytica trophozoite on a monolayer RT1J cells showing the fractures. Arrows illustrate pores of the nucleopore filter. Long mucoid threads (Th) are seen attached to the amoeba. x 3700

Fig. 88d Section of a RT1J cell on a millipore filter. Attachment onto the filter is enhanced by inserting cytoplasmic processes (arrows) from the underside of the cells into the pores (See Knight et al., 1975). x 9600

88b

88c

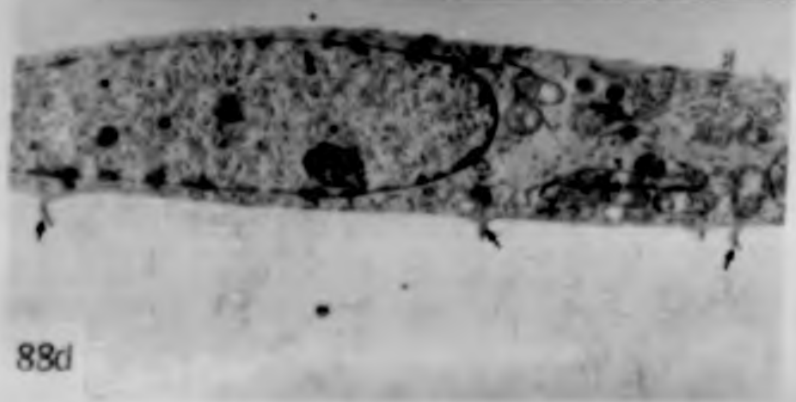

88d

Fig. 89 Acid phosphatase activity in culture RV13 monolayer. Gomori method using sodium β-glycerophosphate as a substrate. x 1000

Fig. 90 Localisation of acid phosphatase using β-glycerophosphate as a substrate in the RV13 cells in contact with the trophozoite (A). An early stage of interaction. x 2000

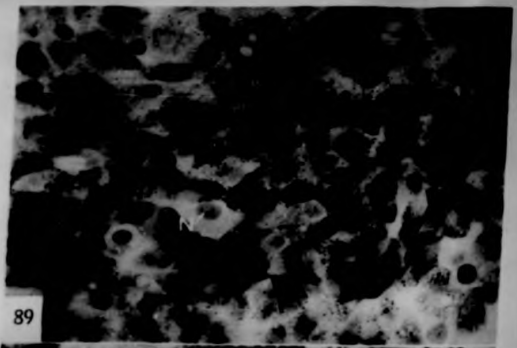

89

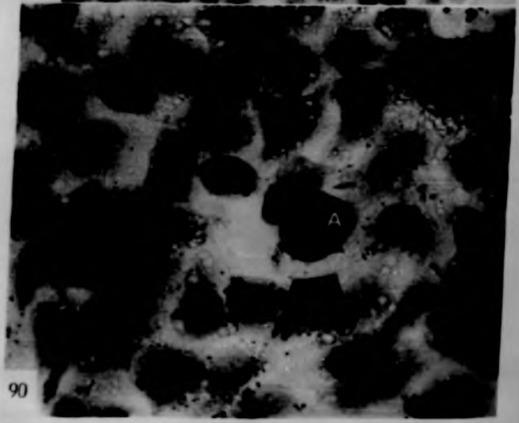

90

Figs. 91 & 92 Later stage of interaction between E. histolytica trophozoites (A) and RK13 cells. Acid phosphatase activity using β-glycerophosphate as substrate. In cells marked 1, there is a progressive enlargement of the lysosomes containing the reaction product. In cells marked 2, the staining is generally diffused; an indication that the lysosomes have disrupted. Note the amoebic phagocytotic channel in Fig. 92 (arrow). x 4000

91

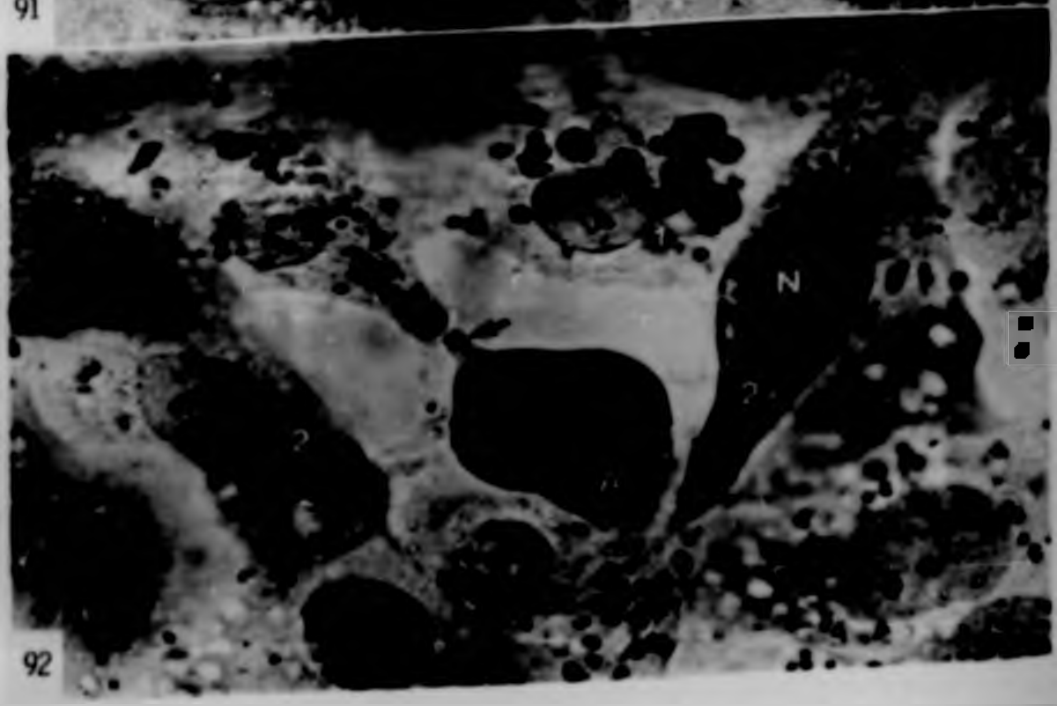

92

Figs. 93 & 94 Acid phosphatase activity in trophozoites of E. histolytica after being added to the RPMI monolayer culture. Incubated in the standard medium for acid phosphatase using Naphthol AS-BI phosphate as a substrate. The reaction product is confined to the cytoplasm (white arrow). None is seen in the pseudopodia (Ps). x 3750

Figs. 95a, b Electron micrographs of RPMI cells from a control monolayer culture showing localisation of acid phosphatase. The reaction product is present in the lysosomes (Arrow indicates artefactual staining.)

Fig. 95a Incubated in Barka and Anderson's medium using β-glycer phosphate as substrate. x 8130

Fig. 95b Incubated in Novikoff's medium using cytidine 5' monophosphate as substrate. x 22,260

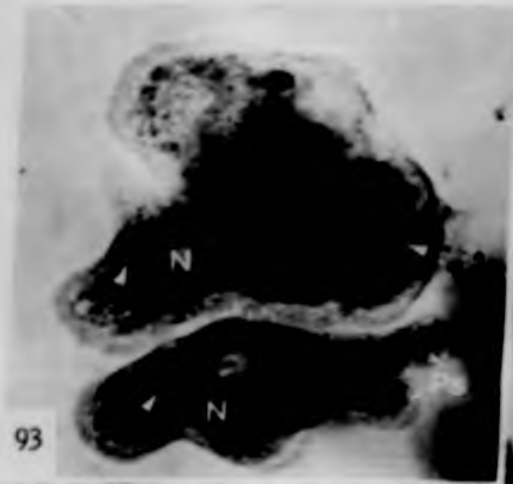

93

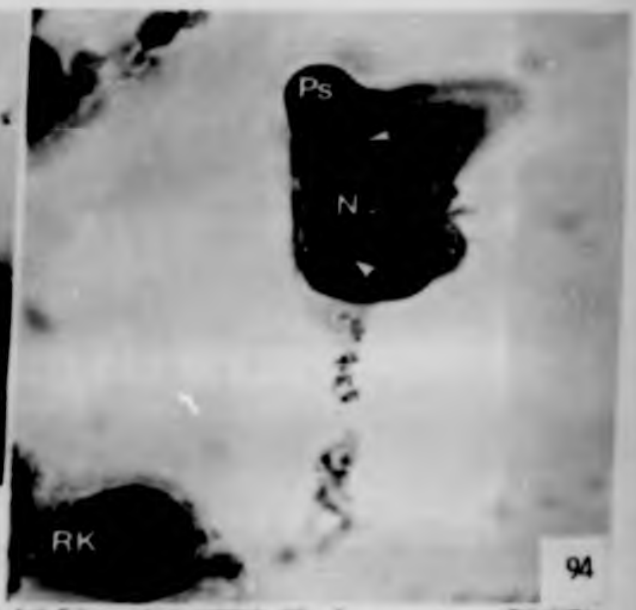

94

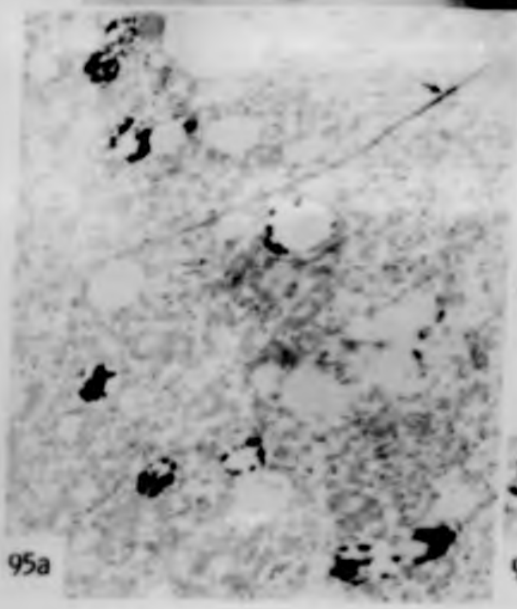

95a

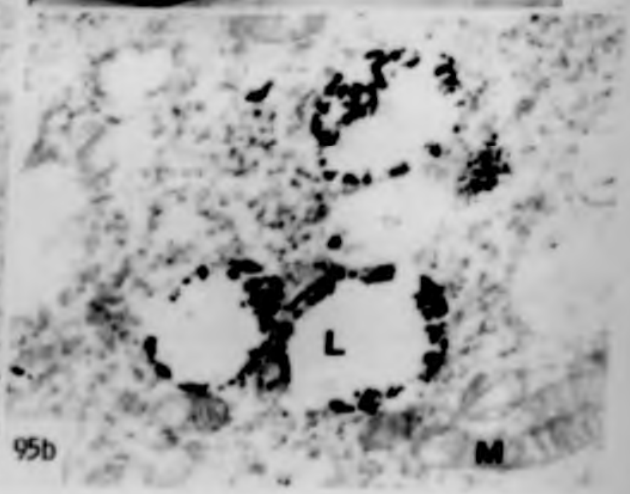

95b

Fig. 96 RK13 cell incubated in substrate-free medium for acid phosphatase localization. Reaction product (arrowhead) due to artefactual staining is evident. x 9040

Fig. 97 Initial stage of interaction between E. histolytica and RK13 cells. Acid phosphatase activity in RK13 cell. Novikoff's cytidene 5' monophosphate (CMP) medium. Slight mitochondrial swelling can be seen. The reaction product is confined to the lysosomes. x 9040

Fig. 98a, b Later stage of interaction. Acid phosphatase activity in RK13 cell. Novikoff's CMP medium. The lysosomes have disrupted releasing their contents, recognized by the reaction product, into the cytoplasm.

Fig. 98a x 24,770
Fig. 98b x 9040

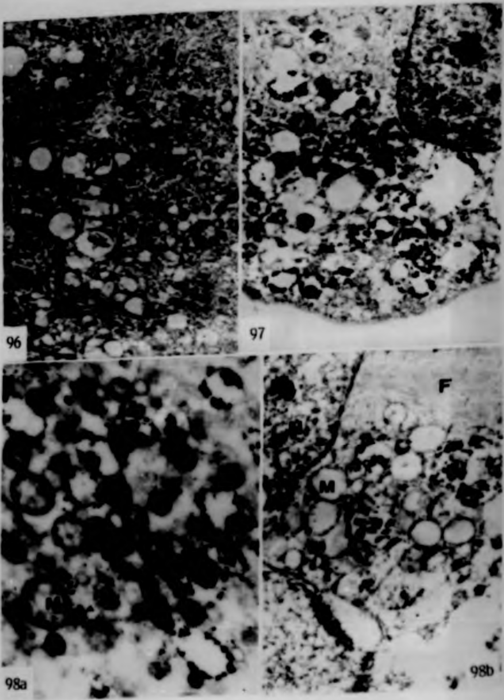
96
97
98a
M
F
98b

Fig. 98c After a prolonged period of interaction between E. histolytica and RW13 cells. Acid phosphatase activity in RW13 cells using Novikoff's CMP medium. General view of localization of reaction product in the intact lysosomes. x 6040

98c

Fig. 99 Higher magnification of Fig. 98c showing intact lysosomes. Note the swollen mitochondria.
x 20,520

Fig. 100 RK13 cell in contact with an amoeba (A). Later stage of interaction. Acid phosphatase activity using Novikoff's CMP medium. Most of the cell organelles have disaggregated except the lysosomes, in which the reaction product is clearly observed. x 7490

Figs. 101 & 102 Acid phosphatase activity using Barka and Ander Anderson's sodium β-glycerophosphate medium. Contents from lysed cells in contact with E. histolytica.

Fig. 101 Intact lysosomes (L) released from lysed cell.

Fig. 102 The lysosomes (L) being irregularly shaped, are ruptured and the reaction product is now confined to the lysosomal membranes.
x 7490

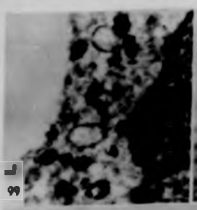

99

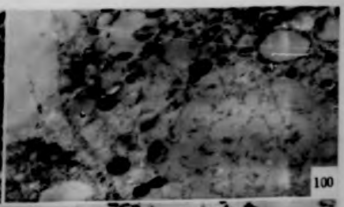

100

101

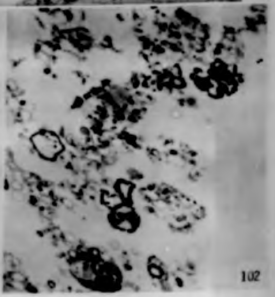

102

Figs. 103 & 104 Amoebae in contact with HV13 cells. In both micrographs, no change in the intensity of acid phosphatase activity in the amoebae is seen throughout the interaction. In Fig. 103, the reaction product in the amoebic vacuoles is probably ingested HV13 components. (Arrows indicate lysosomes).

Fig. 103 Incubated in Barka and Anderson's medium. x 3900

Fig. 104 Incubated in Novikoff's CMF medium x 6700

Fig. 105 Part of amoebic cytoplasm showing a surface vacuole (arrow) which gives an appearance suggestive of a 'surface-lysosome'. Reaction product for acid phosphatase is however absent in such a vacuole. Incubated in medium containing Na-β-glycerophosphate as substrate. x 21,000

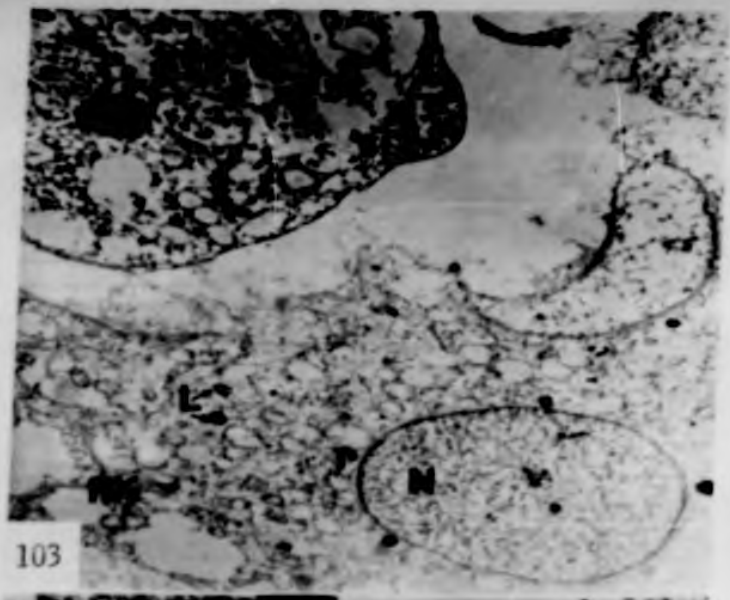

103

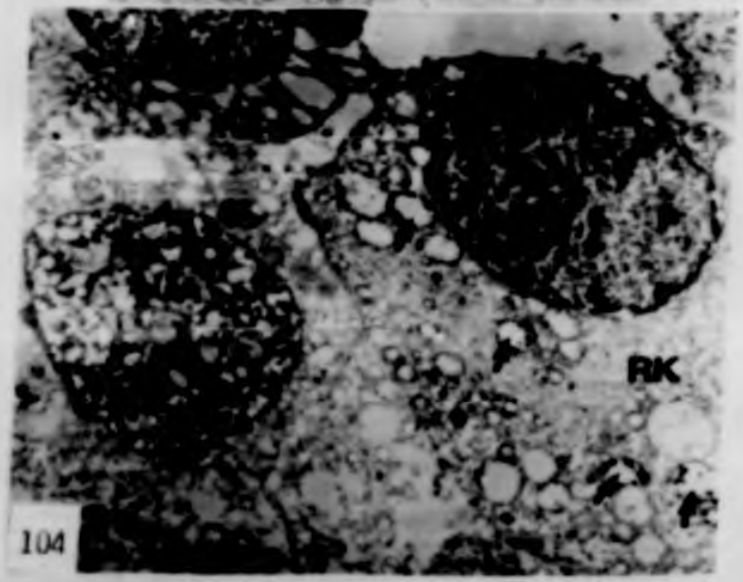

104

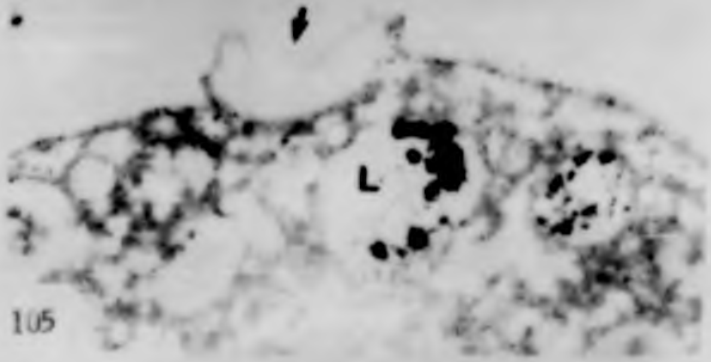

105

Fig. 106 Non-specific esterase activity in culture BY13 monolayer. α -naphthyl acetate method. x 375

Fig. 107 Appearance of lesions (arrows) in culture BY13 monolayer. 15 minutes after an addition of E. histolytica trophozoites. Non-specific esterase localisation using α -naphthyl acetate method. The cells surrounding the lesions show an enhancement of reaction product. x 375

Fig. 108 As for Fig. 107. 120 minutes after an addition of E. histolytica trophozoites. x 375

106

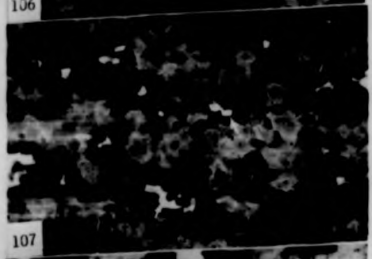

107

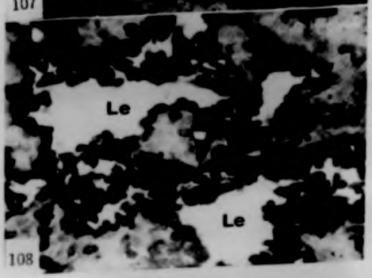

108

Fig. 109 Non-specific esterase activity using α -naphthyl acetate method. Initial stage of interaction between an amoeba (A) and RK13 cells showing an alteration in length of the microvilli (Mv) of RK13 cells. x 3750

Fig. 110 Non-specific esterase activity in culture RK13 monolayer using indoxylase method. Shows a pattern of discrete brown droplets (black arrows) interpreted as sites of lysosomes. The reaction product (white arrow) is also present in the cytoplasm. x 2475

109

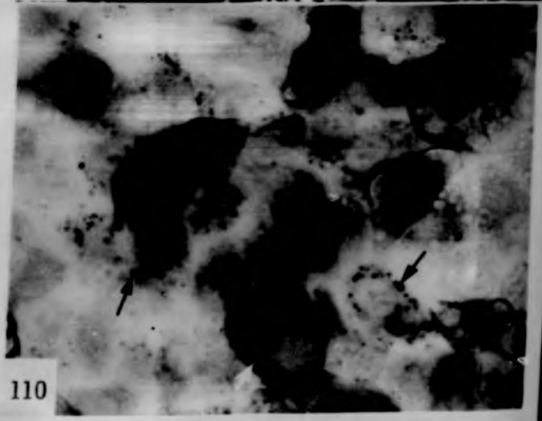

110

Fig. 111 Non-specific esterase activity in a giant multinucleate (M) cell using indoxyl ac method. Shows a definite pattern of brown droplets in the lysosomes (arrowheads). x 3750

Fig. 112 Aryl sulphatase activity in culture RV13 monolayer using Nasi-nitrocatechol sulphate method. x 1500

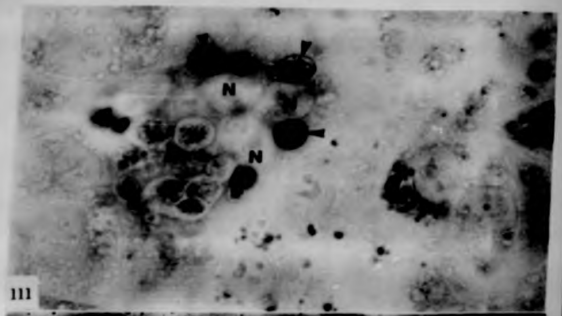

111

112

Fig. 113 Lysosomal staining for aryl sulphatase using lead-nitrocatechol sulphate method is seen to be more pronounced in giant multinucleate cells. x 1500

Fig. 114 E. histolytica trophozoites (A) in contact with HK13 cells. No change in the reaction product is seen in the HK13 cells. Reaction product in the amoebic nucleus (N) is probably an artefact. Aryl sulphatase localisation using lead-nitrocatechol sulphate method.

x 3750

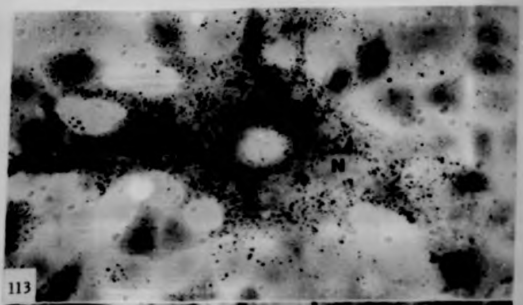

113

114

Fig. 115 Later stage of interaction between trophozoite (A) and HK13 cells. Aryl sulphatase activity using lead-nitrocatechol method. In cells marked 1, there is a progressive enlargement of the lysosomes containing the reaction product. In cells marked 2, no change in the reaction product is seen. x 3750

Figs. 116 & 117a Electron microscopic demonstration of aryl sulphatase activity in HK13 cells. The black deposits over the lysosome-like bodies mark the site of enzyme activity.

Fig. 116 x 6590

Fig. 117a x 18,640

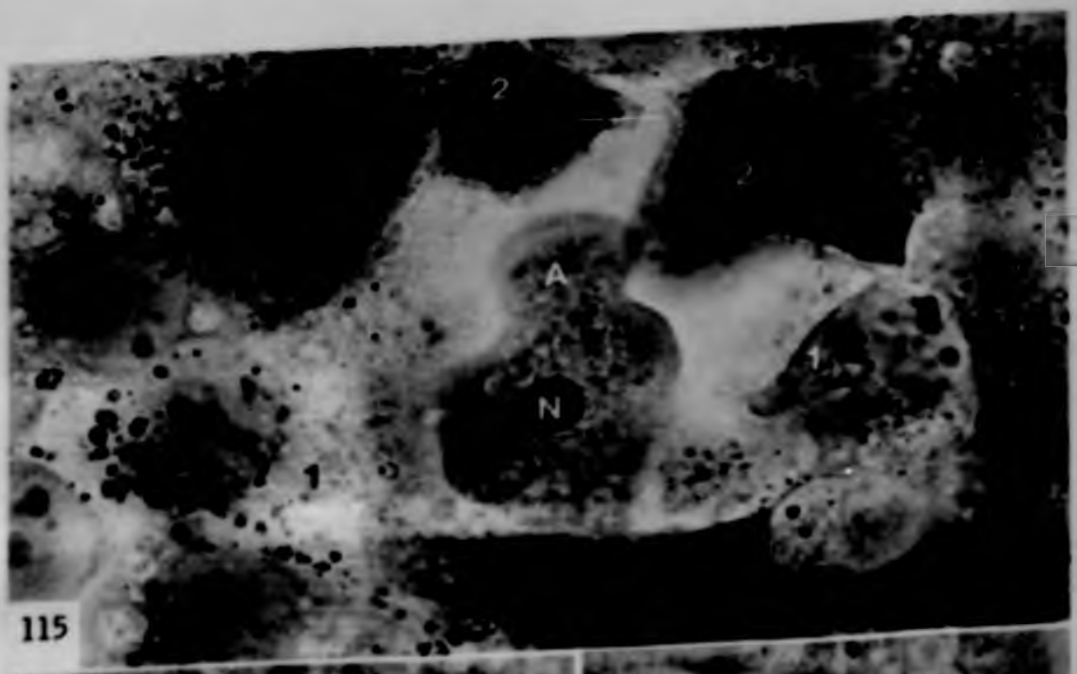

115

116

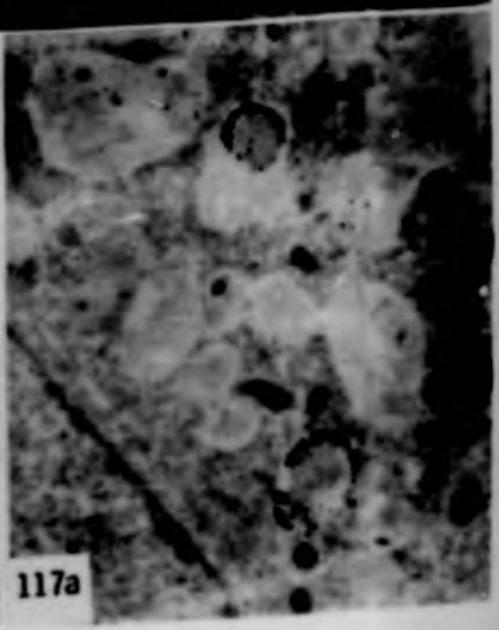

117a

Fig. 117b Another electron microscopic demonstration of aryl sulphatase activity in RV13 cell. Small precipitates (arrowheads) rohably represent primary lysosomes. x 17,490

Fig. 118 No staining is seen in RV13 cells incubated in a substrate-free medium for aryl sulphatase localisation. x 11,660

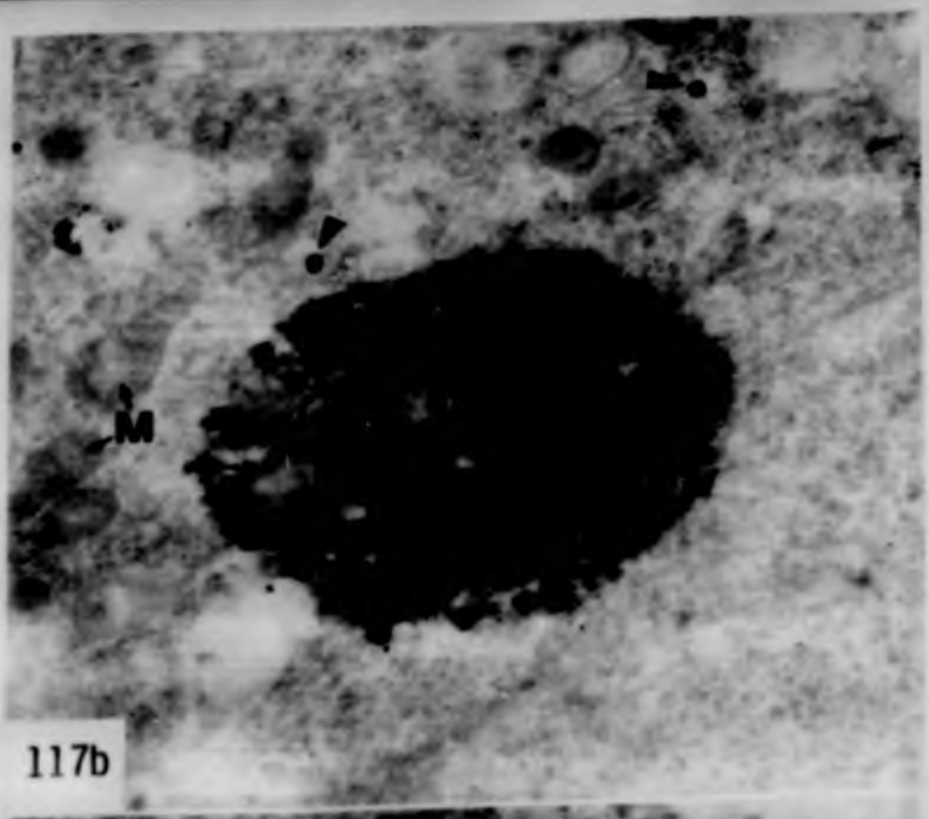

117b

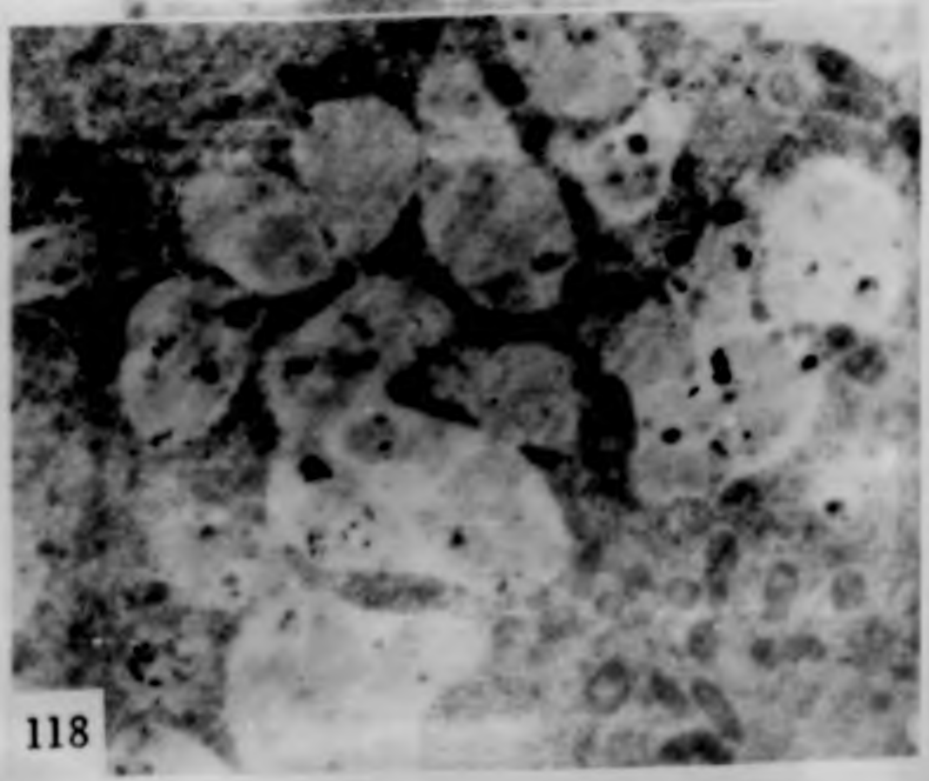

118

Figs. 119 & 120 Electron microscopic demonstration of aryl sulphatase activity in E. histolytica trophozoites.

Fig. 119 No staining is seen in the amoebic nucleus and its nuclear inclusions (Ni). x 8110

Fig. 120 Black deposits are present in the vacuoles. The reaction product is confined to the vacuolar contents, which are probably cellular debris. x 8110

Fig. 121 Initial stage of interaction between E. histolytica and HT13 cells. Aryl sulphatase activity in HT13 cell. Black deposits are confined to the vacuoles. Note mitochondrial swelling. x 8110

Fig. 122 Later stage of interaction. The [illegible], in the affected HT13 cell, containing the reaction product for aryl sulphatase remain intact while other organelles such as mitochondria and endoplasmic reticulum are already swollen. x 22,250

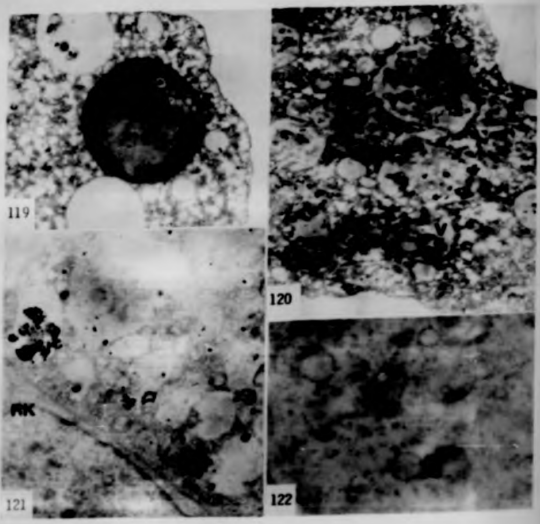
119
120
121
122

Fig. 123 *E. histolytica* (A) penetrating between the HK13 cells. Note the mitochondrial (M) swelling in the affected cells (Ic). x 7225

Figs. 124 & 125 Localisation of β-glucuronidase in HK13 cells in contact with the trophozoite.

Fig. 124 Initial stage of infection. No change in the reaction product in the affected cells although the nuclei are slightly condensed. x 1410

Fig. 125 Later stage of infection. In cells marked 1, the reaction product is grossly enhanced whereas the β-glucuronidase activity in cells marked 2 is moderately enhanced. x 1410

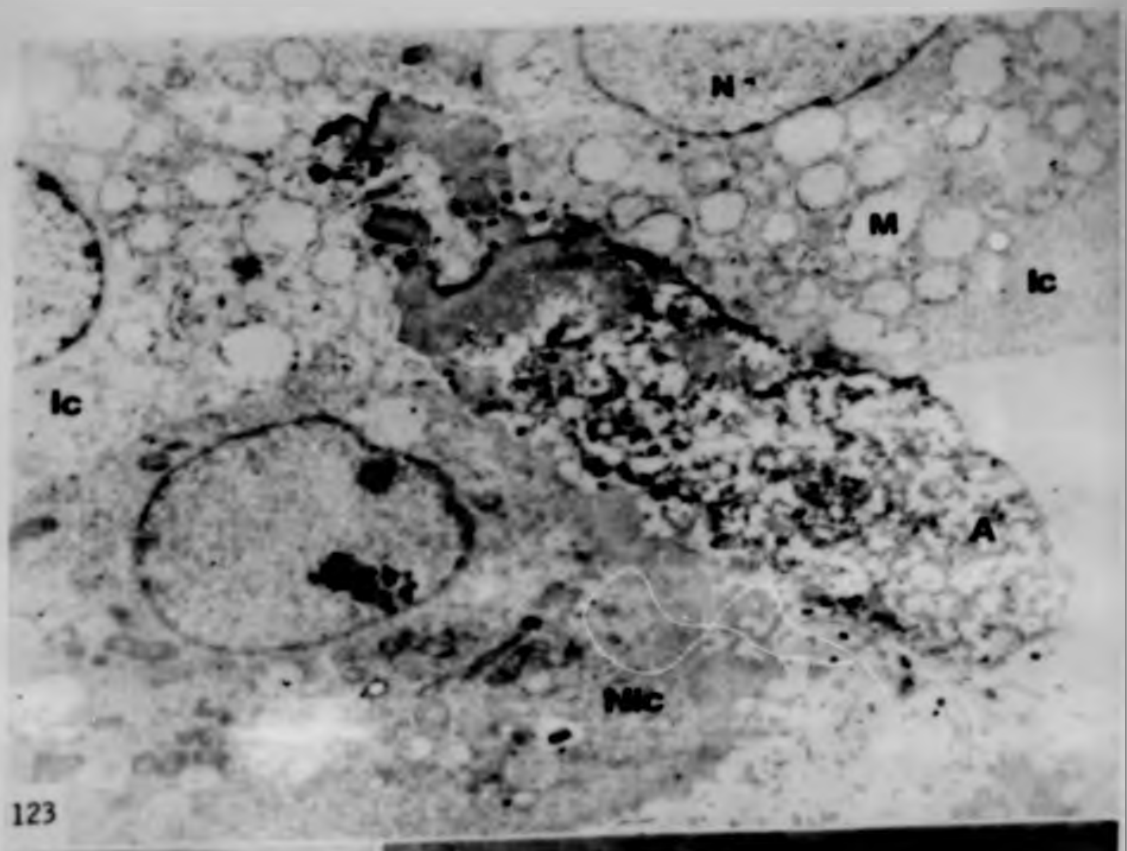

123

124

125

Fig. 126 Section of mouse kidney showing β-galactosidase activity in the tubules. x 1100

Fig. 127 RY13 cell destruction by E. histolytica trophozoite. Reaction product for β-galactosidase activity is present in both the RY13 cells and the amoeba (A). x 1840

Figs. 128a, b Sections of mouse kidney. Light microscopic demonstration of alkaline phosphatase activity. Reaction product is seen around the intima of blood vessels.

Fig. 128a Incubated using Na-β-glycerophosphate as a substrate. x 275

Fig. 128b Incubated using naphthol AS-B1 phosphate as a substrate. x 275

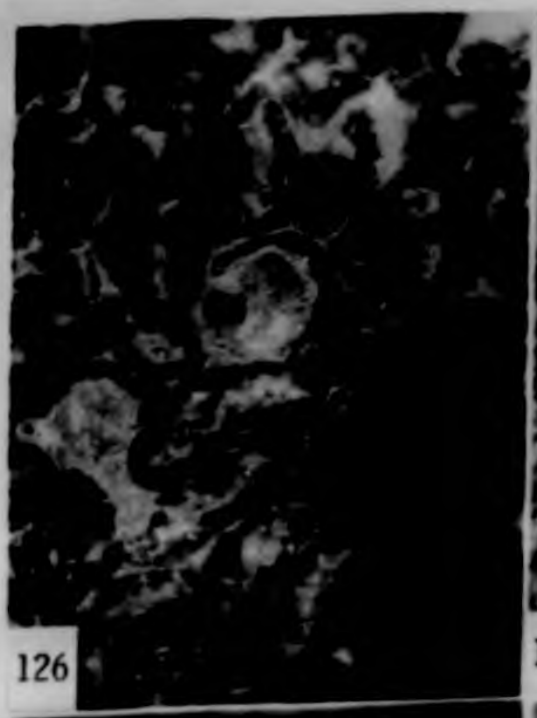

126

127

128a

128b

Fig. 129 Electron micrograph of BT13 cell. Incubated in medium demonstrating alkaline phosphatase using Na-β-glycerophosphate as a substrate. The reaction product (arrows) is present at places along the cell-junctions. x 8400

Fig. 130 Section of mouse kidney showing Mg-activated ATPase activity in the glomeruli (Gl), brush border and basement membrane of the tubules (T). x 900

Fig. 131 Light microscopic demonstration of Mg-activated ATPase activity in BT13 cells. Black deposits are confined to the cell junctions. x 900

Fig. 132 Reaction product for Mg-activated ATPase activity is absent in E. histolytica trophozoites. x 900

129

130

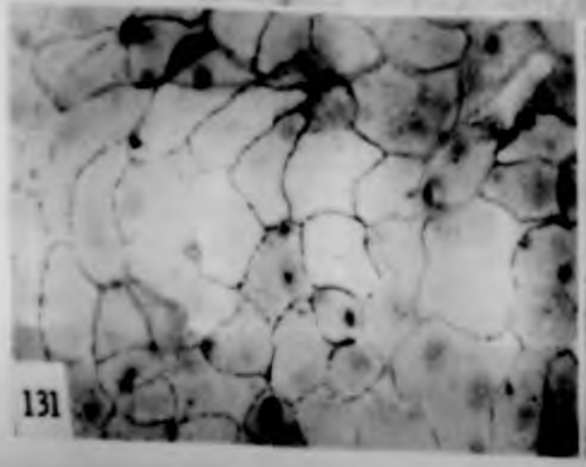

131

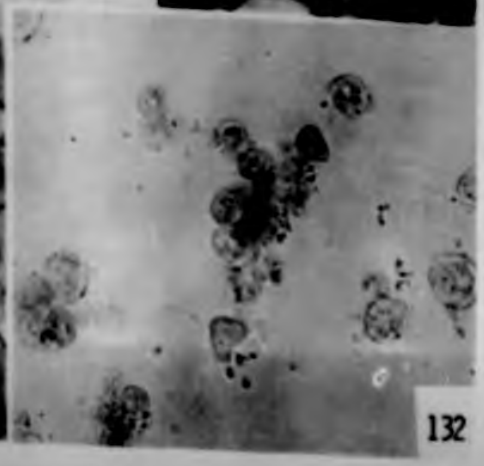

132

Figs. 133 to 135 *E. histolytica* trophozoites in contact with RK13 cells. Light microscopic demonstration of Mg-activated ATPase activity.

Fig. 133 Progressive infection leads to a diffuse pattern of reaction product among the cells surrounding the amoeba (A). x 3750

Fig. 134 Late stage of infection. Mg-activated ATPase activity on plasma membranes of affected cells becoming more intense. The amoebic mucoid threads (Th) are noticeable. x 3750

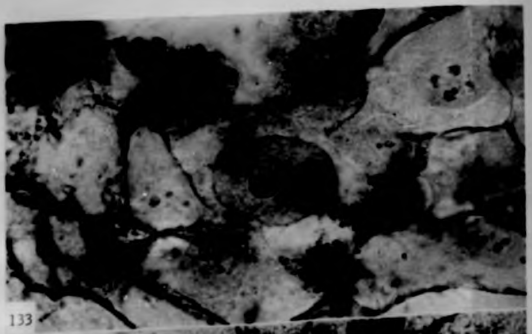

133

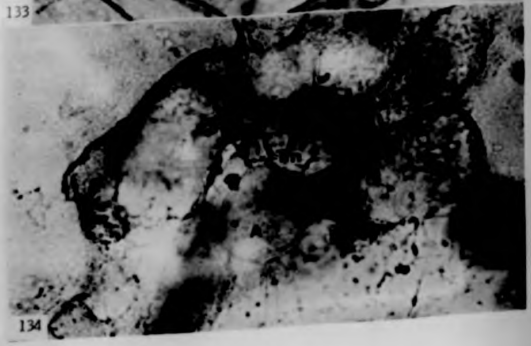

134

Fig. 135 A later stage in RK13 cell destruction. Reaction product for Mg-activated ATPase is now very pronounced on amoebic plasmalemma (P). The black deposits are also seen on the plasma membrane of the affected cells (black arrows). x 3705

Figs. 136a, b Electron microscopic demonstration of Mg-activated ATPase activity in RK13 cells.

Fig. 136a Black deposits are present in the cell-junctions. x 3600

Fig. 136b The reaction product delineates clearly the complex system of interdigitating folds. Reaction product is faintly present in the mitochondria (arrow). x 6400

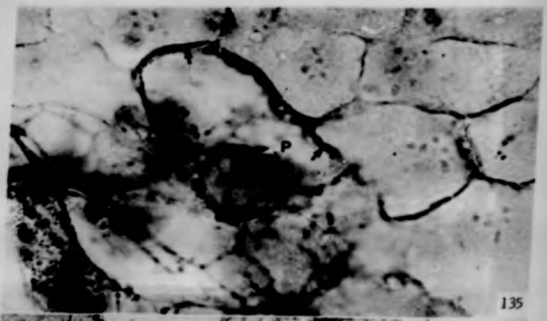

135

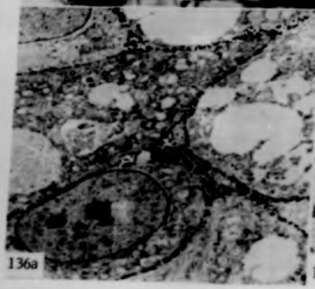

136a

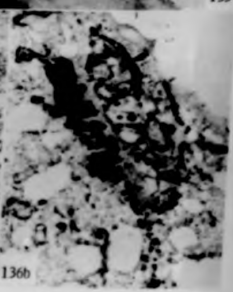

136b

Fig. 137 NK13 cells incubated in substrate-free medium for Mg-activated ATPase localisation. Reaction product (arrows) on the intercellular boundaries is evident here. x 11,290

Fig. 138 Early stage of NK13 cells destruction by E. histolytica trophozoite (A). The plasma membrane of the infected cells is almost completely depleted of reaction product. x 3500

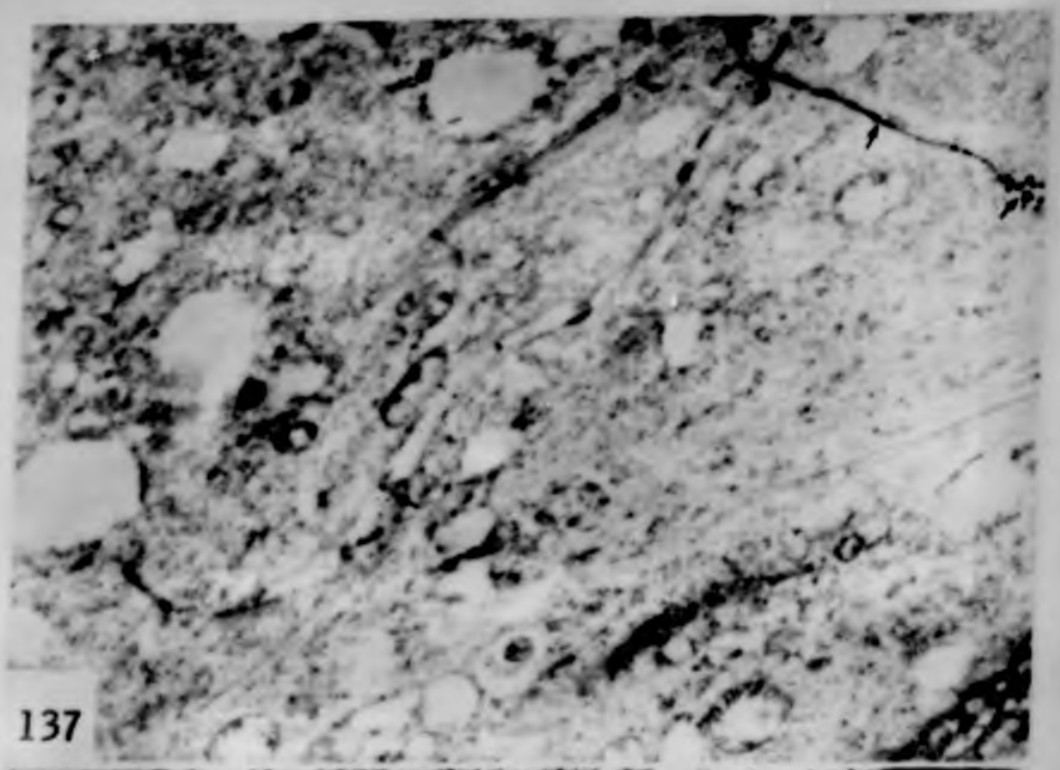

137

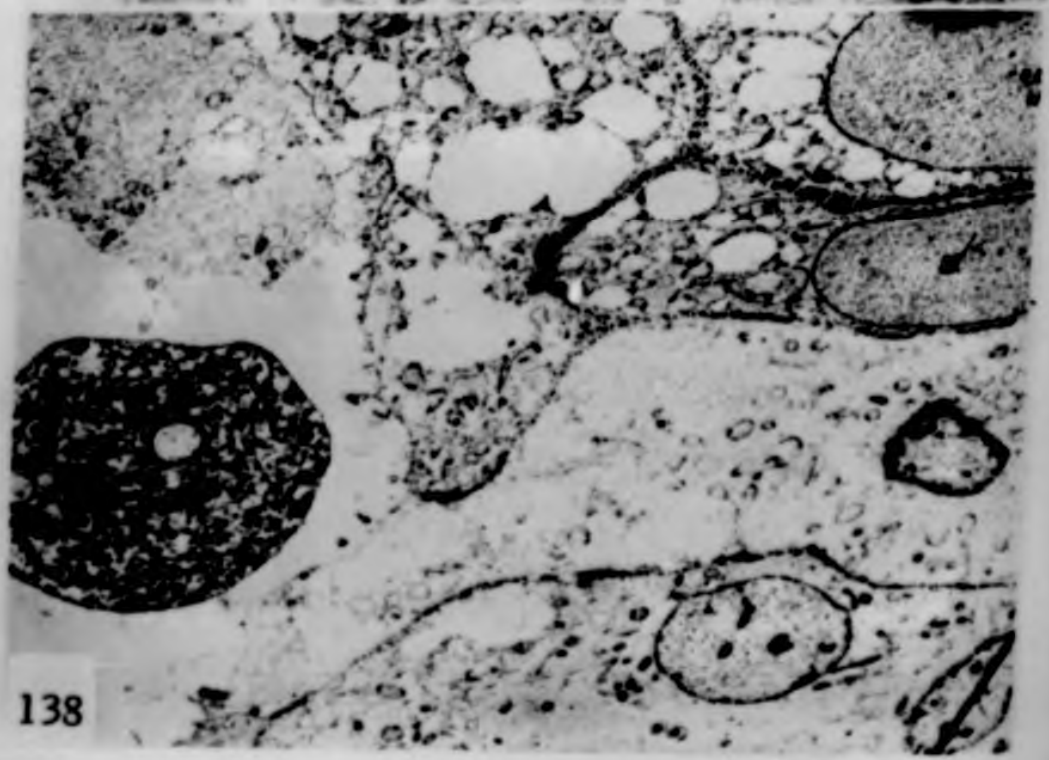

138

Fig. 139 Later stage of cell destruction. A significant increase in the intensity of the reaction product for Mg-activated ATPase on plasma membrane (arrows) of infected cells. x 3300

Fig. 140 A section of a whole amoeba (A) among KB13 cells showing the protrusion of mucoid threads (Tm) from the uroid (U). x 3300

Fig. 141 Higher magnification of the uroid shown in Fig. 140. Particulate matter is seen to enter the uroid (black arrow). No reaction product for Mg-activated ATPase is yet present in this region. x 21,060

Fig. 142 At a later stage of cell destruction, reaction product for Mg-activated ATPase is present at the amoebic uroid (U). x 5040

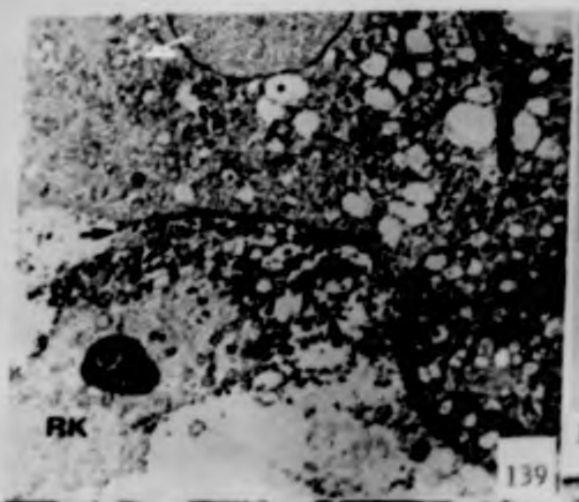

139

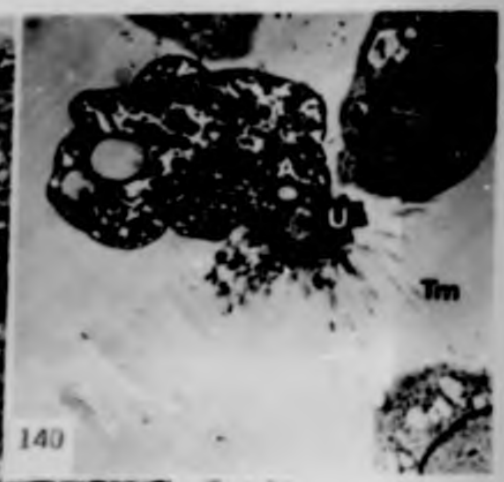

140

141

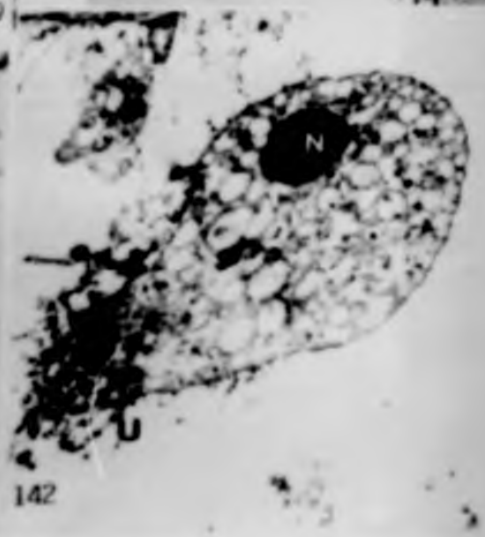

142

Fig. 143 A section of a trophozoite in a lesion showing an uptake of fluid droplets through the ureid (U) by pinocytosis (arrow). Incubated in the medium for demonstrating Mg-activated ATPase.
x 5940

143

Figs. 144a, b
145 a, b

High magnification of the uroid of E. histolytica showing an uptake of cellular debris from lysed RK13 cells. Black deposits are the reaction product for Mg-activated ATPase.

Fig. 144a Uptake by phagocytosis (arrow) x 13,480

Fig. 145a Uptake by pinocytosis leading to a small vesicular-like bulb (arrow). x 24,490

Fig. 144b x 8945

Fig. 145b x 26,340

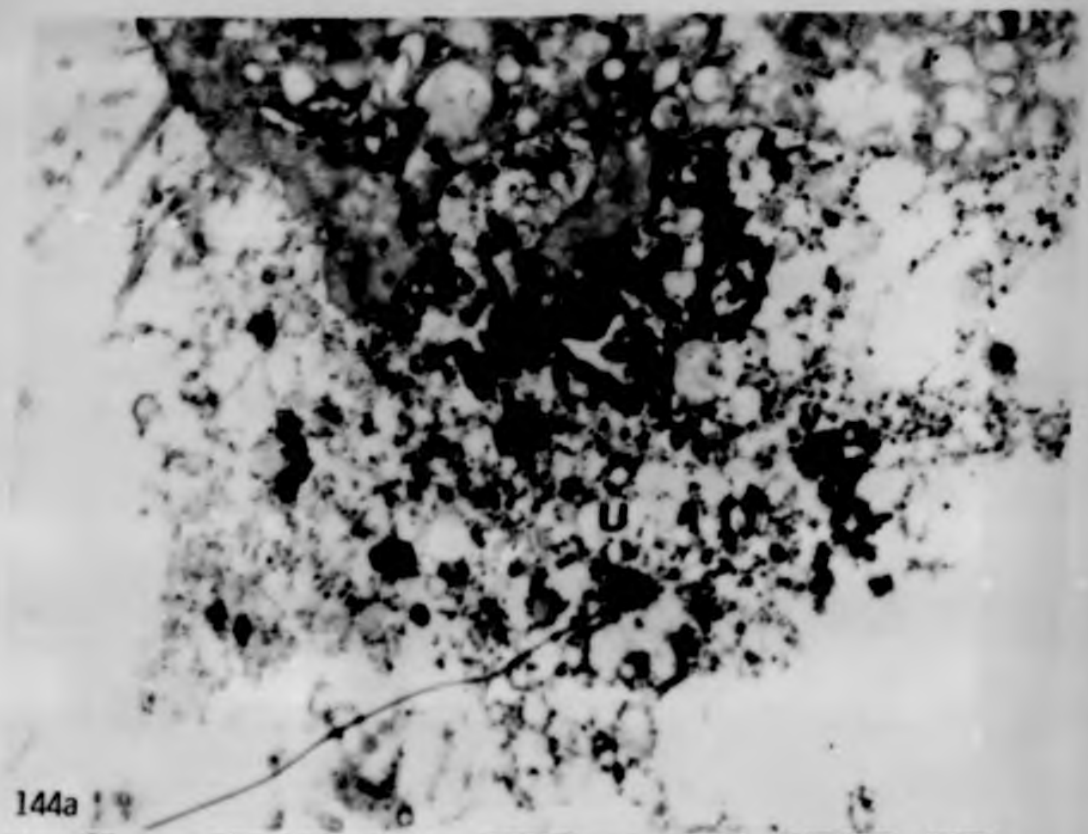

144a

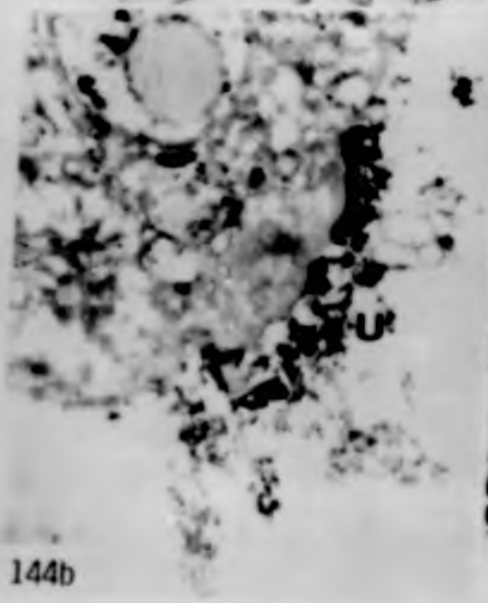

144b

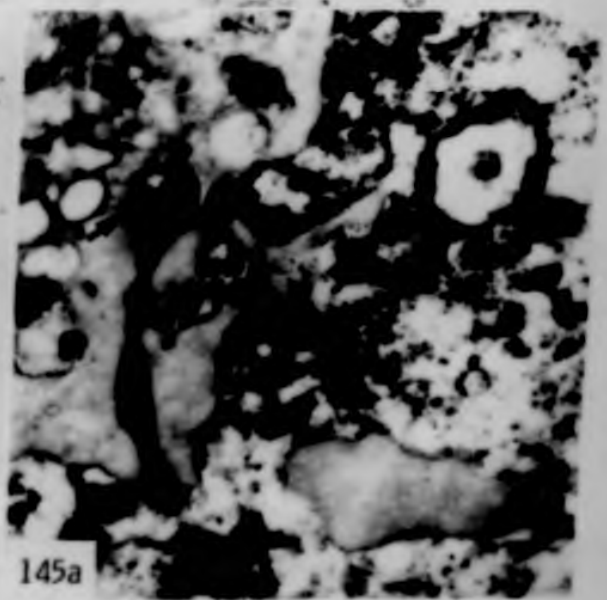

145a

Fig. 145b Uptake by pinocytosis (Pi) leading to a small vesicular-like bulb.

Fig. 146 Part of an amoeba showing the reaction products for Mg-activated ATPase in a vacuole (V). x 26,340

Fig. 147 Part of an amoeba revealing numerous projections or filopodia (Fp). x 9620

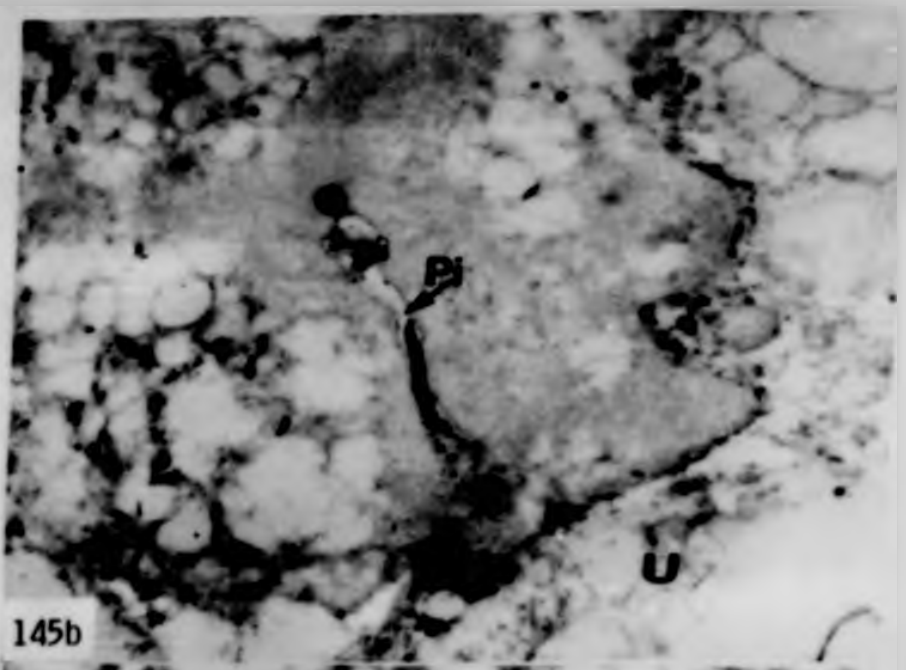

145b

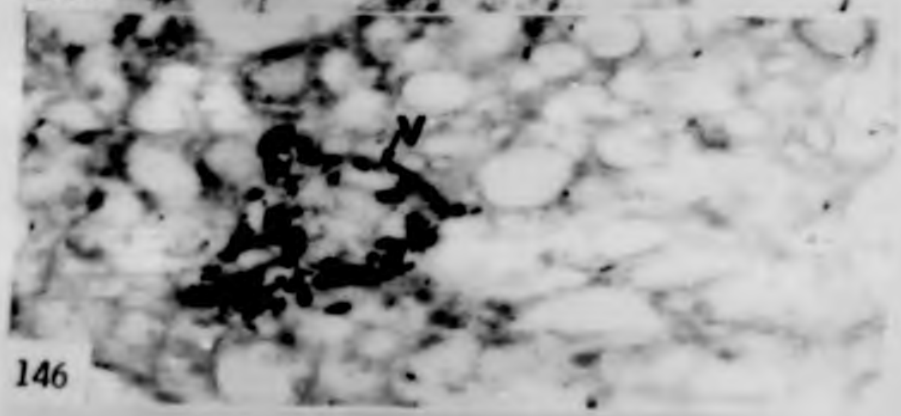

146

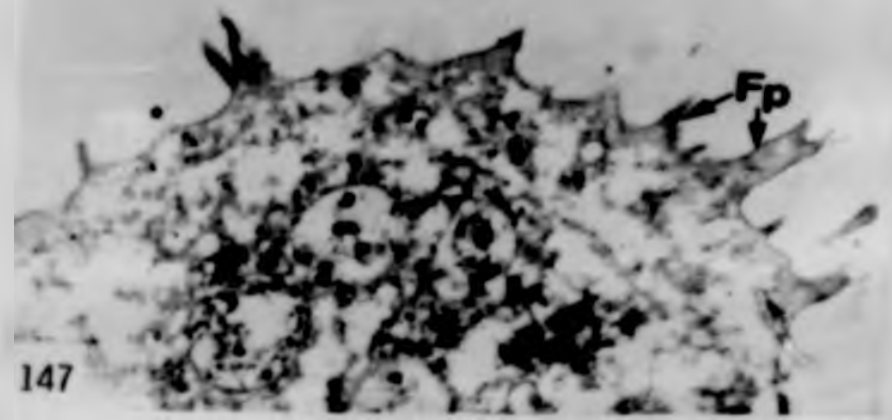

147

Fig. 148 Section of mouse kidney showing Ca-activated ATPase activity in the glomeruli (Gl), brush border and basement membrane of the tubules. x 550

Figs. 149 & 150 E. histolytica trophozoites in contact with BHK cells. Light microscopic demonstration of Ca-activated ATPase activity.

Fig. 149 Staining (arrows) is more pronounced in areas where cells are in contact with the amoeba. x 1820

Fig. 150 The reaction product is seen in the amoebic vacuoles (arrows). x 1820

Fig. 151 Section of mouse kidney showing K-dependent nitrophenyl phosphatase activity. x 550

148

149

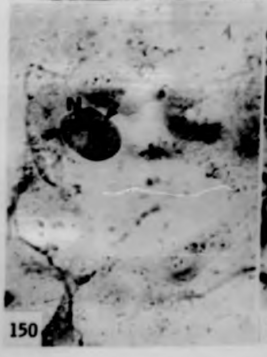

150

151

Fig. 152 As for Fig. 151, except that ouabain was added to the incubation medium. x 450

Fig. 153 Light microscopic demonstration of K-dependent nitrophenyl phosphatase activity in EFlj cells. Black deposits are confined to the intercellular boundaries (arrows). x 3750

Fig. 154 Light microscopic demonstration of TPPase in EFlj cells. Arrows mark the sites of golgi bodies. x 3750


152

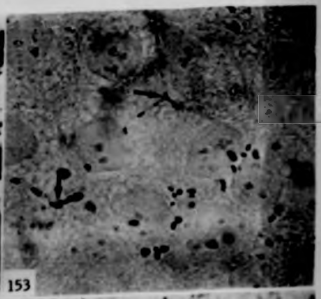
153

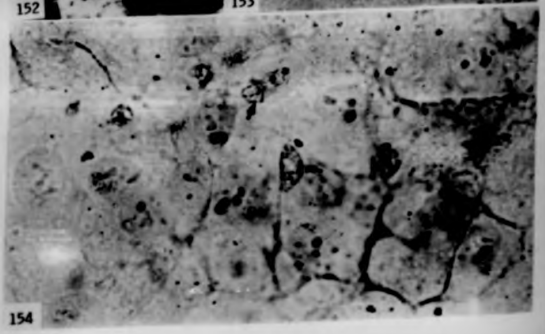
154

Fig. 155 Reaction product for TPPase is also present in the intercellular boundaries of the BK13 cells. x 1200

Fig. 156 Reaction product is also seen in the vacuoles of BK13 cells, after incubation in presence of TPP. x 3000

Fig. 157 Electron microscopic demonstration of TPPase activity in BK13 cells. 4% formaldehyde fixation for 30 minutes. Black deposits are seen in cell junctions (P) and vacuolar-like structures (arrows). x 8400

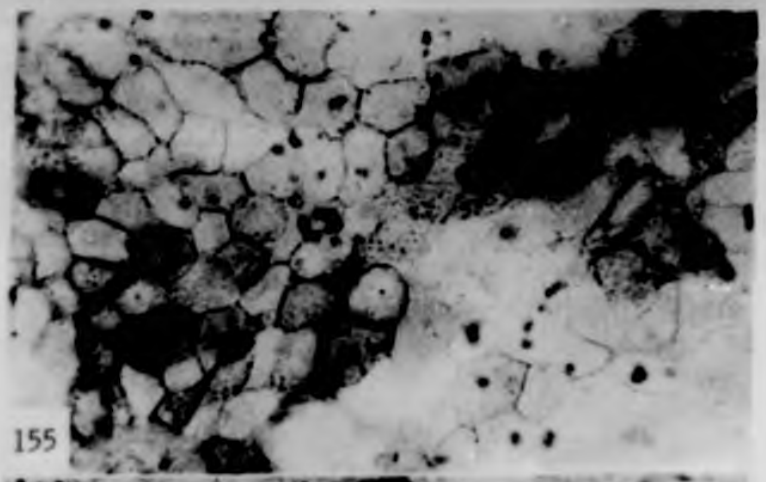

155

156

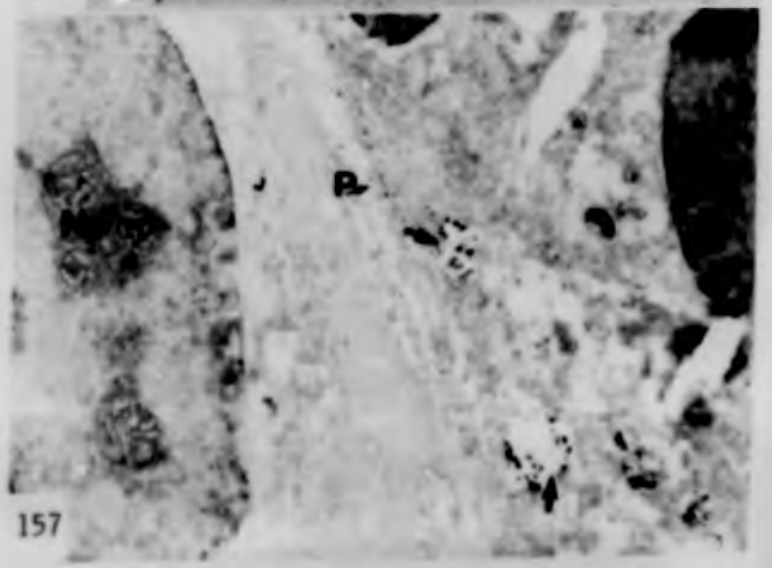

157

Fig. 158 No staining is seen in RF13 cells incubated in a substrate-free medium for TPPase localization.
x 1200

Fig. 159 Initial stage of interaction between *E. histolytica* and RF13 cells. Incubated in presence of TPP. Microvilli (Mv) of affected cells are seen to extend towards the amoeba (A).
x 3750

Fig. 160 Reaction product for inosine diphosphatase (IDPase) activity in vacuoles of RF13 cell.
x 3750

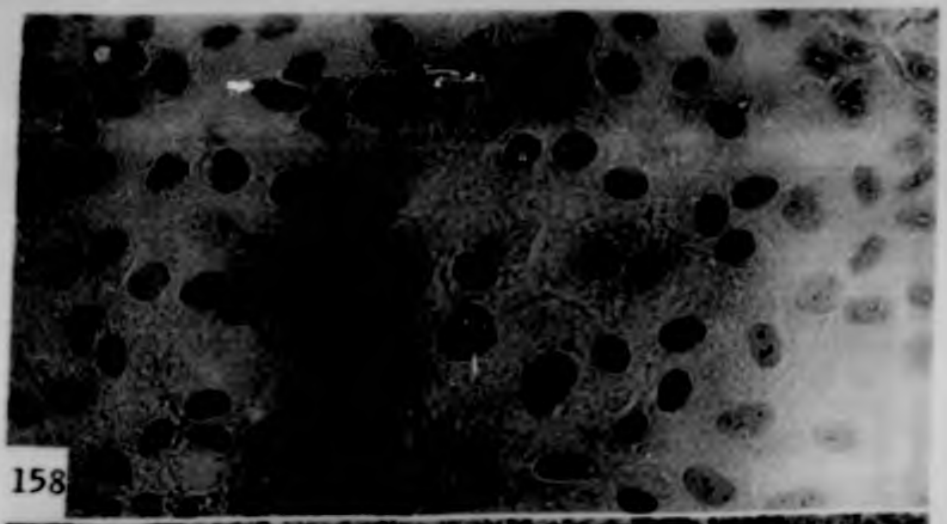

158

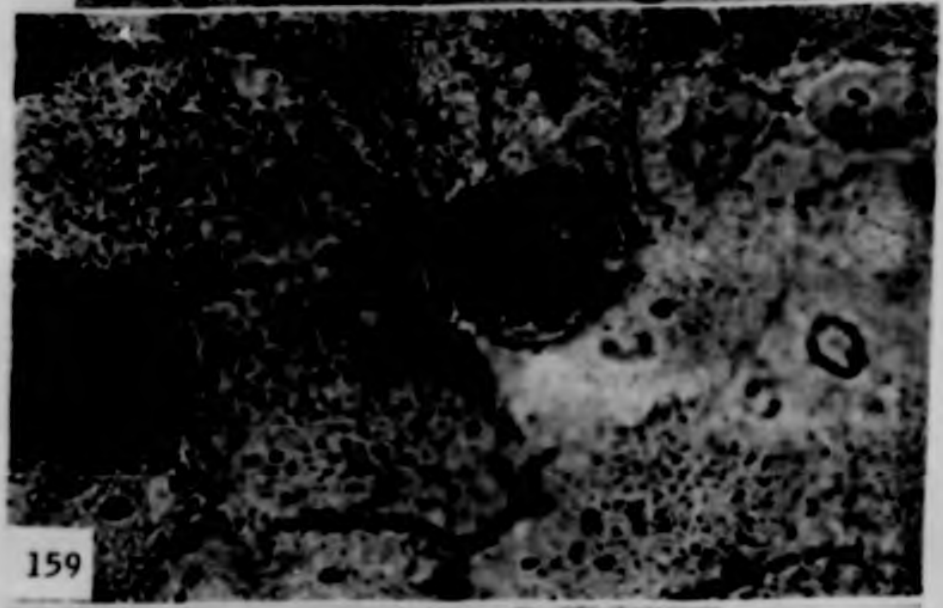

159

160

Fig. 161 No staining is seen in BF1) cells incubated in a substrate-free medium for inosine diphosphatase (IDPase) localisation. x 1290

Fig. 162 A late stage of interaction between E. histolytica and BF1) cells. Incubated for IDPase localisation. Granular deposits (arrows) are seen in the amoebic cytoplasmic vacuoles. x 3220

Fig. 163 E. histolytica trophozoite in contact with BF1) cells. Light microscopic demonstration of catalase activity. Reaction product is restricted to the amoebic vacuoles and uroid (U). x 1610

161

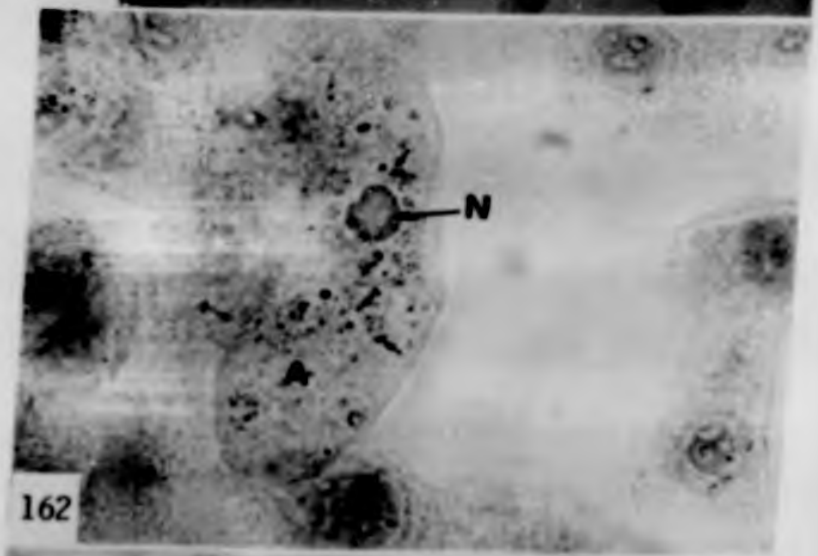

162

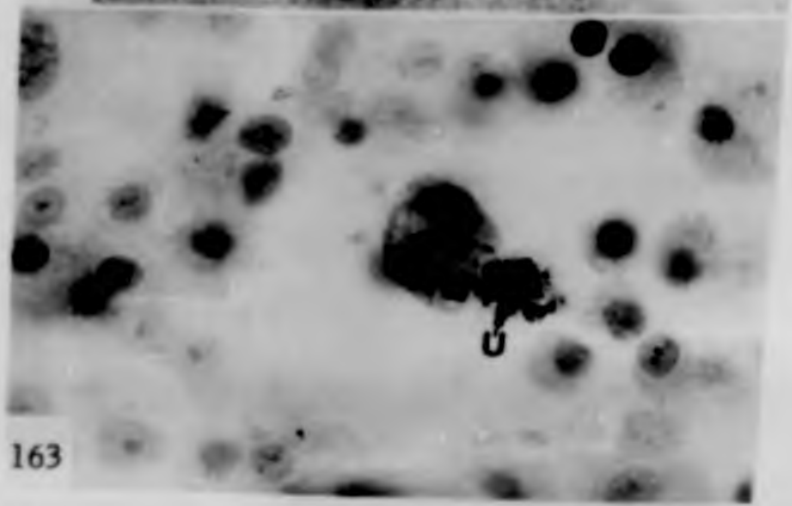

163

Fig. 164 Light microscopic demonstration of mitochondrial ATPase activity in RPMI cells. Cells illustrate long filamentous mitochondria. x 4130

Fig. 165 As for Fig. 164. Arrow indicates a cell showing small, stumpy mitochondria. x 4130

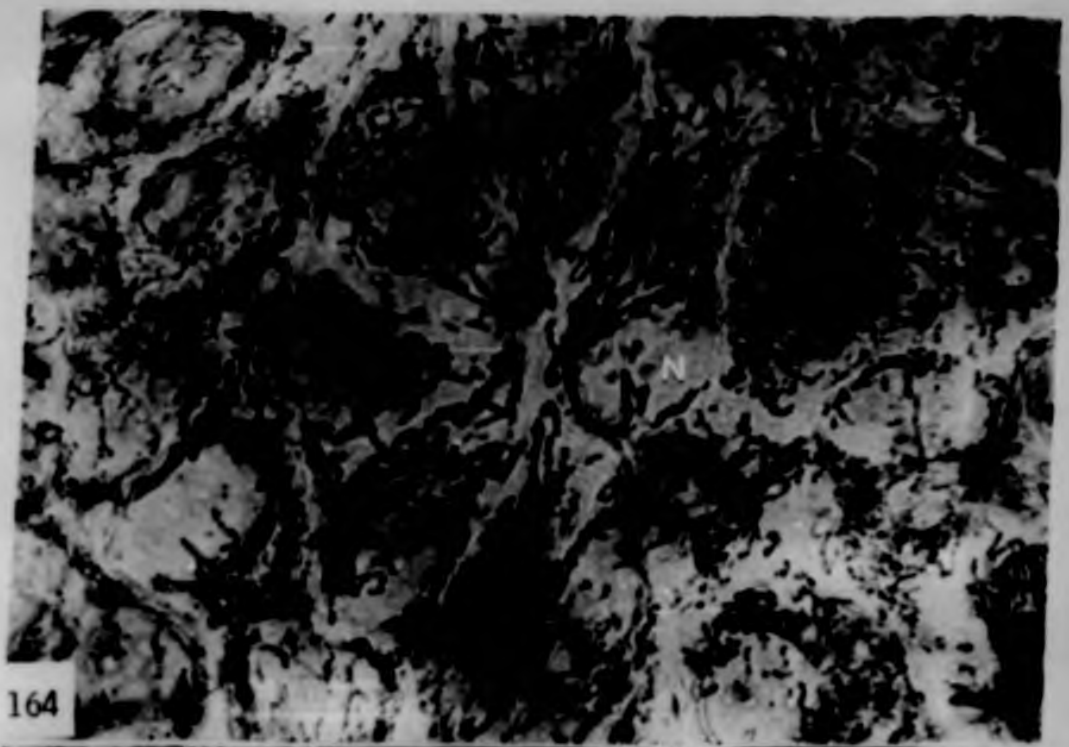

164

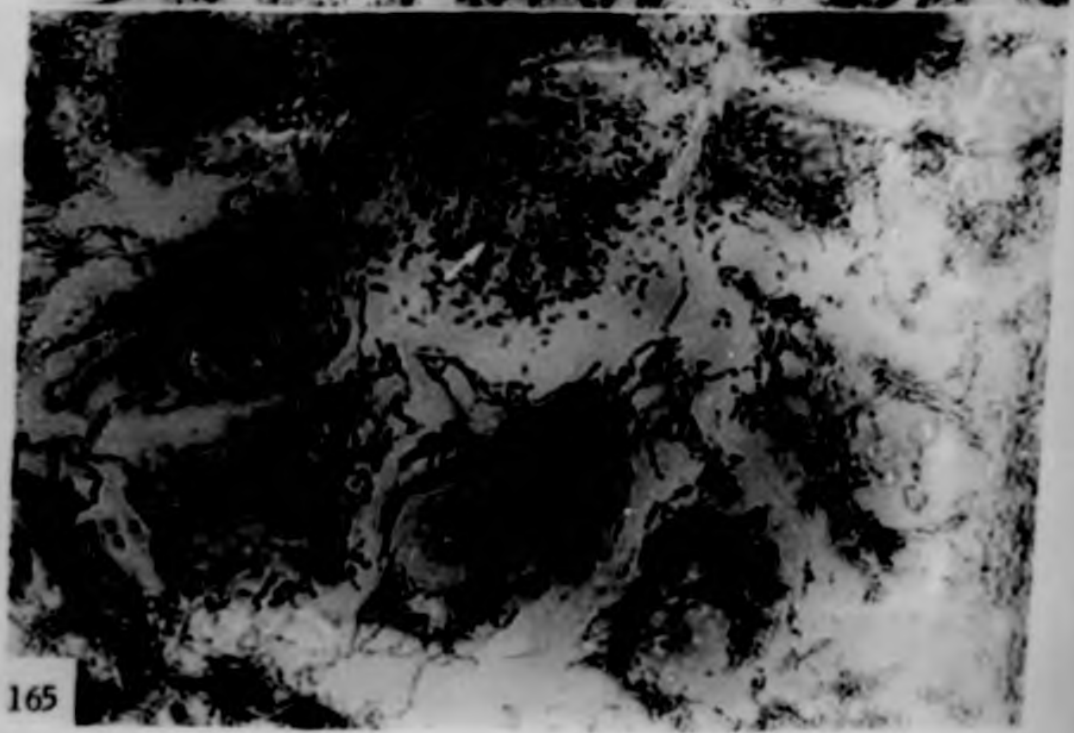

165

Figs. 166 & 167 — *E. histolytica* trophozoites (A) in contact with KT13 cells. Light microscopic demonstration of mitochondrial ATPase activity. In cells marked 1, the mitochondria have changed from an elongated to a rounded shape. In cells marked 2, the staining for mitochondrial ATPase is diffused resulting from breakdown of the mitochondria. ATPase is thus released into the cytoplasm. In Fig. 167 the amoeba has ingested the mitochondria. x 1040

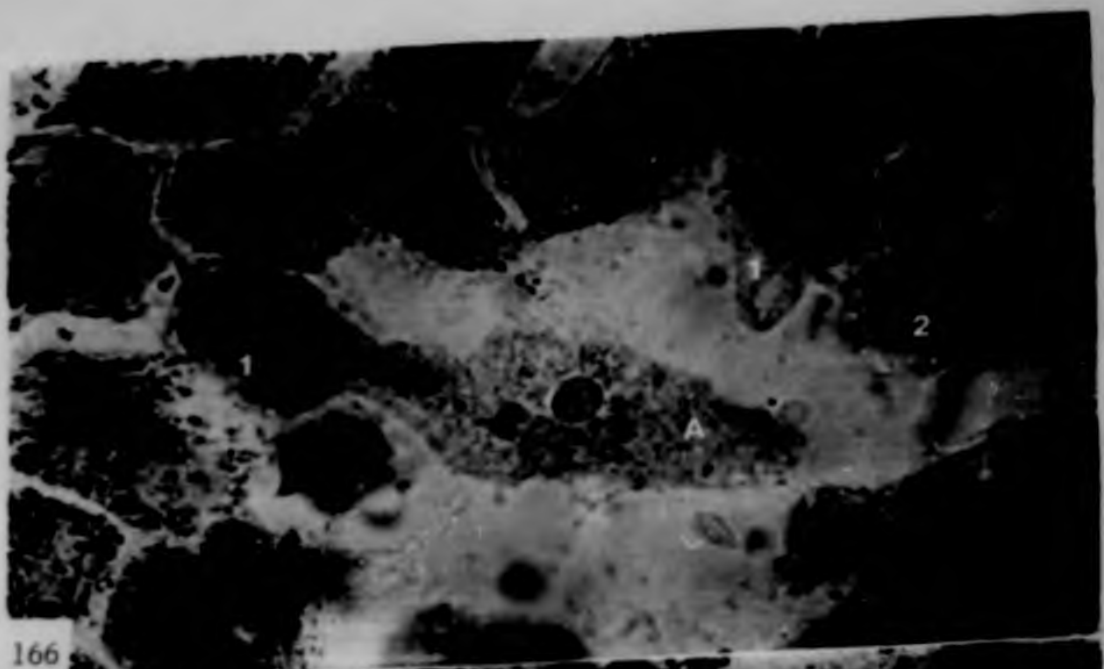

166

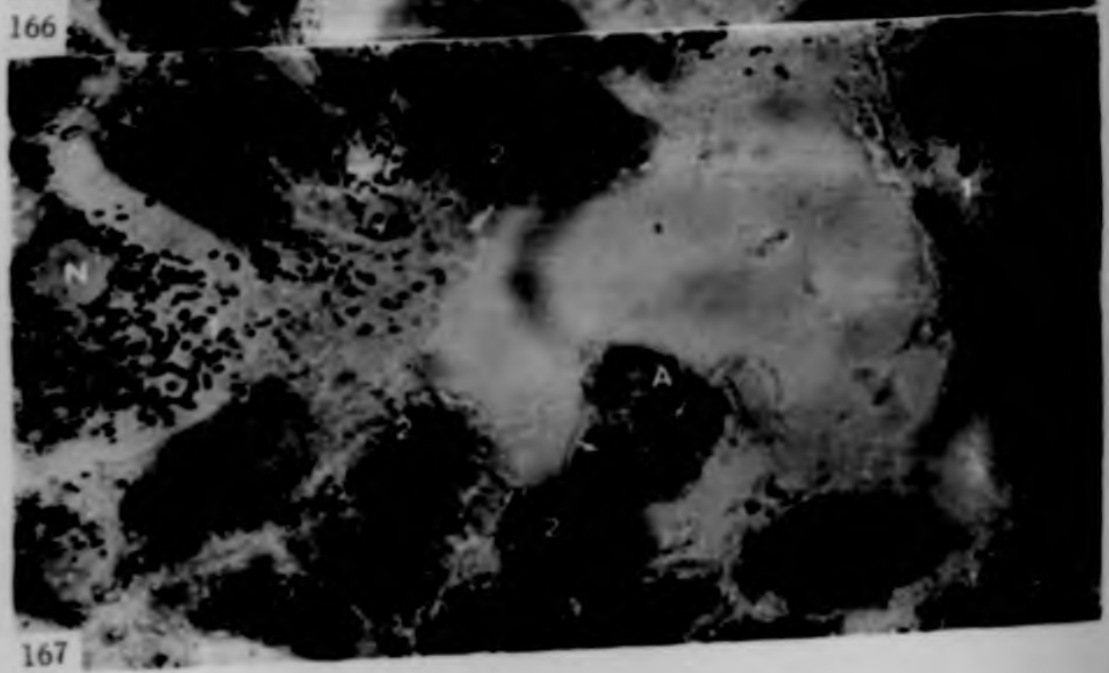

167

Figs. 168 & 169 Sections through healthy BHK cells from a a control monolayer culture.

Fig. 168 The complex interdigitating folds (If) which are thought to help hold cells together are seen. One also finds areas of specialisation of the cell surface, the tight junctions (arrows) which probably represent zones of firmer cell-to-cell attachment.

x 36,080

Fig. 169 Shows the various cellular organelles; rough endoplasmic reticulum (ER), mitochondria (M), Golgi bodies (G), lysosomes (L) and nucleus (N). x 13,150

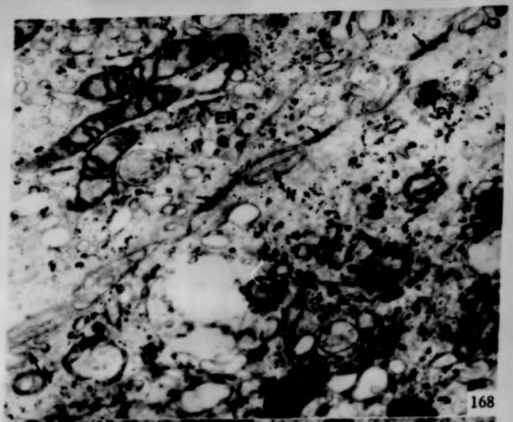

168

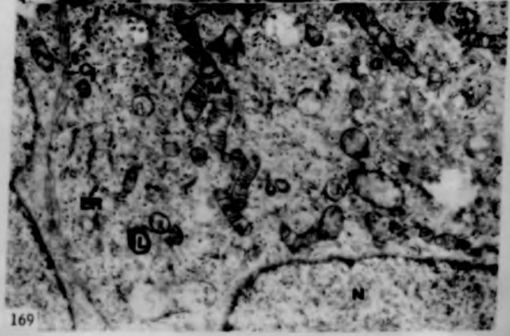

169

Figs. 170, 171 & 173 — Sections through HT13 cells which have been subjected to an homogenate of E. histolytica trophozoites. Shows no effect on the monolayer.

Fig. 170 x 1945
Fig. 171 x 21,300
Fig. 173 x 21,300

Fig. 172 — Section of mouse kidney showing leucine amino-peptidase activity. x 225

170

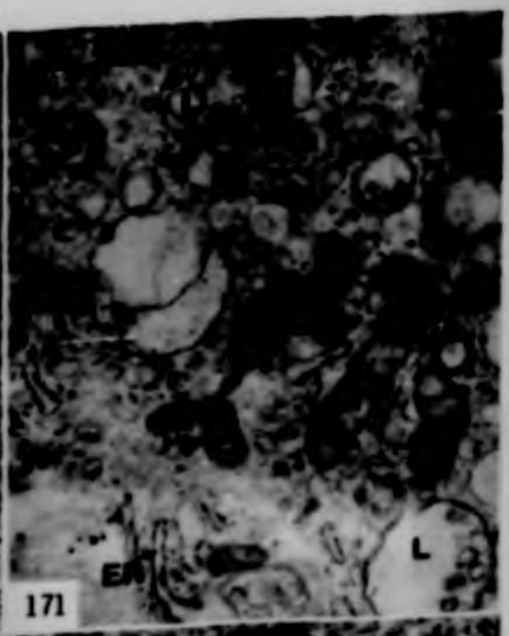

171

172

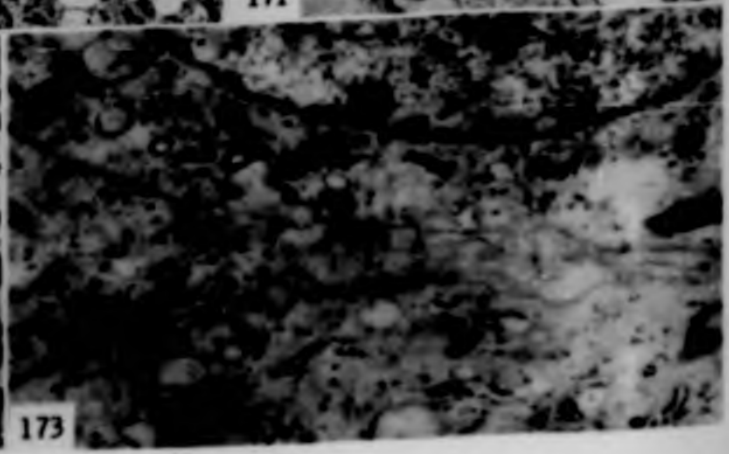

173

Fig. 174 Areas of two adjacent cells (RF13) from a control monolayer culture showing normal cytoplasmic organelles. Microtubules (arrows) are abundant in such a culture. x 12,100

Fig. 175 HM-1:IMSS strain (axenic). Part of an amoeba showing nucleus (N), electron-dense fibrillar structures (Fb), ribosomal helices within double-membraned vacuoles (RH), vacuoles (V), and short smooth-walled vesicles (arrow). x 12,100

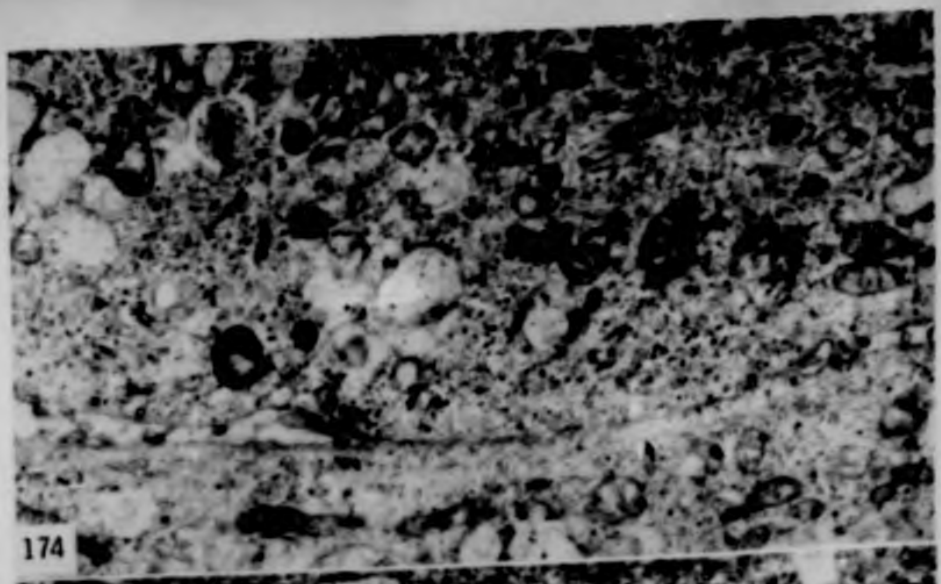

174

175

Fig. 176 A section of E. histolytica trophozoite (HM-1:IMSS strain) in contact with RPIJ cells. The cells surrounding the amoeba are damaged. At one end of the amoeba, initiation of phagocytosis (arrow) is seen. x 3220

Fig. 177 HM-1:IMSS strain (axenic). A section of an amoeba illustrating subpellicular bodies (arrows). x 18,010

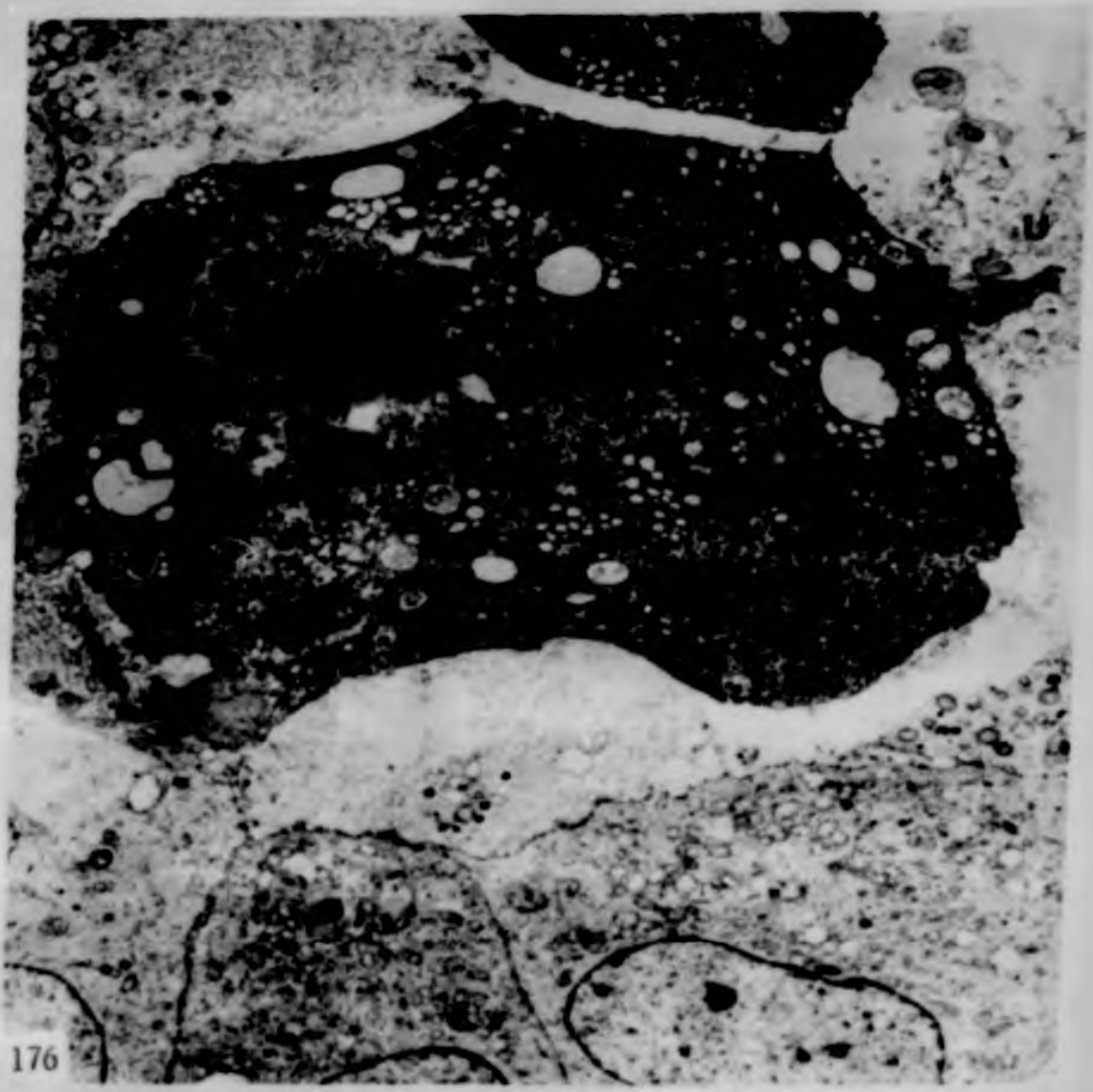

176

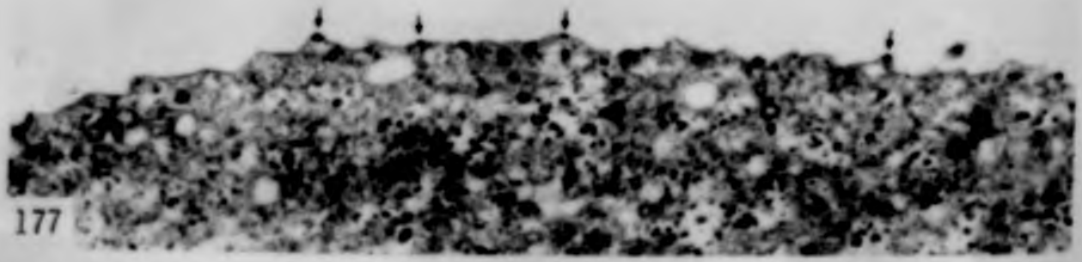

177

Figs. 178, 179, 180, 181

Sections of E. histolytica trophozoites (HM-1: IMSS strain) in contact with BF13 cells.

Fig. 178 Shows swelling of both the mitochondria and the cisternae of the endoplasmic reticulum in the affected cells. Also shown is an amoebic surface vacuole (V) which gives the impression that should this vacuole collapse it would give the appearance of a surface-active lysosome. x 4160

Fig. 179 Note both the swollen mitochondria (M) and the condensed mitochondria (Mi). The lysosomes (L) are not yet affected. The rough endoplasmic reticulum has vesiculated into small cisternae (arrows). x 11,910

Fig. 180 Contact area. x 7940

Fig. 181 Part of the amoebic pseudopodium (Ps) which has penetrated an intracellular cavity between cultured cells. Note condensation of nuclear chromatin (arrows) in the affected BF13 cell. x 7940

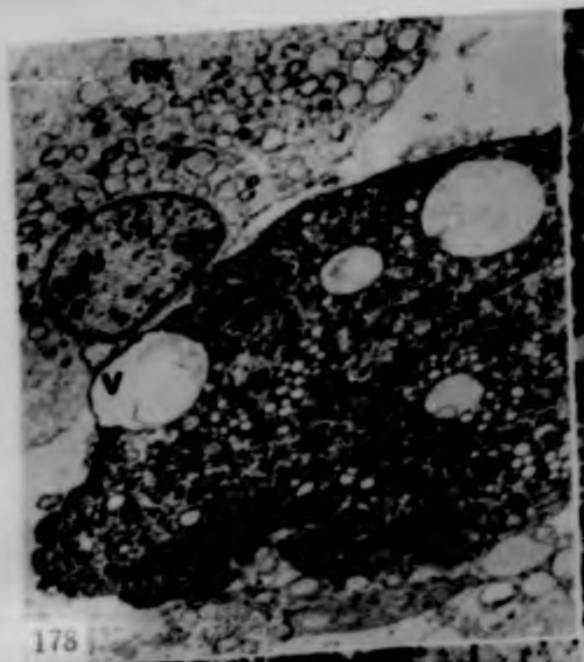

178

179

180

181

Fig. 182a A non-virulent trophozoite (HM-1:IMSS strain) in contact with RF13 cells. Note the amoeba is attempting to phagocytosise a piece of RF13 cell (arrow). x 3340

Fig. 182b Higher magnification of Fig. 182a showing the unaffected organelles in RF13 cell marked 'a'. The cytoplasmic matrix of cell 'a' is denser than that of cell 'b', probably due to the amoeba compressing 'a' against 'b'. The contacted cell 'a' has not lost its attachment with its neighbour as numerous interdigitating folds (arrow) along the cell junction can be seen. x 7790

Figs. 183 & 184 NIH:200 strain (axenic).

Fig. 183 Part of an amoeba showing the nucleus (N) and its intranuclear inclusions. x 3340

Fig. 184 A nuclear inclusion (Ni) is also seen in the cytoplasm. x 21,120

182a

182b

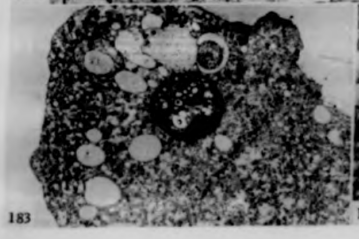

183

184

Figs. 185a, 185b, 186

Sections of E. histolytica trophozoites (200:NIH strain) in contact with HT3 cells.

Fig. 185a The surrounding cells are seen to be unaffected. x 6200

Fig. 185b Cell to cell attachment (arrows) is not lost. x 5030

Fig. 186 High magnification showing both the unaffected mitochondria and endoplasmic reticulum. x 24,000

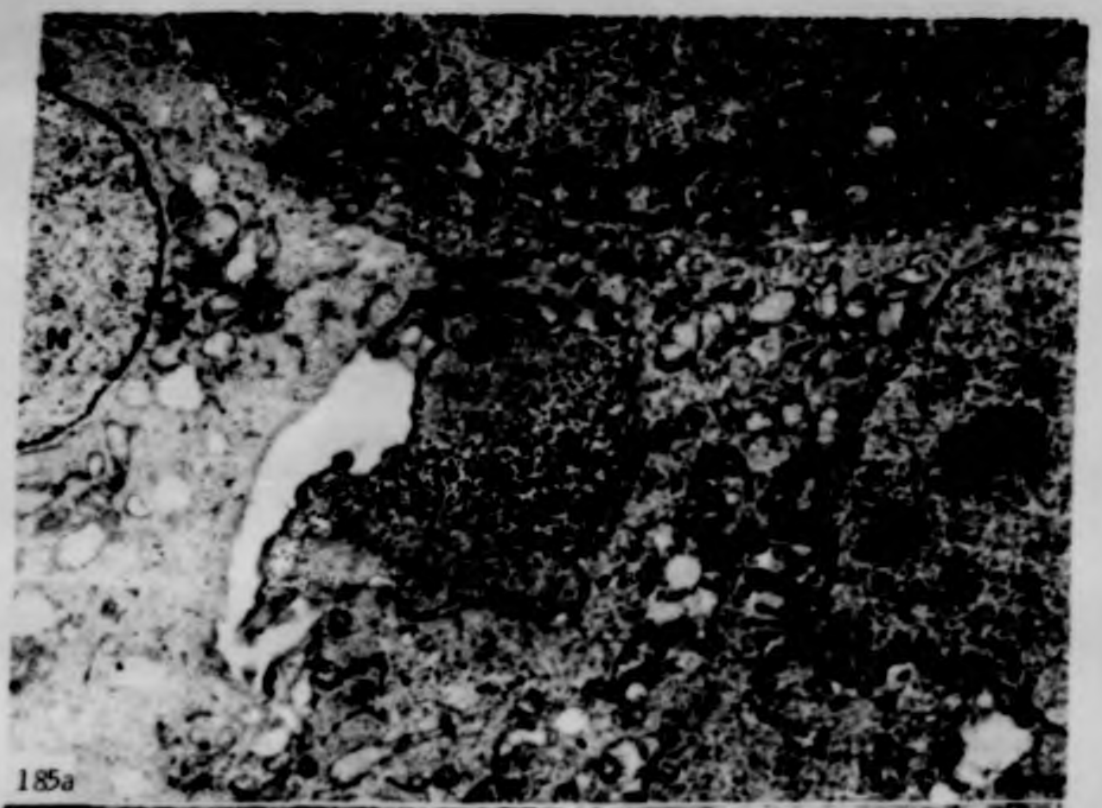

185a

185b

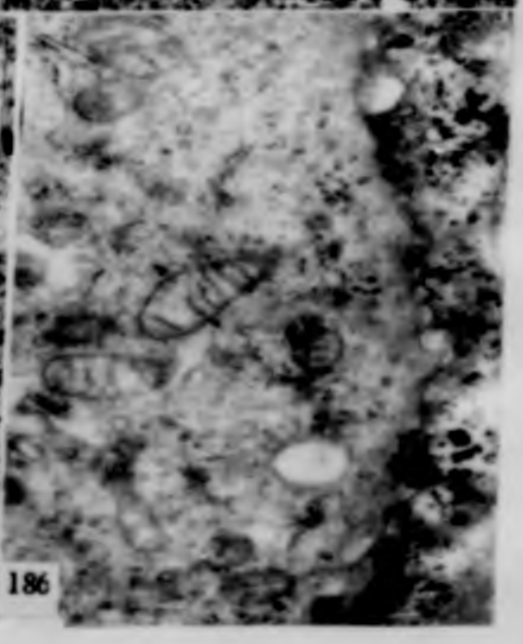

186

Fig. 187 An amoeba (NIH:200 strain) engulfing an unaffected RF13 cell. Part of a phagocytotic channel (Pc) is shown. x 7210

Fig. 188 E. histolytica trophozoite (A) (Evans strain) in cell-denuded area of a RF13 cell monolayer. x 1630

Fig. 189 Contact between E. histolytica trophozoite (Evans strain) and RF13 cell. The mitochondria (M) and the cisternae of the endoplasmic reticulum (small arrows) are swollen. Condensation of the chromatin (large arrows) is seen to occur along the nuclear membrane.

Fig. 190 Later stage of cellular injury. An affected RF13 cell showing disrupted lysosomes (L). Adequate cell-to-cell attachment (arrow) is no longer maintained as interdigitating folds are no longer seen. x 19,750

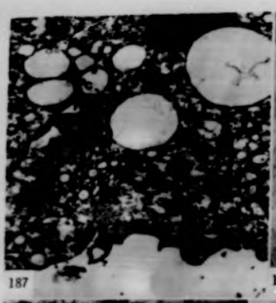

187

188

189

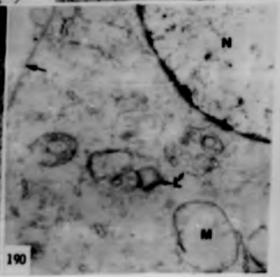

190

Fig. 191 Contact area between an amoeba and a HeLa cell. A piece of the affected cell cytoplasm is taken into the amoeba by phagocytosis. x 11,490

Fig. 192 Shows a collection of cellular debris at the tail end or uroid (U) of the amoeba. x 11,490

191

192

Figs. 193 & 194 Areas of contact between the amoebae and RKl3 cells showing the protective effect of promethazine hydrochloride. In such cells no swelling of either the mitochondria or endoplasmic reticulum is seen. The nucleus is also unaffected.

Fig. 193 x 11,490

Fig. 194 x 31,450

193

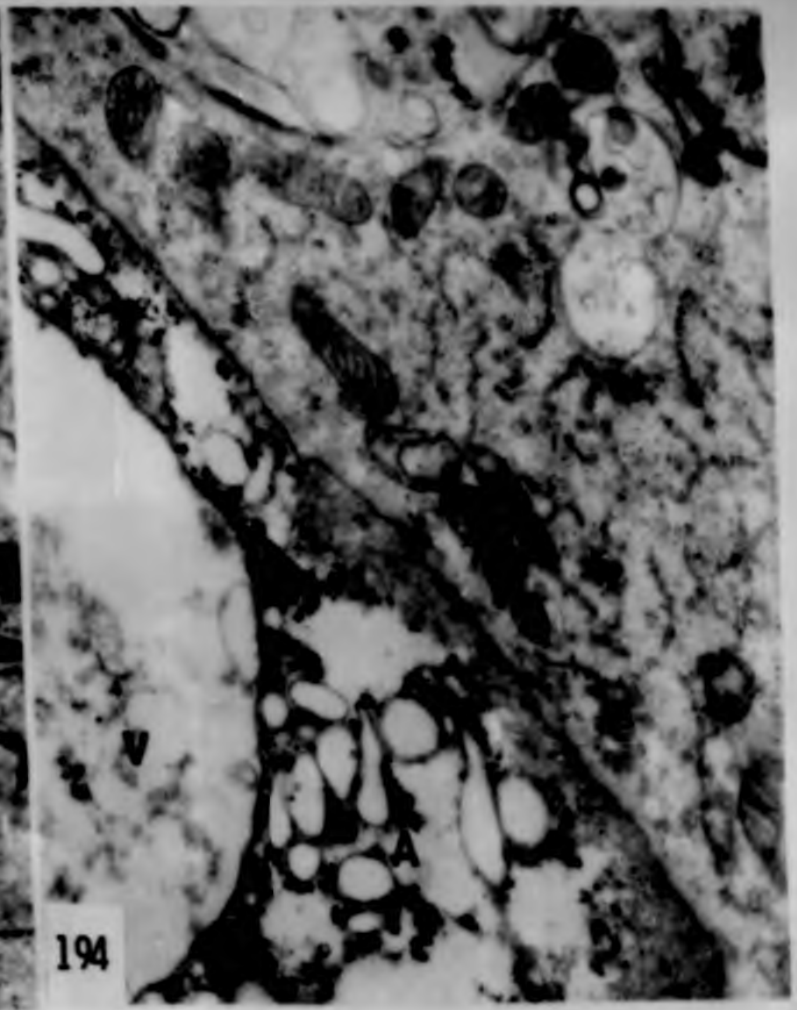

194

Fig. 195 Section showing the protective effect of promethazine hydrochloride on an HTlj cell in contact with an amoeba. Note the indentation of micropseudopodium (Pm) into the HTlj cell. x 34,095

Fig. 196a An amoeba engulfing an intact cell which is protected from cellular injury by the addition of promethazine hydrochloride. x 4890

196
196a

Fig. 196b Higher magnification of the terminal part of the phagocytotic channel (Pc) depicted in Fig. 196a. Vesicles (arrows) are seen to form and may fuse with the amoebic lysosomes where further degradation may take place. x 34,095

Fig. 197 Small filopodia (Pp) are seen to extend along the lateral edges of the amoeba. Note a small bleb (arrow) at end of one filopodium. Such a finding illustrates that promethazine hydrochloride does not affect the amoebic surface morphology. x 34,095

196b

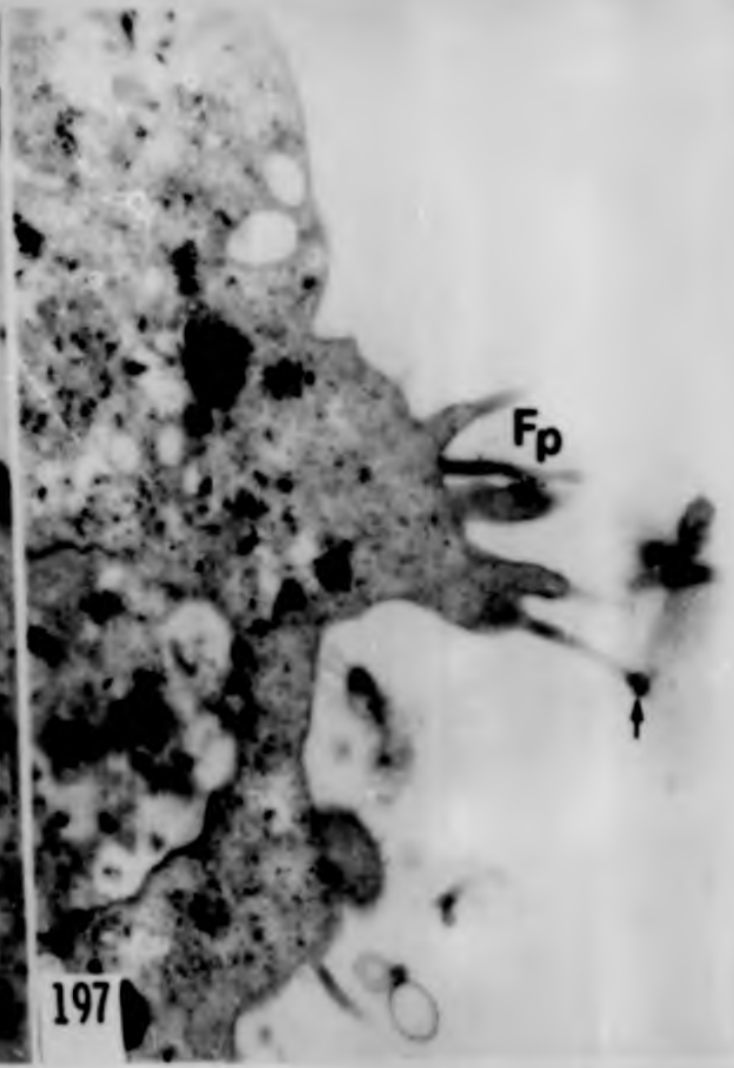

197

Fig. 198 Section of mouse kidney showing non-specific esterase activity in the tubules using α-naphthyl acetate method. x 1500

198

Fig. 199 Light microscopic demonstration of acid phosphatase activity in RF13 cells using azo-dye technique. Red deposits indicate sites of acid phosphatase activity. x 1050

Fig. 200 Acid phosphatase activity in trophozoite of E. histolytica after being added to a RF13 monolayer culture. The reaction product (red deposits) is confined to the amoebic vacuoles and none is seen near the plasmalemma. x 2625

Fig. 201 E. histolytica trophozoite in a lesion. The amoeba initially shows no reaction product for non-specific esterase activity, which is confined to the RF13 cells. The α-naphthyl acetate method is used. x 2625

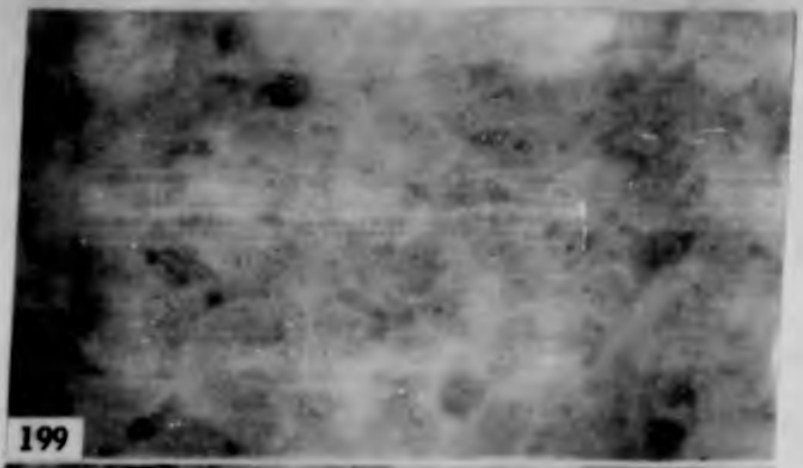

199

200

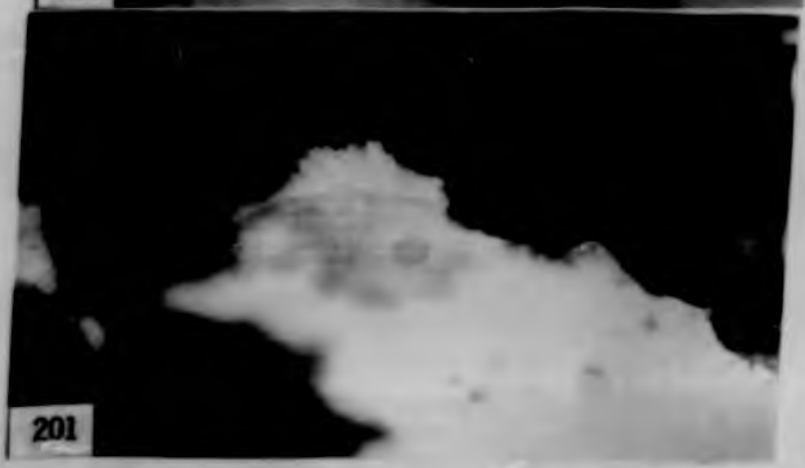

201

Fig. 202 Later stage of interaction between E. histolytica and Fl] cells. The reaction product (brown deposits) for non-specific esterase activity using α-naphthyl acetate method is seen in the amoebic vacuoles. x 2625

Fig. 203 Section of mouse kidney showing non-specific esterase activity in the tubules using indoxyl acetate method. Blue deposits indicate sites of non-specific esterase activity. x 525

Fig. 204 Section of mouse kidney showing β-glucuronidase activity in the tubules (red deposits). No reaction product is seen in the glomeruli. x 265

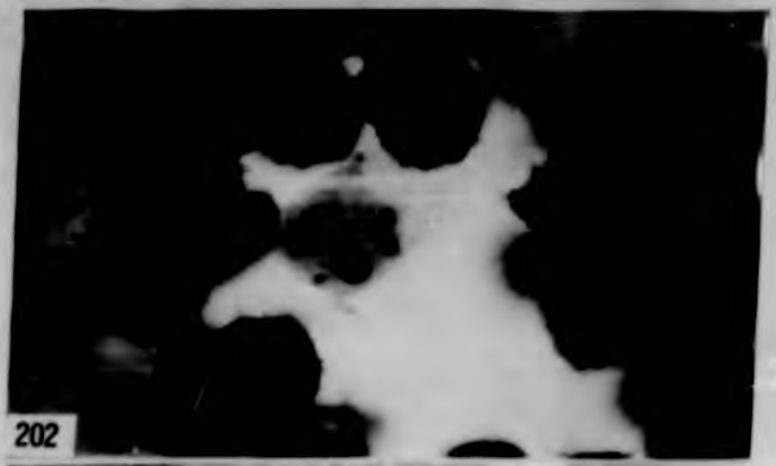

202

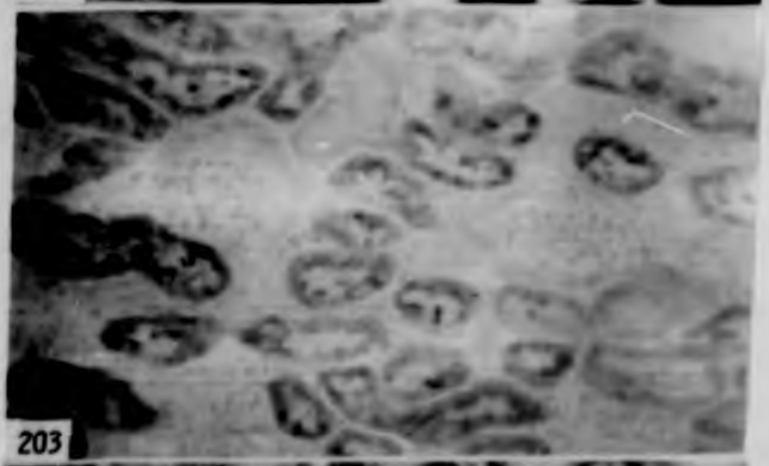

203

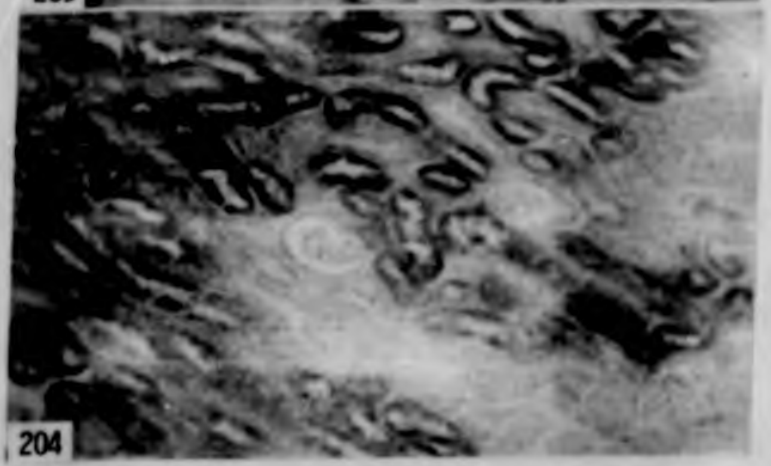

204

Fig. 205 E. histolytica trophozoite in cell-denuded area of an R'1) cell monolayer. An enhancement in the reaction product (red deposits) for β-glucuronidase is noticed in some of the affected cells, especially those with condensed nuclei.
x 1050

Fig. 206 High magnification of an amoeba in a lesion 1 hour after addition. Reaction product for β-glucuronidase is prominent in the amoebic vacuoles. x 2625

Fig. 207 E. histolytica trophozoite in contact with R'1) cells. Light microscopic demonstration of N-acetyl-β-D-glucosaminidase activity. The reaction product (red deposits) is only confined to the amoeba. None is seen in the surrounding cells.

205

206

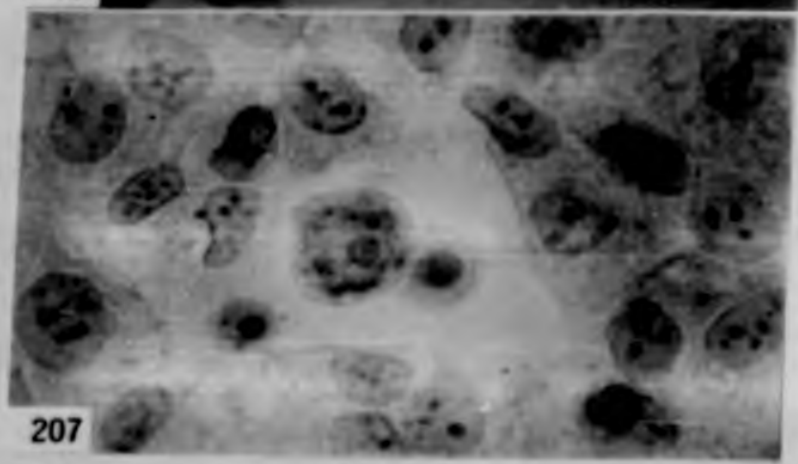

207